Establishment of Novel Cell Culture Models
of Parkinson's Disease
to Study Formation, Modulation, and Toxicity
of α-Synuclein Oligomers

Dissertation der Graduate School of Systemic Neurosciences

der Ludwig-Maximilians-Universität München
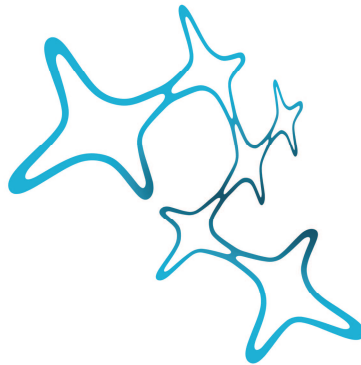
Graduate School of
Systemic Neurosciences
LMU Munich

vorgelegt von

Martin Frank Bartels

aus Kempten (Allgäu)

am 15. Dezember 2016

Dedicated to my parents

for their unconditional support.

List of Contents

List of Figures

List of Tables

1 Abstract

Parkinson's disease (PD) is the second most common neurodegenerative disease following Alzheimer's disease and the most common movement disorder. Clinically, a motor phenotype can be observed only after approximately 50% of dopaminergic neurons in the substantia nigra (SN) have been lost with rigor, resting tremor, bradykinesia or akinesia, and postural instability being the cardinal symptoms. Yet, to date, a definite diagnosis is only possible by analysis of post-mortem brain tissue. Here, a degeneration of the SN can be observed, and Lewy bodies and Lewy neurites in remaining dopaminergic neurites represent the histopathological hallmark of the disease.

On the molecular level, several routes of evidence suggest that the formation of small, soluble αSyn oligomers is causative for the loss of dopaminergic neurons in the SN, yet the toxic αSyn species and the exact mechanism of toxicity remain obscure. To date, agents for symptomatic therapy of PD are available, but no causative therapeutic approaches have been identified so far.

In order to achieve an earlier diagnosis and develop disease-modifying therapies, a better understanding of underlying molecular pathogenic mechanisms is desirable. Established cell lines represent suitable models to identify potential disease-modifying therapeutics and to study αSyn-mediated toxic mechanisms. To the best of our knowledge, by the beginning of this project, overexpression of αSyn in cell models was either constitutive or relied on transient transfection or viral transduction.

In this study, we aimed to develop a strategy for the creation of stable cell lines which inducibly overexpress variants of αSyn by addition of certain chemical agonists. The system should be applicable to a variety of established and primary cell lines for the investigation of aggregation, modulation, and toxicity of αSyn oligomers with regard to PD and other synucleinopathies.

We created vectors for the inducible overexpression of αSyn (S), the fluorescence protein Venus (V), αSyn coupled to Venus (SV), and αSyn coupled to the N-terminal (V1S) or C-terminal Venus fragment (SV2) for a bimolecular fluorescence complementation assay (BiFC). Inducibility was achieved by applying the GAL4_EcR-UAS (GE) or the Cre_ER^{T2}-loxP (CE^{T2}) system, respectively. The expression constructs were stably integrated into the genome of the host cell line by lentiviral transduction.

We here demonstrate the successful application of this strategy for the creation of inducibly αSyn overexpressing cell lines in H4 and LUHMES cells. We observed stronger inducibility of transgene expression in H4_GE cells compared to H4_CE^{T2} cells. Expression characteristics of

inducible H4_GE cells were investigated in detail based on both fluorescence intensity and protein amount. All cell lines showed low background expression and a maximum increase in transgene expression upon incubation with 1 or 10 µM tebufenozide for 4-6 days.

Exposure to heavy metals has been described as risk factor for the development of PD in epidemiological studies. In particular, ferric iron appears to be increased in the SN of PD patients and incubation of recombinant αSyn with DMSO or DMSO and $FeCl_3$ results in the formation of distinct oligomer species. Using the H4_GE cell models described in this work we observed a strong increase in fluorescence intensity in the BiFC assay upon incubation with DMSO in combination with $FeCl_3$ which was not observed for other tri-, di-, or monovalent ions. Additionally, an increase in αSyn protein load and higher molecular αSyn species were detected in western blot and sucrose gradient centrifugation. Taken together, these data suggest increased aggregation of αSyn in the H4_GE cell model upon incubation with DMSO and $FeCl_3$.

In summary, the system presented in this work holds high potential for the creation of αSyn overexpressing cell lines to evaluate risk factors of αSyn aggregation and αSyn-mediated toxicity as well as to screen for anti-aggregative compounds for potential disease-modifying therapeutics for PD and other synucleinopathies.

2 Introduction

2.1 Parkinson's Disease

Neurodegenerative disorders comprise a group of diseases that lead to a progressive loss of neurons resulting in disease-specific symptoms[1]. This loss of neurons is commonly accompanied by the deposition of disease-specific protein aggregates. Exemplarily, these aggregates consist of prion protein in Creutzfeldt-Jakob disease (cytoplasmic), huntingtin in Huntington's disease (cytoplasmic), tau protein (cytoplasmic) and amyloid-beta peptide (extracellular) in Alzheimer's disease (AD), and alpha-synuclein (αSyn) (cytoplasmic) in Parkinson's disease (PD) and other synculeinopathies including dementia with Lewy bodies (DLB) or multiple system atrophy (MSA)[2,3].

PD is the second most common neurodegenerative disease following AD and the most common movement disorder and was first described in 1817 in James Parkinson's *An Essay on the Shaking Palsy*[4]. On the cellular level, degeneration of synapses and axons in the striatum precedes the loss of dopaminergic neurons in the substantia nigra pars compacta (SNpc) leading to a depletion of dopamine in the nigrostriatal circuitry[5]. The typical clinical phenotype is characterized by the four cardinal symptoms rigor (stiffness of muscles), tremor (resting tremor with a frequency of 4-6 Hz), slowness or absence of motion (bradykinesia/akinesia), and postural instability[6] and can only be observed after 50 to 80% of dopaminergic neurons have already been lost (Figure 2-1 A). With further symptoms including sleep disturbances, visual halluzinations and illusions, cognitive deterioration and dementia, depression and anxiety, and a variety of sensory symptoms[7,8], PD places a heavy burden on both patients and relatives.

The loss of dopaminergic neurons in the substantia nigra (SN) (Figure 2-1 B) and Lewy bodies or Lewy neurites in some of the remaining neurons represent the histopathological hallmarks of PD (Figure 2-1 C), but degeneration can also be observed in other brain areas that use different neurotransmitter systems[9]. However, since Lewy body pathology is not proportional to the extent of cell death or the severity of the clinical phenotype and since also asymptomatic individuals show Lewy bodies in an age-dependent manner, it is still under debate if Lewy bodies are a sign of presymptomatic PD[10] or of normal aging[11].
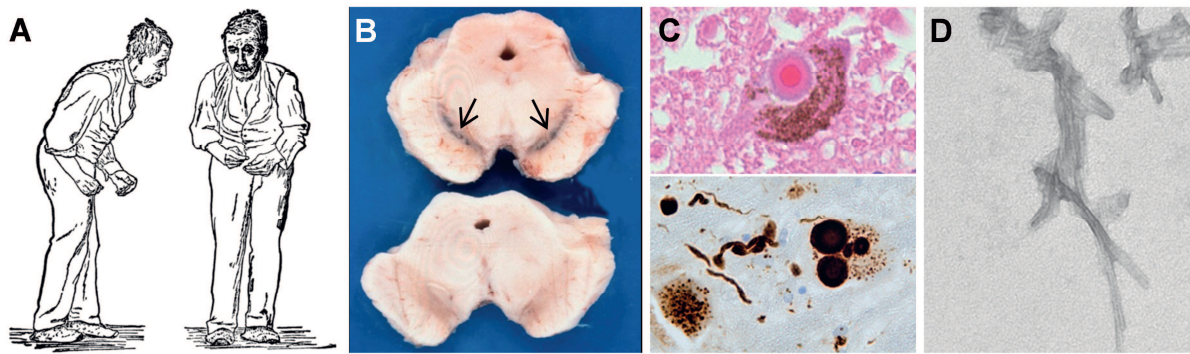
Figure 2-1: Background on Parkinson's disease

A) Illustration of the typical clinical phenotype of a PD patient by Sir William Richard Gowers[12] (source: https://de.wikipedia.org/wiki/Parkinson-Krankheit).

B) Midbrain sections of healthy control (top) and PD patient (bottom). Arrows point to SN which is degenerated in the PD case (pictures from Prof. Dr. med. Armin Giese, LMU Munich).

C) Staining of a brainstem neuron with hematoxylin and eosin (H&E) showing a cytoplasmic Lewy body (top) (pictures from Dr. med. Tobias Högen, LMU Munich). Staining of Lewy bodies and Lewy neurites with an anti-αSyn antibody (αSyn-42) (bottom).

D) αSyn fibrils observed in electron microscopy (from Michael Schmidt and Dr. med. Johannes Levin, LMU Munich).

In industrialized countries approximately 0.3% of the population suffer from PD[13] with probably slightly higher prevalence in men than in women (of approximately 1.5 to 1)[14]. The biggest risk factor for the development of PD is increasing age: The disease occurs only seldom in individuals below the age of 50 years and a strong increase in prevalence can be observed from 60 years on[14]. Thus, approximately 0.6% of the 65-69-year-olds are affected in Europe, and the prevalence increases to approximately 2.6% in the age group of 85-89 years[14-16]. Thus, with an expected prolonged lifespan over the next decades the number of PD patients is likely to further increase in the future. In 2010, approximately 630,000 people had been diagnosed with PD in the United States. It has been estimated that this number will increase to 819,000 by 2020, 1.06 million by 2030, 1.24 million by 2040, and 1.34 million by 2050[17]. With increasing number of patients, medical costs are likely to increase in the future (in the United States from approximately 8 billion $ in 2010 to 18.5 billion $ in 2050)[17].

Clinical diagnosis of PD relies on motor and nonmotor abnormalities, with motor parkinsonism (i.e., bradykinesia plus rest tremor or rigidity) being the core feature[18]. Since the motor phenotype occurs only after a substantial amount of dopaminergic neurons has already been lost, treatment of PD is currently limited to already advanced disease stages. To date, a definite diagnosis of PD is only possible by post-mortem histopathological examination since

parkinsonian symptoms can be observed in patients suffering from a variety of neurological disorders[19]. Indeed, a study from 1992 found that clinical diagnosis of PD was correct in only 76% of cases[20]. For this, better tools to diagnose PD with higher reliability and earlier in the course of disease are urgently required to improve the treatment of PD patients but also to improve clinical trials and epidemiological research[19].

Current treatment of PD patients is largely focused on the compensation for the pathological depletion of dopamine. Thus, PD patients are typically treated with levodopa, a dopamine precursor that can cross the blood-brain barrier (BBB) and is afterwards converted to dopamine by neuronal decarboxylases. Treatment with levodopa is often combined with administration of carbidopa, an inhibitor of peripheral decarboxylases that prevents decarboxylation of levodopa to dopamine and is incapable of crossing the BBB. Unfortunately, the effect of levodopa administration decreases over time. Another possibility to overcome symptoms caused by depletion of dopamine is the treatment with dopamine receptor agonists. Additionally, substances to reduce dopamine metabolism like monoamine oxidase B (MAOB) inhibitors or catechol-O-methyl-transferase (COMT) inhibitors can be given to slow down the degradation of dopamine to inactive metabolites[19,21]. A neurosurgical approach is taken by deep brain stimulation. Here, a neurostimulator, or "brain pacemaker", is implanted that stimulates areas like the globus pallidus, subthalamic nucleus, or thalamus to substitute missing inhibition from the SN and thus decrease inhibition of the motor cortex[22].

To date, there is no cure and no disease-modifying therapy for PD available. Therefore, a better understanding of underlying disease mechanisms is inevitable for the development of better diagnostic tools – allowing an earlier and more reliable diagnosis of PD – and for the development of disease-modifying therapies.

2.2 Alpha-Synuclein and its Physiological Role

Synuclein proteins – purified from *Torpedo californica* – were first characterized by Maroteaux *et al.*[23] in 1988. The acronym "synuclein" refers to the initially described localization in synapses and in the nucleus[23-31]. By now, the synuclein family has been subdivided into three groups, termed alpha-, beta-, and gamma-synuclein (with gamma-synuclein being equivalent to breast cancer specific gene 1 (BCSG-1))[30]. Meanwhile, alpha-synuclein (αSyn) has been found to localize not only to synapses and the nucleus but also to the cytosol, the mitochondria-associated membrane of the endoplasmic reticulum (ER), and the inner membrane of mitochondria. Hence, αSyn appears to travel actively between different compartments[32-34].

In humans, αSyn is expressed from the *SNCA* gene located on 4q21, i.e., the long (q) arm of chromosome 4 at position 21. It belongs to the family of natively unfolded proteins and accounts for approximately 0.5% to 1% of total protein in soluble cytosolic brain fractions[19,25,35]. The highest expression of αSyn is observed in neurons in both the central and peripheral nervous system[32,35]. αSyn exists mainly as a small soluble protein of 140 residues with a molecular weight of 14 kDa whose primary structure can be subdivided into three distinct regions[19,25]: the N-terminal lipid-binding region (1-60), the central NAC region (non-amyloid-beta component) (61-95), and the hydrophilic C-terminal region (96-140)[19,25] (Figure 2-2 A). Two further isoforms can be observed as a result of alternative splicing: αSyn-126 (lacking the amino acids 41 to 54 in exon 3) and αSyn-112 (lacking the amino acids 103-130 in exon 5)[35,36].

The physiological function of αSyn is still subject of ongoing research. It has been shown that mice lacking alpha- and/or beta-synuclein show normal survival and no obvious brain defects[19,37]. The only observed phenotype in mice with a depletion of αSyn expression was a different modulation in dopamine release and recycling pool homeostasis. However, the lack of more obvious phenotypes might be due to an artificial environment without evolutionary pressure and compensatory mechanisms or a redundancy of other synucleins[32,38-41], since age-related neurodegeneration and endocytosis abnormalities can be observed in mice lacking alpha-, beta-, and gamma-synuclein[42,43] and acute knockdown using RNAi expressed from adeno-associated viruses promotes degeneration in neurons of the SN[32,44].

Although it has been observed in a variety of cell compartments, αSyn has been described to be mainly enriched in presynaptic vesicles of vertebrates[32,45-47]. A lipid-binding property of αSyn can already be postulated based on its primary structure since its N-terminal region consists almost entirely of imperfect 11-mer repeats with a degenerate KTKEGV consensus motif[35,48] which is related to an alpha-helical lipid-binding motif of apolipoproteins (Figure 2-2 A).

A

N-terminal lipid binding region

MDVFMKGLSK AKEGVVAAAE KTKQGVAEAA GKTKEGVLYV GSKTKEGVVH GVATVAEKTK

Central NAC region

EQVTNVGGAV VTGVTAVAQK TVEGAGSIAA ATGFV

Hydrophilic C-terminal region

KKDQL GKNEEGAPQE GILEDMPVDP DNEAYEMPSE EGYQDYEPEA

B

A53T
A53E
H50Q
G51D
E46K
A30P
C
N

Figure 2-2: Background on αSyn

A) Amino acid sequence of αSyn (140-amino-acid isoform) with three distinct regions: N-terminal lipid-binding region (1-60), central NAC region (61-95), and hydrophilic C-terminal region (96-140). 11-mer repeats with degenerate KTKEGV consensus motif are underlined. All known disease-associated mutations are located within the N-terminal region (affected sequence positions are highlighted in color and amino acid substitutions are indicated below) (modified after Beyer, 2007[48]).

B) 3D structure of micelle-bound human αSyn according to Ulmer et al., 2005[49]. Position of disease-associated mutations are highlighted in color (figure kindly provided by Dr. Viktoria Ruf, LMU, modified).

Indeed, it has been shown that the exposure of αSyn to lipid micelles leads to a change in secondary structure from unfolded to alpha-helix in the N-terminal region[19,49,50] (Figure 2-2 B) and that a fraction of αSyn interacts with the presynaptic membrane and membranes of synaptic vesicles[51-54]. It has been hypothesized that this binding of αSyn to vesicles inhibits their fusion with other membranes. The association of αSyn to lipid membranes seems to be supported by a topologically stressed bilayer–water interface: Accordingly, it appears to be critically dependend on surface curvature and lipid composition favored by strong surface curvature and negatively

charged lipids or membranes composed of zwitterionic lipids in the gel state but not in the liquid-crystalline state[48,55,56].

In line with its lipid-binding properties, the physiological function of αSyn may play a role in the regulation of the homeostasis of the presynaptic vesicular pool, of synaptic vesicle cycling and endocytosis[23,32,35,37,57-59], and the regulation of neurotransmitter release[19,60,61], especially for dopamine[39,62-65]. Apart from direct lipid-binding, there may also be an indirect effect of αSyn towards the regulation of synaptic transmission. In line with this, it has been described that αSyn can bind to and inhibit phospholipase D2 (PLD2) which is involved in vesicular trafficking and breakdown of phosphatidylcholine[66-69].

Several members of the family of natively unfolded proteins have been shown to have chaperone function[19]. For αSyn, the C-terminal region has been suggested to show chaperone activity (Figure 2-2 A). Thus, αSyn may act as auxiliary chaperone for the cysteine string protein alpha (CSPalpha) which acts as co-chaperone for soluble N-ethylmaleimide-sensitive factor attachment protein receptor (SNARE) proteins located in synaptic vesicles[19,51]. By this, αSyn may be involved in the facilitation and stabilization of SNARE complexes with overexpression of αSyn leading to decreased exocytosis in cultures of embryonic hippocampal neurons[32,70,71]. It has also been suggested that the C-terminal region can prevent the self-assembly of αSyn by interacting with its hydrophobic core region[32,72,73] which is involved in the aggregation process of monomers into aggregates and amyloid fibrils[19,74].

The control of αSyn activity and/or its localization could be mediated by post-translational modifications (such as phosphorylation) for which the C-terminal region shows several putative sites[32,75,76]. Thus, αSyn can be phosphorylated at S129 by casein kinase I and G protein-coupled receptor kinases, modulating its lipid-binding properties[69,77]. Moreover, the C-terminal region has been shown to target recombinant αSyn into the nucleus, whereas the N-terminal and core region were required to target αSyn to the presynapse[24,78].

However, the functions of αSyn described above are by far not complete and a variety of additional mechanisms with involvement of αSyn have been suggested. According to this, its expression has been shown to be upregulated in early development[79]. Additionally, αSyn conveys protection against oxidative stress by inhibiting the c-Jun N-terminal kinase (JNK) stress signaling pathway in neuronal cells[80]. It has also been shown to bind to histones[81] and affect histone acetylation[24,82] and to influence the function of nuclear proteins[32,78,81,82].

2.3 Evidence for αSyn as Important Factor in Neurodegeneration

The first evidence for an involvement of αSyn in neurodegenerative disorders came in 1993, when αSyn was identified as non-amyloid-beta component in amyloid preparations from patients suffering from AD[27,28]. Later on, αSyn was also found to be the principal component of Lewy bodies[24,45,83] where it occurs as highly ordered amyloid-type fibril[45,84,85] (Figure 2-1 D) and usually appears to be subjected to post-translational modifications like cleavage, S129 phosphorylation, oxidation, and nitration, which increase the rate of oligomer formation[19,32,86-92]. The aggregation of αSyn can also be observed in solution *in vitro* where full-length αSyn and peptides derived from it form aggregates and amyloid fibrils with a morphology comparable to fibrils purified from Lewy bodies[19,93,94].

Critically important for the aggregation process appears to be the NAC-region (comprising amino acids 61-95) (Figure 2-2 A) which consists largely of hydrophobic amino acids: The aggregation behavior of beta-synuclein (βSyn) – which differs from αSyn by the absence of eleven amino acids (73-83) in the NAC-region – has been discussed controversially, but overall a reduced aggregation propensity compared to αSyn can be postulated[95-99]. Moreover, an area of 12 amino acids inside the NAC region (71-82) was shown to be necessary and sufficient for αSyn fibrillization[100].

A causal part of αSyn in disease progression can be assumed due to the presence of aggregated αSyn in neuronal populations which correlates to the onset of cell loss[32,101-103]. This αSyn pathology precedes cell loss in a model where mice had been injected with preformed fibrils, suggesting that pathological αSyn species are the main driver of neurodegeneration[32,103-105].

Although the vast majority of PD cases is sporadic[106], clues for an involvement of αSyn in the development of PD also come from gene mutations detected in familial PD cases. Thus, several disease-associated mutations leading to single amino acid exchanges have been identified in the *SNCA* gene: A53T[107], A30P[108], E46K[109], H50Q[110], G51D[111], and A53E[112] (Figure 2-2 A, B). The pathological mode of action of these mutations is currently largely unsolved, but A30P, E46K, and A53T have been shown to increase the aggregation rate of αSyn[94,113]. Additionally, duplication or triplication of the *SNCA* gene cause parkinsonian symptoms with the age of onset and severity of symptoms correlating with the gene copy number[19,105,114-116]. Recently, a number of polymorphisms in the promoter region of αSyn has been described as risk factors for PD[117], and genome-wide association studies indicate a connection between the *SNCA* locus and PD[32,118,119]. In line with this are experiments in mice and flies where overexpression of human αSyn was accompanied by neuronal dysfunction, loss of neurons and synaptic terminals, and an unphysiological motor phenotype[19,120,121].

Interestingly, several genetic risk factors for PD comprising mutations in other genes than *SNCA* might actually exert their pathological potential via αSyn. Accordingly, mutations in gluocerebrosidase which cause Gaucher's disease also increase the amount of αSyn and the risk for PD[122,123]. In addition, Lewy pathology has been observed for mutations in a variety of proteins including DJ-1, PINK1, GBA and likely also LRRK2, Parkin, and ATP13A2[124-129].

Not only genetic risk factors but also several environmental risk factors for the development of PD have been shown to influence αSyn aggregation[130]. According to epidemiological studies, the exposure to heavy metals like iron represents one such risk factor[131]. Indeed, alterations in brain iron levels with an increased iron load in the SN have been described in PD [132-134]. Elevated brain iron levels in PD patients can be detected using magnetic resonance tomography or transcranial sonography (TCS). This might already be possible early in the course of disease, and elevated brain iron levels might precede neurodegeneration since several persons rated as healthy subjects showed increased echogenicity and were clinically diagnosed with PD several years later[135,136]. In the post-mortem tissue of PD patients, elevated brain iron levels and a shift in the ferrous-to-ferric iron ratio towards ferric iron can be observed[137,138]. In line with this, iron chelators show a neuroprotective effect in the SN in PD models[139-143].

In vitro, ferric iron and other metal ions have been shown to increase αSyn aggregation[131,144,145], and αSyn promotes the production of reactive oxygen species (ROS) in the presence of iron[146]. Interestingly, oxidative stress in turn increases the formation of iron-induced αSyn oligomers[144], presumably resulting in a vicious circle. According to post-mortem studies in PD brains, several molecules appear to be damaged as a result of oxidative stress including lipids, proteins, and DNA[132,147].

Additionally, pesticides like paraquat[148] or rotenone[149,150] have been suggested to increase αSyn aggregation and to promote PD-like progression via increased release of αSyn from enteric neurons[151]. The interaction with αSyn and the stabilization of a protofibril stage of aggregation by dopamine and related catecholamines[152,153] might in parts explain, why dopaminergic neurons in the SNpc are particularly vulnerable to αSyn-mediated toxicity in PD. Taken together, several lines of evidence point to a central role of αSyn in the development of PD.

2.4   The Toxic αSyn Species and the Pathological Mechanism

To date, the toxic species and the pathological mechanism(s) of αSyn aggregation remain obscure[24].

Besides the prototypical amyloid fibrils with a typical width of 12-15 nm that can be found in LBs several different molecular species have been described[24,32,152,154-156]. These include short β-sheet-rich fibril-like intermediates, termed protofibrils, that can assemble linearly forming chains[154] or circularly forming ring structures consisting of 25 to several hundred αSyn molecules[32,152,156]. Since cell death cannot be explained by the presence of fibrillar αSyn aggregates, and since overexpression of αSyn can lead to disruption of organelles and cell death in the absence of detectable fibrillary deposits, it was suggested that such smaller, oligomeric species – which may be on- or off-pathway to amyloid fibrils – might comprise the cytotoxic αSyn species[157-160]. To date, this hypothesis has not been proven but is supported by several lines of (indirect) evidence[19,161,162].

Concerning their structural features, αSyn oligomers show similarities to oligomers of other disease-associated peptides such as amyloid-beta, polyglutamine, or prion peptide 106-126, supporting the hypothesis of a common pathological mechanism in different neurodegenerative disorders[163]. Iron has been shown to promote aggregation of αSyn resulting in toxicity in cell culture[164-166], and the inhibition of αSyn oligomer formation reduces cytotoxicity, suggesting a toxic effect of αSyn oligomers[165]. Moreover, large iron-induced αSyn oligomers lead to increased intracellular calcium dyshomeostasis and excitotoxic neuronal death by enhancing pre- and post-synaptic α-amino-3-hydroxy-5-methylisoxazole-4-propionate (AMPA) receptor-mediated synaptic transmission[167]. Further indirect evidence comes from αSyn-expressing cells which show increased but unspecific cation permeability[162,168]. Moreover, αSyn oligomers were shown to increase calcium permeability and cause cell death[32,169]. *In vivo*, the overexpression of αSyn with mutations that favor oligomer formation (E57K and E35K) in the midbrain of rats results in increased loss of dopaminergic neurons, whereas mutations that lead to a quick fibrillization of αSyn are less toxic[32,169].

Since αSyn protofibrils can display an annular structure that is reminiscent of bacterial pore-forming toxins[161,170], a common hypothesis for the oligomer-mediated toxicity is the formation of pore-like structures in cellular membranes leading to membrane permeabilization[170,171]. This is supported by the finding that the binding affinity of αSyn to membranes depends on its aggregation state with intermediates – formed during the conversion from monomeric αSyn to fibrils – showing highest affinity[19,172]. Moreover, the binding of αSyn protofibrils to phospholipid vesicles is much stronger than that of monomeric or fibrillar αSyn[161,170,173]. Interestingly, αSyn

oligomers show a modified lipid-binding behavior compared to monomeric αSyn: In contrast to monomeric αSyn, iron-induced oligomers can bind to membranes independently of charge, lipid composition, or surface curvature with high affinity[56]. Recently, our group was able to show that iron-induced αSyn oligomers lead to the insertion of distinct pore species in lipid bilayers *in vitro*[171]. Taken together, this might account for a pathological mechanism in which αSyn oligomers can bind to the plasma membrane or membranes of cell organelles such as ER or mitochondria with high affinity, where the insertion of pores results in impaired organell function leading to reduced cell viability.

Meanwhile, a number of studies suggests a role of oxidative stress and mitochondrial dysfunction in αSyn-mediated toxicity[19]. First hints for an involvement of mitochondria came in 1976, when Barry Kidston, a 23-year-old chemistry graduate student, developed parkinsonian symptoms three days after consumption of the self-synthesized opioid drug MPPP (1-methyl-4-phenyl-4-propionoxypiperidine or desmethylprodine). When Kidston died 18 months later (from a cocaine overdose), brain autopsy revealed destruction of dopaminergic neurons in the SN. Some years later, several young adults developed sudden, severe parkinsonism after consumption of synthetic heroin. In both cases, contaminations with MPTP (1-methyl-4-phenyl-1,2,3,6-tetrahydropyridin), a selective inhibitor of mitochondrial complex-I, were detected[174-176]. Treatment of squirrel monkeys with MPTP-induced permanent parkinsonism[177], while mice lacking αSyn appeared to be resistant against MPTP induced degeneration of dopaminergic neurons[178,179]. Additionally, it has been described that αSyn binds to mitochondria and that changes in the amount of αSyn can influence mitochondrial function[32,180-183]. Furthermore, the expression of mutant αSyn leads to mitochondrial defects, promotes cell death and enhances susceptibility to oxidative stress[19].

It has also been suggested that αSyn exists mainly as physiological tetramer[184] and that the interaction of αSyn multimers with membranes is a physiological event. Then, disease-associated mutations located within a small part of the N-terminal region could lead to disruption of physiological αSyn multimers and thus decrease membrane binding affinity of αSyn[32,184-189]. Furthermore, the disruption of tetrameric αSyn to unfolded monomers has been discussed as starting point for pathological αSyn aggregation[32,190]. However, the tetramer hypothesis is under strong debate and the scientific relevance remains questionable[191].

Several additional mechanisms have been described for αSyn-mediated toxicity such as ER stress and unfolded protein response (UPR) activation, which are likely to be both cause and effect in the pathogenesis of PD, or dysfunction of the ubiquitin proteasome system, calcium homeostasis dysregulation, and neuroinflammation[19,32].

All in all, to date it, remains unclear if one specific pathological oligomeric αSyn species or several different pathological species can act via one specific or several different pathological mechanisms. Yet, the development of small molecule modulators of αSyn oligomerization appears to represent a promising strategy towards new treatment options for neurodegenerative disorders in general and PD in particular[192]. Indeed, inhibition of polyglutamine oligomerization has shown beneficial effects in models of Huntington's disease[193], and anle138b – which inhibits αSyn oligomer formation and prion propagation *in vitro* – also displays beneficial effects on pathology in *in vivo* models of synucleinopathies and prion diseases[192].

2.5   Cell Models for the Investigation of Synucleinopathies

Using models to study disease mechanisms is inevitable, yet every model system will differ from the process being modelled. Moreover, since studying disease mechanisms is usually performed for diseases where the pathomechanism is not fully understood yet, models will rely on an incomplete assembly of well-known characteristics of the disease of interest and, thus, will not necessarily represent a complete picture of it[194]. For this, choosing a combination of different suitable models should increase the probability of gaining relevant information concerning the process being modelled.

While *in vitro* methods hold high potential to study principle mechanisms in short time and a simplified environment, no information concerning cytotoxicity can be obtained. Animal studies, on the other hand, hold the benefit of investigating mechanisms in a complex environment but are usually much more expensive and time-consuming, more restricted concerning the number of independent experiments and require some lead time due to governmental regulations. Besides, the use of rodent models and rodent cells has been discussed critically since these models may have low predictivity for human disease states[195,196].

A promising strategy to improve the poor translation rate from animal models to human patients is represented by a more detailed characterization of drug candidates in combinations of more and better *in vitro* and *in vivo* models. Thus, attempts to provide elaborated disease models based on human cells are ongoing[197,198]. Cell models with a human background provide the opportunity to close a fundamental gap between *in vitro* studies and experiments performed in animals since they represent a more complex experimental setup than *in vitro* experiments with the potential to assess complex interactions and cytotoxicity on a much shorter time scale than experiments performed in animal models. Concerning αSyn-mediated toxicity, they also

enable the investigation of timing of αSyn aggregation relative to downstream events, hereby increasing the chance of identifying αSyn-mediated toxic effects[162].

The investigation of αSyn oligomers is hampered by the fact that oligomers represent transient intermediates whose formation depends on non-covalent interactions and appears to be highly dynamic[162]. Thus, oligomerization is influenced by external conditions like concentration, temperature, and medium composition[95,199-201]. Since αSyn oligomers are submicroscopic particles, their detection requires indirect biochemical methods such as native gel electrophoresis, density gradient centrifugation, or size exclusion chromatography. Alternatively, microscopic methods can be applied that include additional preparatory steps such as atomic force microscopy, or fluorescence labeling like fluorescence intensity distribution analysis[200,202-205]. However, apart from being time-consuming and labor-intensive, none of these methods enables the investigation of the formation of αSyn oligomers in a cellular environment in real time[206]. To overcome this problem, a bimolecular protein fragment complementation assay (PCA) has been developed to study αSyn aggregation[207,208] applying both luminescence using *Gaussia princeps* luciferase and fluorescence using a variety of fluorescence proteins including Venus, a variant of the yellow fluorescent protein (YFP)[209-216].

Several cell culture models have been established to study αSyn oligomerization and αSyn-mediated toxicity. Over the last years, more and more studies using human induced pluripotent stem cells (iPSCs) have been published[217-219], and these models will certainly gain further relevance in the future. However, by now, the usage of iPSCs has two important drawbacks compared to established cell lines: It is very money- and time-consuming[1].

Cultures of primary midbrain dopaminergic neurons, usually derived from mice or rats, hold high potential to study the effect of αSyn aggregation and cytotoxicity[220]. These primary neurons are suited to dissect mechanisms of neurodegeneration including neurite retraction and neuronal death. Moreover, they enable the investigation of pharmacological compounds and their underlying mechanism(s)[1,221]. On the other hand, the preparation of primary cultures from midbrain dopaminergic neurons requires some experience and is time-consuming. Moreover, primary neurons are usually less susceptible to transient transfection mechanisms[1]. Furthermore, breeding and maintenance of transgenic rodents requires man power and the existence of an animal facility. Finally, the use of rodent dopaminergic neurons might be limited since humans are the only known species which is affected by the development of PD[32,222].

Several established human cell lines have been used to unravel mechanisms of αSyn-mediated neurodegeneration. In contrast to iPSCs or cultures from primary dopaminergic neurons, established cell lines tend to acquire some artificial features over time. HEK293 cells or H4 cells,

e.g., show multiplication of chromosomes. Thus, their phenotype might be more different from human dopaminergic neurons compared to iPSCs or primary dopaminergic neurons, although the existence of more than one cell type in primary cultures can often not be excluded. On the other hand, established cell lines have several advantages compared to iPSCs and primary cultures: Most of them, such as HEK293 cells and H4 cells, are quite easy in handling and susceptible to transient transfection. Furthermore, the cell populations are very comparable between different experiments.

The commonly used HEK293 cells were derived from human embryonic kidney[1,223] and have been used extensively to study pathological mechanisms of PD[1,224-228]. However, a drawback of HEK293 cells is the lack of a neuronal phenotype.

Another group of established cell lines with neuronal background has been derived from brain tumors. SH-SY5Y cells, for example, have been derived from human neuroblastoma cells and are commonly used to investigate neurodegenerative mechanisms[1] including the overexpression of αSyn[1,229] and transmembrane seeding of αSyn aggregation[230]. However, SH-SY5Y cells are hard to differentiate into a postmitotic mature dopaminergic state[1]. NT2 and hNT are human cell lines that have been derived from embryonic teratocarcinomas and can be differentiated to a postmitotic neuronal phenotype[231,232]. H4 cells, derived from human neuroglioma represent another commonly used cell line for the investigation of αSyn oligomerization and related toxicity[210,233,234]. Based on H4 cells, Outeiro *et al.* established a cell line which stably overexpresses variants of αSyn[213]. A drawback of all of these tumor-derived cell lines is that they show only a moderate neuronal phenotype[1].

Since brain cells physiologically show very low proliferation rates, they are naturally more difficult to cultivate than established cell lines. This problem can be overcome by Lund human mesencephalic (LUHMES) cells. This cell line was derived from 8-week-old human fetal ventral mesencephalic cells and immortalized by tetracycline-regulated expression of *v-myc* using the LINX*v-myc* retroviral vector[235]. In the absence of tetracycline, expression of *v-myc* from a minimal human cytomegalovirus (CMV) promoter is enhanced by a tetracycline transactivator resulting in continuous proliferation. Upon addition of tetracycline, the tetracycline transactivator is inactivated and expression of *v-myc* is turned off. Additional incubation with glial cell line-derived neurotrophic factor (GDNF) and cyclic adenosine monophosphate (cAMP) induces differentiation to a neuronal phenotype within five days[236]. Once differentiated, LUHMES cells show features of dopaminergic neurons: They release dopamine and show neuronal electric properties[237,238]. LUHMES cells have been used to study dopamine-related cell death mechanisms[236,238,239] but also other features of neurodegeneration[239,240] and seem to become more and more popular in PD research. Moreover, the cultivation of LUHMES cells does

not require addition of components obtained from animals (like fetal bovine serum, FBS). Thus, using LUHMES cells is in line with the development of alternative systems to reduce the amount of sacrificed animals in science. Unfortunately, transient transfection is very inefficient in LUHMES cells. Thus, for efficient transfection a lentiviral approach is necessary[1].

So far, formation, modulation, and toxicity of αSyn oligomers have mainly been studied in two kinds of cell models: First, cell models in which the overexpression of αSyn is induced by transient transfection[241] or viral transduction[242]. Second, cell models in which the gene coding for αSyn is stably inserted and constitutively overexpressed[243]. Both strategies hold several drawbacks: (1) When using transient transfection or viral transduction, the fraction of transgene expressing cells and the strength of overexpression are subject to great inter-experimental variation. Moreover, individual experiments are rather time-consuming and expensive. Additionally, the initiation of expression cannot be defined accurately, and for several cells (such as primary cells and LUHMES cells) transient transfection is very inefficient. (2) Constitutive overexpression of αSyn enables the investigation of αSyn oligomers only in steady state but not the investigation of *de novo* oligomer formation. This hinders the identification of compounds which prevent αSyn aggregation but are not capable of degrading preformed αSyn aggregates. Moreover, the constitutive overexpression of αSyn and the resulting αSyn-mediated toxicity may result in selection for cells that are resistant to αSyn-mediated toxicity. This might interfere with the investigation of potential toxic effects. For these reasons, a system for the fast and easy creation of stable and inducible αSyn overexpression that is applicable to a variety of cell lines to investigate αSyn-mediated effects in different synucleinopathies would be desirable.

2.6   Aim of this Study and Project Strategy

The aim of this study was to develop a system for the fast and easy creation of cell lines which inducibly overexpress variants of αSyn upon incubation with certain chemical agonists that can be applied to a variety of established and primary cell lines for the investigation of aggregation, modulation, and toxicity of αSyn oligomers with regard to PD and other synucleinopathies.

We decided to overexpress different kinds of αSyn constructs based on untagged human wildtype αSyn-140 which is the most abundant splice-variant of αSyn in humans (Figure 2-3 A). Since this variant can only be visualized indirectly, we also used a construct where αSyn-140 is coupled to the fluorescence protein Venus for direct visualization (Figure 2-3 B). Venus is a YFP-variant and holds the advantage over GFP[244-248] that it shows improved maturation (especially at 37°C) and brightness, and is less sensitive towards environmental influences[249,250]. Since

fluorescence tags might interfere with the protein function, results obtained with this kind of construct have to be controlled carefully. Moreover, we used a bimolecular fluorescence complementation (BiFC) system in order to study the aggregation of αSyn (Figure 2-3 C). BiFC assays have widely been used to study protein-protein interactions[251] and have been established for studying αSyn interaction by Outeiro *et al.*[213]. In short, the protein of interest (here: αSyn) is coupled to the N-terminal or C-terminal part of a fluorescence protein (here: Venus), respectively. Each construct alone does not show any fluorescence signal. Upon interaction of two suited αSyn proteins the N-terminal and C-terminal part of Venus are brought into close proximity. This results in complementation of these fragments and a fluorescence signal can be detected. Thus, the BiFC assay enables the detection of αSyn oligomers without background signals from monomeric αSyn. Moreover, if we assume that the complementation of N- and C-terminal Venus is a statistic event, the fluorescence intensity should be directly proportional to the extent of aggregation. This allows a fast and easy readout for high-throughput screening assays for anti-aggregative compounds. On the other hand, it has been described that the complementation of fluorescence proteins might stabilize pre-existing protein-protein interactions[213]. Moreover, the signal-to-noise ratio is a common problem in BiFC systems which is difficult to control for[251]. Additionally, we planned to establish cell lines that overexpress Venus alone as a control. To be able to estimate the fraction of transduced cells we also established cell lines which inducibly overexpress untagged αSyn and constitutively overexpress mCherry-NLS, a fluorescence protein which is coupled to a nucleotide localization sequence. In this case, all cells that took up the αSyn construct will show a fluorescence signal with an emission maximum of 610 nm in the nucleus[248].

Inducible expression in cell lines is often achieved using Tet-On or Tet-Off systems[252,253]. Since differentiation of LUHMES cells is mediated by a Tet-Off system, we decided to apply induction systems which act independently of tetracycline and followed two different strategies:

First, we used a modified GAL4-UAS system[254], GAL4_EcR-UAS (GE), which has been established in zebrafish by Esengil *et al.*[255] and has been optimized for cell culture application by Peer-Hendrik Kuhn (unpublished) (Figure 2-3 D-E). In this system, the DNA-binding and homodimerization regions of GAL4 (a yeast transcription factor) have been coupled to the activation domain of the herpes simplex virus regulatory protein VP16 and the ligand binding domain of the insect-specific ecdysone receptor from *Bombyx mori* (GAL4_EcR). There are no known vertebrate orthologues of EcR, and EcR agonists have no known effect in vertebrates[255-258]. The GAL4_EcR protein is constitutively expressed from a human ubiquitin-C promoter (Ubi), while the gene of interest (GOI) is located downstream of an upstream activation sequence (UAS) and requires binding of GAL4 to the UAS in order to be transcribed from a minimal E1b

promoter. In the absence of an ecdysone agonist, binding of GAL4_EcR to the upstream activation sequence (UAS) is prevented by unclear mechanisms[255]. Thus, transcription of the GOI does not take place (Figure 2-3 D). The interaction of an ecdysone agonist, such as tebufenozide, with the EcR induces binding of GAL4_EcR to the UAS. As a consequence, transcription of the GOI is induced, resulting in its expression and production of the protein of interest (POI) (Figure 2-3 E).

Second, we also established viruses for inducible expression using the Cre_ER[T2]-loxP (CE[T2]) system[259-261]. Here, Cre recombinase is coupled to the modified estrogen receptor ER[T2], which shows higher affinity for 4-OH-tamoxifen over estrogen compared to wildtype (wt) ER[260]. The Cre_ER[T2] protein is constitutively expressed from a human ubiquitin-C promoter. The GOI is located downstream of a constitutively active human phosphoglycerol kinase (hPGK) promoter and a floxed puromycin resistence gene (i.e., it is flanked by two loxP sites). In the absence of tamoxifen, Cre cannot interact with the loxP sites. Thus, translation of the mRNA stops at the termination codon in puromycin and the GOI is not expressed (Figure 2-3 F). Upon binding of 4-OH-tamoxifen to ER[T2], Cre will interact with the loxP sites and excise the floxed puromycin gene, leading to expression of the GOI (Figure 2-3 G).

In order to insert the required machineries for inducible expression we used lentiviruses. It has been shown that expression rates are more stable when using lentiviruses compared to transient transfection and antibiotic selection[262]. The transduction of cells with lentivirus particles leads to the stable insertion of the expression constructs into the host genome. To insert all components of the induction system into the host genome the cells have to be transduced with two different kinds of viruses: a driver virus carrying the GAL4_EcR system (GAL4 driver) or the Cre_ER[T2] system (Cre driver) and a corresponding receiver virus carrying the UAS-GOI system (UAS-GOI receiver) or the loxP-GOI system (loxP-GOI receiver).

For the BiFC system, an equimolar expression rate of the two hemi-Venus constructs (V1S and SV2) would be desirable. Expressing two GOIs from one promoter via an IRES sequence holds the disadvantage that expression of the GOI downstream of the IRES is usually lower than expression of the GOI upstream of the IRES sequence[263]. To overcome this problem, we decided to couple the hemi-Venus constructs by a "self-cleaving" P2A sequence derived from porcine teschovirus-1. Several 2A sequences have been described of which the P2A sequence showed the highest "cleavage" efficiency in a variety of model system[264-266]. Separation of transgenes coupled via 2A sequences occurs on the level of translation due to ribosomal skipping of a peptide bond[267]. In contrast to IRES sequences, 2A sequences are shorter and show stoichiometric expression of multiple proteins[264].

In summary, we here present a valuable system for the fast and easy creation of cell lines with inducible αSyn overexpression relying on the CE^{T2} system or the GE system. The system applies a strategy based on lentiviral transduction to stably integrate the expression machinery of both systems into the host genome. Overexpression of αSyn only occurs upon incubation with a certain agonist (4-OH-tamoxifen or tebufenozide).

The system was first established in H4 cells, a human neuroglioma cell line which has become a well-established model in research for neurodegenerative diseases. H4 cells are very robust and quite easy and cheap in handling, making them a valuable model to establish the above described expression systems and for high-throughput screening assays. Since the H4 cell lines relying on the GE system (H4_GE cells) showed higher transgene induction than the H4 cell lines relying on the CE^{T2} system (H4_CE^{T2} cells), the H4_GE cells were further characterized and the GE system was applied for the creation of additional cell lines.

We show a detailed analysis of the expression characteristics of the tebufenozide-dependent transgene expression in H4_GE cells. Using the H4_GE cell model we found that incubation with DMSO and ferric iron led to a stronger increase in fluorescence intensity in a bimolecular fluorescence complementation (BiFC) model for αSyn aggregation compared to other tri-, bi-, and monovalent metal ions. Additionally, incubation with DMSO and $FeCl_3$ increased αSyn protein load in all tested αSyn overexpressing H4_GE cells and led to the detection of higher molecular αSyn species after sucrose gradient centrifugation. Taken together, these results suggest that incubation with DMSO and $FeCl_3$ increased aggregation of αSyn in the H4_GE cell model. Furthermore, the strategy for the creation of stable inducible cell lines was not limited to H4 cells but was also succesfully applied to LUHMES cells.
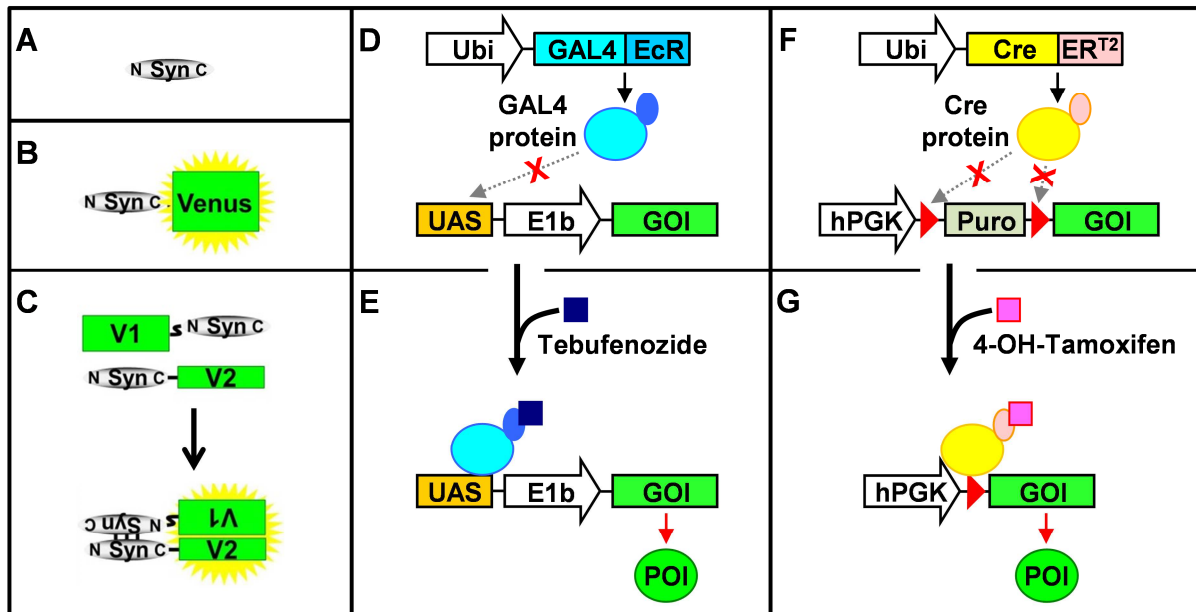
Figure 2-3: Overview of αSyn constructs and induction systems

Cell models were generated for the inducible overexpression of different αSyn constructs:

A) Unmodified human αSyn.

B) αSyn coupled to the fluorescent protein Venus.

C) αSyn coupled to the N-terminal part of Venus (V1; 1-157) or the C-terminal part of Venus (V2; 158-240) for a BiFC assay.

Inducible overexpression using the GAL4_EcR-UAS (GE) system:

D) No expression of the GOI in the absence of tebufenozide since binding of GAL4 to the UAS is inhibited.

E) Expression of the GOI is induced upon interaction of tebufenozide with EcR resulting in binding of GAL4 to the UAS.

Inducible overexpression using the Cre_ER^{T2}-loxP (CE^{T2}) system:

F) No expression of the GOI in the absence of 4-OH-tamoxifen since binding of Cre recombinase to the loxP sites is inhibited and translation is terminated at the stop-codon of puro.

G) Expression of the GOI is induced upon interaction of 4-OH-tamoxifen with ER^{T2} resulting in excision of the floxed puro gene by Cre recombinase.

Syn: αSyn; V1: N-terminal Venus fragment; V2: C-terminal Venus fragment; Ubi: human ubiquitin-C promoter; EcR: ecdysone receptor; UAS: upstream activation sequence; E1b: minimal E1b-promoter; GOI: gene of interest; POI: protein of interest; Cre: Cre recombinase; ER^{T2}: estrogen receptor, optimized for tamoxifen over estrogen; hPGK: human phosphoglycerol kinase promoter; Puro: puromycin resistance gene; red triangle: loxP site

3   Materials and Methods

3.1   Creation and Transformation of XL2-Blue Competent *E. coli*

In order to obtain competent cells for transformation, 10 ml of antibiotic-free LB medium (5 g/l yeast extract (Carl Roth, 2363.1), 10 g/l tryptone/peptone (Carl Roth, 8952.3), 10 g/l NaCl (Carl Roth, 3957.1)) were inoculated with 2 µl of XL2-Blue competent cells (kind gift from Klaus Förstemann) and incubated in a shaker at 37°C and 225 rpm overnight. 1 ml of the overnight culture was then added to 100 ml LB medium and incubated in a shaker at 37°C and 130 rpm until it reached an optical density (OD_{600}) of 0.7-0.8. Optical density was measured using a photometer (Eppendorf AG, Hamburg). Afterwards the culture was cooled on ice and transferred to two 50-ml Falcons and centrifuged at 4°C and 3220 relative centrifugal force (rcf) for 15 min (5810 R, Eppendorf, Hamburg). The supernatant was discarded and the pellet was resuspended in 25 ml of freshly diluted precooled and sterile filtered 0.1 M $CaCl_2$ solution and incubated on ice for 30 min. Afterwards the cells were centrifuged for 15 min at 3,320 rcf and 4°C. The supernatant was discarded and the pellet was resuspended in 2.5 ml of precooled 0.1 M $CaCl_2$ solution supplemented with 10% glycerol. The competent cells were then frozen in liquid nitrogen in 100 µl aliquots and stored at -80°C.

For transformation cells were thawed on ice before 1 to 100 ng of plasmid (but not more than 10 µl total volume) was added. Cells were incubated on ice for 30 min and afterwards heat-shocked for 1 minute at 42°C without shaking in a thermomixer (Eppendorf, 5355000.011). After incubating the cells on ice for 3 min, 900 µl of antibiotic-free LB medium was added and the mixture was incubated at 37°C and 225 rpm for 1 h in a shaker (CERTOMAT IS, Braun). 10 to 200 µl were plated on LB-Amp plates (100 µg/ml ampicillin (Carl Roth, K029.2)), LB-Kan plates (100 µg/ml kanamycin (Carl Roth, T832.1)), or LB-Spec plates (100 µg/ml spectinomycin (Sigma, S4014), respectively.

3.2   Plasmid Cloning

Plasmids were expanded in XL2-Blue cells and extracted using the NucleoSpin Plasmid Mini kit (Macherey-Nagel, 740588.250). Glycerol stocks of transformed XL2-Blue cells were generated by mixing 600 µl of cell suspension with 200 µl glycerol (AppliChem, A1123.1000).

The plasmids and primers used in this work are summarized in Table 3-1 and Table 3-2, respectively.

The constructs αSyn (S), Venus$_{\text{N-terminal fragment}}$ (V1), V1-αSyn (V1S), αSyn-Venus$_{\text{C-terminal fragment}}$ (SV2), SV2-P2A-sequence-V1S (SV2-P2A-V1S), SV2-P2A-sequence-V1 (SV2-P2A-V1), αSyn-Venus$_{\text{full-length}}$ (SV), and Venus (V) (see Figure 2-3 A, B, C) were amplified from plasmids #1-#4 (see also Figure 8-1, kind gift from Pamela McLean) using polymerase chain reaction (PCR) and primers that carry a suitable restriction site. Plasmids #1-#4 were sequenced using primers MB1 and MB2. The different constructs were amplified according to Table 3-3.

Following PCR amplification, amplificates were separated via agarose gel electrophoresis and purified using the NucleoSpin® Gel and PCR Clean-up kit (Macherey-Nagel, 740609.250). For ligation into the desired plasmids, constructs were cut with the corresponding restriction enzymes. In order to insert the construct SV2-P2A-V1S, the construct SV2-P2A-V1 was cut with the restriction enzymes HindIII and ClaI and the construct P2A-V1S was cut with the restriction enzymes ClaI and NotI. Both restricted constructs were ligated simultaneously into the desired plasmid. For transient transfection and constitutive expression, constructs were cloned between the HindIII and NotI site of the P12-HA-TGFa-FLAG-plasmid (Table 3-1, kind gift from Peer-Hendrik Kuhn and Stefan Lichtenthaler).

For the creation of lentiviral expression plasmids, αSyn constructs were first inserted between the HindIII and NotI site of the entry vector pCR8/GW/TOPO+pCS2-MCS (Figure 8-2 A, kind gift from Peer-Hendrik Kuhn and Stefan Lichtenthaler) and later on transferred to the destination vectors using the Gateway® Technology (Table 3-4, see also chapter 3.3). Destination vectors F2P-Delta Zeo-LoxP-Ko.Puro-LoxP-STNST-GW(DEST) (db 636, Figure 8-2 B), F2-Delta Zeo-Kozak-Puro-5XUAS-E1b-(GW)Dest (db 597, Figure 8-2 C), F2-Delta Zeo-Kozak-Hygro-5XUAS-E1b-(GW)Dest (db #44, Figure 8-2 D), and F2-Delta Zeo-Kozak-Zeo-5XUAS-E1b-(GW)Dest (db #45, Figure 8-2 E) were kindly provided by Stefan Lichtenthaler and Peer-Hendrik Kuhn. Destination vector F-Delta Zeo-Kozak-mCherry-NLS-5X UAS-E1b-(GW)Dest (db #92, Figure 8-2 F) was created by amplifying mCherry-NLS from template plasmid #87 (addgene, plasmid #39319) using primers 42MB_SalI-mCherry_f and 43MB_NsiI_mCherry_r and subcloning between the XhoI and NsiI restriction sites of plasmid #45.

Point mutations I152L in V1 and L201V in V2 were inserted using Pfu Turbo Cx hotstart DNA Polymerase (Agilent Technologies, 600412) in template plasmid #21 with primers MB31_V1_I152L_f and MB32_V1_I152L_r and in template plasmid #20 using primers MB33_V2_L201V_f and MB34_V2_L201V_r, respectively. After PCR, template plasmids were DpnI-digested for 1 h at 37°C followed by inactivation for 10 minutes at 80°C resulting in plasmids #63 and #53, respectively.

To create plasmid #71, $V1S_{I152L}$ was amplified from template plasmid #63 using primers MB24_V1_HindIIIf and MB6_V1S_Not1_r. For plasmid #73, $V1_{I152L}$+Spacer was amplified from template plasmid #63 using primers MB24_V1_HindIIIf and MB39_V1+Sp_Not1_r. For plasmid #75, $SV2_{L201V}$ was amplified from template plasmid #53 using primers MB3_SV2_Hind3_f and MB25_V2_NotI_r. All constructs were then subcloned between the HindIII and NotI restriction sites of plasmid #14.

The inserts of all newly created plasmids were sequenced (Eurofins Scientific, Luxemburg). For sequencing of inserts in plasmids with P12-HA-TGFa-FLAG backbone we used Eurofins standard primer T7 (5'-TAATACGACTCACTATAGGG-3'). For sequencing of inserts in plasmids with pCR8/GW/TOPO+pCS2-MCS backbone we used primer MB37_pCR8_r or Eurofins standard primer M13 uni (-21) (5'-TGTAAAACGACGGCCAGT-3'). For sequencing of inserts in plasmids with F2-Delta Zeo-Kozak-Puro-5XUAS-E1b-(GW)Dest (597) backbone we used primers MB26_691_fw and MB28_636+691_r. For sequencing of inserts in plasmids with F2P-Delta Zeo-LoxP-Ko.Puro-LoxP-STNST-GW(DEST) (636) backbone we used primers MB27_636_fw and MB28_636+691_r.

3.3 Gateway® Reaction

In order to transfer the generated constructs into different expression plasmids we used the Gateway® Technology[268]. This technology utilizes the site-specific recombination provided by bacteriophage lambda[269]. Here, the gene of interest (GOI) is cloned between optimized attachment (*att*) sites *att*L1 and *att*L2 of the *entry clone* which serve as binding sites for recombination proteins. The *destination vector* carries a control of cell death B *(ccd*B) gene flanked by an *att*R1 and *att*R2 site. In the LR reaction, the recombination of the *entry clone* and the *destination vector* results in the creation of an *expression clone* which carries the GOI between two attB sites, and a by-product carrying ccdB between attP sites. *Ccd*B is a bacterial toxin that targets the GyrA subunit of DNA gyrase[270,271] and thus inhibits proliferation of most *E. coli* strains by preventing cleavage of double-stranded DNA. This results in a negative selection for bacteria that take up *ccdB*-containing vectors like unreacted *destination vector* or LR reaction by-product.

Table 3-1: List of plasmids

This table summarizes information on plasmids that have been used in this study. #DB: Database number.

#DB	Insert	Backbone
#1	V1S	pCS2
#2	SV2	pCS2
#3	SV	pCS2
#4	Venus	pCS2
#11	SV2-P2A-V1S	P12-HA-TGFa-FLAG
#12	SV2-P2A-V1	P12-HA-TGFa-FLAG
#13	SV	P12-HA-TGFa-FLAG
#14	αSyn	P12-HA-TGFa-FLAG
#15	Venus	P12-HA-TGFa-FLAG
#20	SV2	pCR8/GW/TOPO+pCS2-MCS
#21	V1S	pCR8/GW/TOPO+pCS2-MCS
#22	V1	pCR8/GW/TOPO+pCS2-MCS
#23	SV	pCR8/GW/TOPO+pCS2-MCS
#24	αSyn	pCR8/GW/TOPO+pCS2-MCS
#25	Venus	pCR8/GW/TOPO+pCS2-MCS
#32	SV2	F2P-Delta Zeo-LoxP-Ko.Puro-LoxP-STNST-GW(DEST) (636)
#33	V1S	F2P-Delta Zeo-LoxP-Ko.Puro-LoxP-STNST-GW(DEST) (636)
#34	V1	F2P-Delta Zeo-LoxP-Ko.Puro-LoxP-STNST-GW(DEST) (636)
#35	SV	F2P-Delta Zeo-LoxP-Ko.Puro-LoxP-STNST-GW(DEST) (636)
#36	αSyn	F2P-Delta Zeo-LoxP-Ko.Puro-LoxP-STNST-GW(DEST) (636)
#37	Venus	F2P-Delta Zeo-LoxP-Ko.Puro-LoxP-STNST-GW(DEST) (636)
#38	SV2	F2-Delta Zeo-Kozak-Puro-5XUAS-E1b-(GW)Dest (597)
#39	V1S	F2-Delta Zeo-Kozak-Puro-5XUAS-E1b-(GW)Dest (597)
#40	V1	F2-Delta Zeo-Kozak-Puro-5XUAS-E1b-(GW)Dest (597)
#41	SV	F2-Delta Zeo-Kozak-Puro-5XUAS-E1b-(GW)Dest (597)
#42	αSyn	F2-Delta Zeo-Kozak-Puro-5XUAS-E1b-(GW)Dest (597)
#43	Venus	F2-Delta Zeo-Kozak-Puro-5XUAS-E1b-(GW)Dest (597)
#44	ccdB	F2-Delta Zeo-Kozak-Hygro-5XUAS-E1b-(GW)Dest
#45	ccdB	F2-Delta Zeo-Kozak-Zeo-5XUAS-E1b-(GW)Dest
#46	SV2 in 44	F2-Delta Zeo-Kozak-Hygro-5XUAS-E1b-(GW)Dest
#47	Venus in 44	F2-Delta Zeo-Kozak-Hygro-5XUAS-E1b-(GW)Dest
#48	SV2 in 45	F2-Delta Zeo-Kozak-Zeo-5XUAS-E1b-(GW)Dest
#49	Venus in 45	F2-Delta Zeo-Kozak-Zeo-5XUAS-E1b-(GW)Dest
#53	L201V in MB20	pCR8/GW/TOPO+pCS2-MCS
#63	I152L in V1S	pCR8/GW/TOPO+pCS2-MCS

Table 3-1: List of plasmids (continued)

#DB	Insert	Backbone
#71	V1S	P12-HA-TGFa-FLAG
#73	V1+Spacer	P12-HA-TGFa-FLAG
#75	SV2	P12-HA-TGFa-FLAG
#87	mCherry-NLS	pmCherry-C1
#88	V1_I152L+Spacer	P12-HA-TGFa-FLAG
#90	SV2_L201V	P12-HA-TGFa-FLAG
#91	V1S_I152L	P12-HA-TGFa-FLAG
#92	ccdB	F-Delta Zeo-Kozak-mCherry-NLS-5X UAS-E1b-(GW)Dest
#97	psPAX2	
#98	VSV-G	pcDNA3.1
#99	Zeo-GAL4-VP16	FUGW
#100	Zeo-GAL4-VP16-EcR	FUGW
#101	F2U-Delta Zeo-iCre	FUGW
#102	F2U-Delta Zeo-iCre_ER^{T2}	FUGW
#120	S	F-Delta Zeo-Kozak-mCherry-NLS-5X UAS-E1b-(GW)Dest
597	ccdB	F2-Delta Zeo-Kozak-Puro-5XUAS-E1b-(GW)Dest
636	ccdB	F2P-Delta Zeo-LoxP-Ko.Puro-LoxP-STNST-GW(DEST) (636)
---	Empty	pCR8/GW/TOPO+pCS2-MCS

For the LR reaction, 75 ng of the *entry clone* and 0.5 µl of the *destination vector* (150 ng/µl) were incubated in a 1.5-ml microcentrifuge tube. TE buffer, pH 8.0, was added to a total volume of 4 µl. Afterwards the LR Clonase™ II enzyme mix (Invitrogen, 11791-020) was thawed on ice, briefly vortexed and spun down. 1 µl of LR Clonase™ II enzyme mix was added to the reaction followed by vortexing briefly and short centrifugation. The reaction mixture was incubated at 25°C for 1 h before 1 µl of Proteinase K solution was added to stop the reaction. Afterwards the samples were incubated for 10 min at 37°C. XL2-Blue competent cells were transformed with 2 µl of the LR reaction mixture, plated on LB plates containing 100 µg/ml ampicillin (Carl Roth, K029.2), and incubated at 37°C overnight. A summary of entry clones, destination vectors (Figure 8-3 A-D), and resulting plasmids is shown in Table 3-4.

Table 3-2: List of primers

This table summarizes information on primers that have been used for molecular cloning or sequencing reactions in this study.

Primer Name	Sequence (5'-3')
MB1_BGH_r	TAGAAGGCACAGTCGAGG
MB2_SV40_polyA_r	GAAATTTGTGATGCTATTGC
MB3_SV2_Hind3_f	GATCAAGCTTGCCACCATGGATGTATTCATGAAAGG
MB4_SV2_P2A_r	CACGTCTCCAGCCTGCTTCAGCAGGCTGAAGTTAGTAGCTCCGCTTCCCTTGTA CAGCTCGTCCATGC
MB5_V1S_P2A_f	GCTGAAGCAGGCTGGAGACGTGGAGGAGAACCCTGGACCTATGGTGAGCAA GGGCGAGGAGC
MB6_V1S_Not1_r	GATCGCGGCCGCTTAGGCTTCAGGTTCGTAG
MB7_Ven1_Not1_r	GATCGCGGCCGCCTACTTGTCGGCGGTGATATAGACG
MB8_SV_Hind3_f	GCGCAAGCTTGCCACCATGGATGTATTCATGAAAGG
MB9_SV_PspOMI_r	GATCGGGCCCTCTACAAATGTGGTATGGCTG
MB10_V_Hind3_f	GATAAAGCTTGCCACCATGGTGAGCAAGGGCGAGG
MB11_Syn_Not1_r	GATCGCGGCCGCCTAGGCTTCAGGTTCGTAGTCTTG
MB24_V1_HindIIIf	GATCAAGCTTGCCACCATGGTGAGCAAGGGCGAGGAGC
MB25_V2_NotI_r	GATCGCGGCCGCTTACTTGTACAGCTCG
MB26_691_fw	CGACTCTAGAGGGTATATAATGG
MB27_636_fw	AGCCCGGTGCCTGAATGCATTAGATAACTTCG
MB28_636+691_r	GGAGCAACATAGTTAAGAATACC
MB31_V1_I152L_f	CCACAACGTCTATCTCACCGCCG
MB32_V1_I152L_r	CGGCGGTGAGATAGACGTTGTGG
MB33_V2_L201V_f	CGACAACCACTACGTGAGCTACC
MB34_V2_L201V_r	GGTAGCTCACGTAGTGGTTGTCG
MB37_pCR8_r	CAGGAAACAGCTATGACC
MB39_V1+Sp_Not1_r	GATCGCGGCCGCCTACTTAAGGGACCCACCACC
42MB_SalI_mCherry_f	GATCGTCGACGCCACCATGGTGAGC
43MB_NsiI_mCherry_r	GATCATGCATTTATCTAGATCCGGTGGATCC

Table 3-3: Overview of the amplification of the different constructs

This table summarizes information on the PCR amplification for the moleclular cloning of the different constructs for inducible overexpression.

Construct	Template	Forward Primer	Reverse Primer
αSyn	Plasmid #3	MB8_SV_Hind3_f	MB11_Syn_Not1_r
V1	Plasmid #1	MB24_V1_HindIIIf	MB7_Ven1_Not1_r
V1+Spacer	Plasmid #1	MB24_V1_HindIIIf	MB39_V1+Sp_Not1_r
V1S	Plasmid #1	MB24_V1_HindIIIf	MB6_V1S_Not1_r
SV2	Plasmid #2	MB3_SV2_Hind3_f	MB25_V2_NotI_r
SV2-P2A	Plasmid #2	MB3_SV2_Hind3_f	MB4_SV2_P2A_r
P2A-V1S	Plasmid #1	MB5_V1S_P2A_f	MB6_V1S_Not1_r
P2A-V1	Plasmid #1	MB5_V1S_P2A_f	MB7_Ven1_Not1_r
SV2-P2A-V1	SV2-P2A P2A-V1	MB3_SV2_Hind3_f	MB7_Ven1_Not1_r
SV	Plasmid #3	MB8_SV_Hind3_f	MB9_SV_PspOMI_r
V	Plasmid #3	MB10_V_Hind3_f	MB9_SV_PspOMI_r

3.4 Cell Maintenance

All cell lines were tested regularly for mycoplasma contamination using PCR Mycoplasma Test Kit I/C (PromoKine, PK-CA91-1096) and following the manufacturer's instructions.

3.4.1 HEK293T Cells

HEK293T cells (ATCC, CRL-3216, kind gift from Peer-Hendrik Kuhn) were maintained in T75 flasks (Hartenstein, ZF12) in normal growth medium consisting of DMEM (PAN, P04-03600) supplemented with 1% glutamine (PAN, P04-80100) and 10% fetal bovine serum (FBS; Pan, P30-3702) and grown at 37°C in a humidified 95% air/5% CO_2 atmosphere. Cells were passaged twice a week by washing with DPBS (PAN, P04-36500) once and subsequent enzymatic dissociation by incubation with 2 ml trypsin-EDTA (Sigma, T3924) for 2 min. Subsequently, 8 ml of normal growth medium were added and cells were aspirated and transferred to fresh culture vessels using a subcultivation ratio of 1:3 to 1:10.

Table 3-4: Overview of plasmids of the Gateway® reaction

This table summarizes information on plasmids used as *entry clone* and *destination vector* and the resulting *expression clone (viral plasmid)*. #DB: Database number.

Entry Clone			Destination Vector		Viral Plasmid
#DB	Backbone	Construct	#DB	Backbone	#DB
#20	pCR8/GW/TOPO+pCS2-MCS	SV2	636	F2P-Delta Zeo-LoxP-Ko.Puro-LoxP-STNST-GW(DEST)	#32
#21	pCR8/GW/TOPO+pCS2-MCS	V1S	636	F2P-Delta Zeo-LoxP-Ko.Puro-LoxP-STNST-GW(DEST)	#33
#23	pCR8/GW/TOPO+pCS2-MCS	SV	636	F2P-Delta Zeo-LoxP-Ko.Puro-LoxP-STNST-GW(DEST)	#35
#24	pCR8/GW/TOPO+pCS2-MCS	S	636	F2P-Delta Zeo-LoxP-Ko.Puro-LoxP-STNST-GW(DEST)	#36
#25	pCR8/GW/TOPO+pCS2-MCS	V	636	F2P-Delta Zeo-LoxP-Ko.Puro-LoxP-STNST-GW(DEST)	#37
#20	pCR8/GW/TOPO+pCS2-MCS	SV2	597	F2-Delta Zeo-Kozak-Puro-5XUAS-E1b-(GW)Dest	#38
#21	pCR8/GW/TOPO+pCS2-MCS	V1S	597	F2-Delta Zeo-Kozak-Puro-5XUAS-E1b-(GW)Dest	#39
#23	pCR8/GW/TOPO+pCS2-MCS	SV	597	F2-Delta Zeo-Kozak-Puro-5XUAS-E1b-(GW)Dest	#41
#24	pCR8/GW/TOPO+pCS2-MCS	S	597	F2-Delta Zeo-Kozak-Puro-5XUAS-E1b-(GW)Dest	#42
#25	pCR8/GW/TOPO+pCS2-MCS	V	597	F2-Delta Zeo-Kozak-Puro-5XUAS-E1b-(GW)Dest	#43
#20	pCR8/GW/TOPO+pCS2-MCS	SV2	#44	F2-Delta Zeo-Kozak-Hygro-5XUAS-E1b-(GW)Dest	#46
#25	pCR8/GW/TOPO+pCS2-MCS	V	#44	F2-Delta Zeo-Kozak-Hygro-5XUAS-E1b-(GW)Dest	#47
#20	pCR8/GW/TOPO+pCS2-MCS	SV2	#45	F2-Delta Zeo-Kozak-Zeo-5XUAS-E1b-(GW)Dest	#48
#25	pCR8/GW/TOPO+pCS2-MCS	V	#45	F2-Delta Zeo-Kozak-Zeo-5XUAS-E1b-(GW)Dest	#49
#24	pCR8/GW/TOPO+pCS2-MCS	S	#92	F-Delta Zeo-Kozak-mCherry-NLS-5X UAS-E1b-(GW)Dest	#120

For long-term storage cells were enzymatically dissociated as described above upon reaching 80% confluency. After addition of normal growth medium cells were transferred to 15-ml or 50-ml centrifuge tubes (Hartenstein, ZR97 or ZR82, respectively) and centrifuged at 180 rcf for 8 min. Medium was discarded and cells were resuspended in cryoprotectant medium consisting of 90% normal growth medium and 10% DMSO (Sigma, D2438), transferred to cryogenic vials and frozen in a Mr. Frosty Freezing Container (Thermo Scientific, 5100-0001) at -80°C overnight. Afterwards, the vials were stored at about -140°C in the gas phase of a liquid nitrogen cell tank.

3.4.2   H4 Cells

H4 human neuroglioma cells (ATCC, HTB-148) were maintained in T75 flasks (Hartenstein, ZF12) in normal growth medium consisting of Opti-MEM (Invitrogen, 31985-070) supplemented with 10% FBS (Pan, P30-3702) and grown at 37°C in a humidified 95% air/5% CO_2 atmosphere. Cells were passaged twice to three times a week by washing with DPBS (PAN, P04-36500) once and subsequent enzymatic dissociation by incubation with 2 ml trypsin-EDTA (Sigma, T3924) for 6 min. Subsequently, 8 ml of normal growth medium were added and cells were aspirated and transferred to fresh culture vessels using a subcultivation ratio of 1:3 to 1:10.

For long-term storage cells were enzymatically dissociated as described above upon reaching 80% confluency. After addition of normal growth medium cells were transferred to 15-ml or 50-ml centrifuge tubes (Hartenstein, ZR97 or ZR82, respectively) and centrifuged at 180 rcf for 8 min. Medium was discarded and cells were resuspended in cryoprotectant medium consisting of 95% normal growth medium supplemented with 5% DMSO (Sigma, D2438), transferred to cryogenic vials and frozen in a Mr. Frosty Freezing Container (Thermo Scientific, 5100-0001) at -80°C overnight. Afterwards the vials were stored at approximately -140°C in the gas phase of a liquid nitrogen cell tank.

3.4.3   LUHMES Cells

The Lund human mesencephalic (LUHMES) cell line is a subclone of the MESC2.10 cell line[272]. This cell line was derived from 8-week-old human fetal ventral mesencephalic cells and immortalized by tetracycline-regulated expression of *v-myc* using the LINX*v-myc* retroviral vector[235].

3.4.3.1 Maintenance

LUHMES cells (ATCC, CRL-2927) were maintained in precoated T75 flasks (Hartenstein, ZF12) in complete growth medium consisting of DMEM-F12 (Invitrogen, 31985-070) supplemented with 1% 100-fold N2 supplement (Invitrogen, 17502-048) and human basic fibroblast growth factor (bFGF; Invitrogen, 13256-029) and grown at 37°C in a humidified 95% air/5% CO_2 atmosphere.

Flasks were precoated with 7 ml of freshly diluted 50 µg/ml poly-L-ornithin (PLO; Sigma, P3655) overnight at room temperature. Afterwards PLO was removed and flasks were rinsed three times with sterile double distilled water and allowed to air-dry uncapped standing upright in a biological cabinet for 10 min. Subsequently, 5 ml of freshly diluted 1 µg/ml human fibronectin (Sigma, F0895) was added and flasks were incubated at 37°C. After 3 h, fibronectin solution was removed and discarded and flasks were rinsed three times with sterile double distilled water and allowed to air-dry uncapped standing upright in a biological cabinet for 10 min. Flasks were either used immediately afterwards or stored at 4°C for up to 5 days.

Cells were passaged every two to three days by washing with DPBS (PAN, P04-36500) once and subsequent enzymatic dissociation by incubation with 4 ml of 1x trypsin solution (2 ml 2x trypsin (137mM NaCl (Carl Roth, 3957.1), 5.4 mM KCl (Sigma, P5405), 6.9 mM $NaHCO_3$ (Sigma, S-5761), 5.6 mM D-Glucose (Carl Roth, HN06.3), 0.68 mM EDTA (Carl Roth, 8043.1), 0.5 g/l trypsin (Sigma, T7409)) and 2 ml DPBS (PAN, P04-36500)) for 3 min. Subsequently, 6 ml of wash medium (DMEM-F12 (Invitrogen, 31985-070) supplemented with 1% 100-fold N2 supplement (Invitrogen, 17502-048)) were added and cells were aspirated and transferred to 15-ml or 50-ml centrifuge tubes (Hartenstein, ZR97 or ZR82, respectively) and centrifuged at 180 rcf for 8 min. Medium was discarded and cells were resuspended in complete growth medium and transferred to fresh precoated culture vessels using a subcultivation ratio of 1:3 to 1:10.

For long-term storage cells were enzymatically dissociated as described above upon reaching 80% confluency. After centrifugation medium was discarded and cells were resuspended in cryoprotectant medium consisting of 70% complete growth medium, 20% FBS (Pan, P30-3702) and 10% DMSO (Sigma, D2438), transferred to cryogenic vials and frozen in Mr. Frosty Freezing Containers (Thermo Scientific, 5100-0001) at -80°C overnight. Afterwards, the vials were stored at approximately -140°C in the gas phase of a liquid nitrogen cell tank.

3.4.3.2 Differentiation

V-myc expression in LUHMES cells occurs from a minimal human cytomegalovirus (CMV) promoter under control of a tetracycline transactivator, resulting in continuous proliferation in the absence of tetracycline. Differentiation of LUHMES cells is induced by addition of tetracycline, glial cell line-derived neurotrophic factor (GDNF) and N^6,2'-O-Dibutyryladenosine 3',5'-cyclic monophosphate (db-cAMP)[272].

LUHMES cells were differentiated following the two-step protocol described in Scholz *et al.*[237]. Cells were enzymatically dissociated and centrifuged as described above and diluted to a concentration of 437,000 cells/ml in 8 ml of complete growth medium and transferred to a precoated T75 flask. 24 h later, complete growth medium was replaced with differentiation medium consisting of DMEM-F12 (Invitrogen, 31985-070) supplemented with 1 µg/ml tetracycline (Sigma-Aldrich, T7660), 2 ng/ml recombinant human GDNF (R&D Systems, 212-GD-010) and 1 mM db-cAMP (Sigma-Aldrich, D0627-250MG). 48 h later, cells were enzymatically dissociated by incubation with 4 ml of 2x trypsin solution for 4 min. Subsequently, 6 ml of wash medium were added and cells were aspirated and transferred to 15-ml or 50-ml centrifuge tubes and centrifuged at 180 rcf for 8 min. Medium was discarded and cells were resuspended in differentiation medium, diluted to a concentration of 350,000 cells/ml and transferred to fresh precoated culture vessels. Differentiation medium was replaced every two days.

Alternatively, LUHMES cells were differentiated following a one-step protocol. For this, LUHMES cells were immediately diluted in differentiation medium at a concentration of 300,000 cells/ml after enzymatic dissociation and centrifugation. Differentiation medium was replaced every two days without additional enzymatic dissociation.

3.5   Virus Production and Purification

To produce infectious but replication-incompetent virus particles two different packaging plasmids encoding for viral enzymes (db #97, Figure 8-3 E) and surface proteins (db #98, Figure 8-3 F), and expression plasmids were transiently transfected into HEK293T cells (see Table 3-5). The virus production protocol described here was provided by Peer-Hendrik Kuhn and has been slightly adapted.

To produce virus in one 10-cm dish, HEK293T cells were maintained in normal growth medium and expanded to approximately 1.5 T75 flasks. Cells were then washed once with DPBS and then

enzymaticly dissociated by incubation with 2 ml trypsin-EDTA (Sigma, T3924) for 2 min. Subsequently, 8 ml of normal growth medium were added and the cells were aspirated and transferred to 15-ml or 50-ml centrifuge tubes and centrifuged at 180 rcf for 8 min. Medium was discarded, cells were resuspended in room temperature Opti-MEM supplemented with 10% FBS, counted using a Neubauer counting chamber (VWR, 631-0926), and diluted to a final concentration of 600,000 cells/ml in a volume of 1.5 ml.

For each 10-cm dish a DNA mix and a Lipofectamine® 2000 mix was generated. The DNA mix consisted of 5 μg of psPAX2 (#97), 2.7 μg of VSV-G (#98) and 5.5 to 6.5 μg of the expression plasmid (Table 3-5) in 750 μl Opti-MEM. For the Lipofectamine® 2000 mix 750 μl Opti-MEM and 38 μl of Lipofectamine® 2000 (Invitrogen, 11668-019) were mixed and incubated for 5 min at room temperature. Afterwards the Lipofectamine® 2000 mix was mixed with the DNA mix and incubated for 15 min at room temperature before the cell mix was added.

Afterwards, 6 ml of Opti-MEM supplemented with 10% FBS were pipetted into a 10-cm dish (Hartenstein, GK03). 3 ml of the DNA Lipofectamine® 2000 cell mixture were added and incubated at 37°C in a humidified 95% air/5% CO_2 atmosphere. After 24 h the transfection mix was carefully replaced with 8.5 ml of normal growth medium. 24 h later, the virus-containing medium was carefully aspirated, pipetted into a 50-ml centrifuge tube and stored for 24 h at 4°C (1st harvest). The cells in the 10-cm dish were again incubated in normal growth medium for another 24 h at 37°C in a humidified 95% air/5% CO_2 atmosphere before viruses were harvested for a second time and pooled with the 1st harvest.

To get rid of cellular debris, the 50-ml tube was centrifuged at 3000 rcf for 15 min. Afterwards, the supernatant was filtered using a 0.45-μm filter (Carl Roth, KH55.1) to remove further cellular particles. Centrifuge polymer tubes (Beckman Coulter, 358126) were thoroughly washed with 70% ethanol in a biological cabinet. Ethanol was aspirated and tubes were allowed to air-dry for 20 min. Afterwards the virus supernatant was loaded into the tubes and centrifuged at 22,000 rpm in an SW28 rotor (Beckman Coulter, 342196) for 2 h at 4°C in an ultracentrifuge (Sorvall Discovery 90SE). The supernatant was discarded and the pellet was incubated in TBS-5 buffer (50 mM Tris-HCl (pH 7.8), 130 mM NaCl, 10 mM KCl, 5 mM $MgCl_2$, 10% BSA weight per volume (w/V)), sterile filtered through a 0.22-μm filter (Hartenstein, FI02)) overnight. The pellet was carefully resuspended without producing air bubbles, transferred to a 1.5-ml reaction tube (Hartenstein, RSL1), and centrifuged at 800 rcf for 2 min at 4°C. Supernatant was frozen in 20-μl aliquots in 0.5-ml reaction tubes (Hartenstein, RSL0) or PCR tubes (Eppendorf, 0030 124359) at -80°C.

Table 3-5: List of viruses

This table summarizes the plasmids used for production of infectious but replication-incompetent viruses. Co-transfection of HEK293T cells with viruses #97 and #98 and an expression plasmid resulted in production of viruses shown in the right column. #DB: Database number.

Plasmid #DB	Kind of Plasmid	Insert	Comment	Virus #DB
#97	Packaging	psPAX2	Encodes for viral enzymes gag-pol to generate lentiviruses	
#98	Packaging	VSV-G	Encodes for the envelope glycoprotein VSV-G from Vesicular Stomatitis Virus (broad tropism)	
#99	Expression	Zeo-GAL4-VP16	Constitutive GAL4 driver	V99
#100	Expression	Zeo-GAL4-VP16-EcR	Inducible GAL4_EcR driver (+tebufenozide)	V100
#101	Expression	F2U-Delta Zeo-iCre	Constitutive Cre driver	V101
#102	Expression	F2U-Delta Zeo-iCre_ER^{T2}	Inducible Cre_ER^{T2} driver (+4-OH-tamoxifen)	V102
#32	Expression	SV2	Cre-loxP receiver (puromycin resistance)	V32
#33	Expression	V1S	Cre-loxP receiver (puromycin resistance)	V33
#34	Expression	V1	Cre-loxP receiver (puromycin resistance)	V34
#35	Expression	SV	Cre-loxP receiver (puromycin resistance)	V35
#36	Expression	S	Cre-loxP receiver (puromycin resistance)	V36
#37	Expression	V	Cre-loxP receiver (puromycin resistance)	V37
#38	Expression	SV2	GAL4-UAS receiver (puromycin resistance)	V38
#39	Expression	V1S	GAL4-UAS receiver (puromycin resistance)	V39
#40	Expression	V1	GAL4-UAS receiver (puromycin resistance)	V40
#41	Expression	SV	GAL4-UAS receiver (puromycin resistance)	V41
#42	Expression	S	GAL4-UAS receiver (puromycin resistance)	V42
#43	Expression	V	GAL4-UAS receiver (puromycin resistance)	V43
#46	Expression	SV2	GAL4-UAS receiver (hygromycin resistance)	V46
#47	Expression	V	GAL4-UAS receiver (hygromycin resistance)	V47
#48	Expression	SV2	GAL4-UAS receiver (zeocin resistance)	V48
#49	Expression	V	GAL4-UAS receiver (zeocin resistance)	V49
#120	Expression	S	GAL4-UAS receiver (mCherry-NLS)	V120

3.6 Transient Transfection of H4 Cells

In order to transiently transfect H4 cells, cells were enzymatically dissociated as described above and seeded at a concentration of 100,000 cells/ml and incubated at 37°C, 5% CO_2 for 24 h before the transfection mix was added. Per 1 ml cell-containing medium the transfection mix consisted of 100 µl serum-free Opti-MEM, 0.5 µg plasmid and X-tremeGENE™ HP DNA Transfection Reagent (3 µl/µg$_{plasmid}$; Roche Diagnostics, 06366236001). The transfection mix was incubated for 15 to 30 min at room temperature before it was pipetted into the wells. The medium was mixed by rocking the plate gently. Afterwards, the cells were incubated at 37°C in a humidified 95% air/5% CO_2 atmosphere. 24 to 72 h after transfection cells were processed according to the following analysis.

3.7 Compound Testing Using Transiently Transfected H4 Cells

In order to test compounds using transiently transfected H4 cells, cells were seeded at a concentration of 100,000 cells/ml and incubated with different compounds at different concentrations at a final DMSO concentration of 0.1% or 1% DMSO as a control at 37°C in a humidified 95% air/5% CO_2 atmosphere. After 24 h, the medium was aspirated, cells were carefully washed once with DPBS and fresh normal growth medium was added. Afterwards, the cells were transiently transfected as described above and incubated at 37°C in a humidified 95% air/5% CO_2 atmosphere for 2 h. Then, medium was aspirated, cells were carefully washed once with DPBS and fresh normal growth medium containing the corresponding compound or DMSO as a control was added. 48 h after transfection, cells were processed according to the following analysis.

3.8 Creation of Stable Cell Lines

3.8.1 H4 Cells

3.8.1.1 Optimization of the H4 Transduction Protocol

In order to obtain as many transduced cells as possible we tested the transduction efficiency of viruses V99 and V41 (see Table 3-5) using different protocols. For all protocols H4 cells were handled as described in chapter 3.4.2.

Protocol A$_{H4}$:

Virus was diluted 1:200 in cell-containing medium. H4 cells were diluted to a concentration of 50,000 cells/ml. 2 ml of cell suspension was pipetted into one well of a 6-well plate and 10 μl of both V99 and V41 were added. The composition was mixed by rocking the plate gently.

Protocol B$_{H4}$:

Virus was diluted 1:50 in cell-containing medium. H4 cells were diluted to a concentration of 50,000 cells/ml. 2 ml of cell suspension were pipetted into one well of a 6-well plate and 40 μl of both V99 and V41 were added. The composition was mixed by rocking the plate gently.

Protocol C$_{H4}$:

Virus was diluted 1:12 in cell-containing medium. H4 cells were diluted to a concentration of 100,000 cells/ml. 200 μl of the cell suspension were mixed with 20 μl V99 and 20 μl V41 in a 0.5-ml reaction tube and incubated for 5 min at room temperature. Afterwards, the mixture was seeded into a 24-well plate.

Protocol D$_{H4}$:

Virus was diluted 1:3.5 in cell-containing medium. H4 cells were diluted to a concentration of 50,000 cells/ml. 50 μl of the cell suspension were mixed with 20 μl V41 in a 0.5-ml reaction tube and incubated for 5 min at room temperature. Afterwards the mixture was seeded into a 96-well plate. 72 h after transduction virus-containing medium was aspirated and replaced with normal growth medium. Cells were expanded to 6-well plates and then expanded to T75 flasks when they reached 80% confluency and maintained as described above. After two weeks, the obtained H4_41 cells were diluted to a concentration of 50,000 cells/ml. 50 μl of the cell suspension were mixed with 20 μl V99 in a 0.5-ml reaction tube and incubated for 5 min at room temperature. Afterwards the mixture was seeded into a 96-well plate and the cells were expanded as described in chapter 3.4.2.

For all protocols, cell nuclei were stained with 10 μg/ml DAPI (Carl Roth, 6335.2) or 0.5 μg/ml Hoechst33342 (Invitrogen, H1399) 72 h after transduction and pictures were taken using a fluorescence microscope (Hundt, Wetzlar or Olympus, Hamburg). The fraction of fluorescing

cells was determined manually using the *ImageJ* software. Alternatively, virus-containing medium was aspirated and replaced with normal growth medium. Cells were expanded to T25 flasks and then expanded to T75 flasks when they reached 80% confluency and maintained as described in chapter 3.4.2.

3.8.1.2 Creation of Stable Inducible H4 Cell Lines

H4 cells were diluted to a concentration of 50,000 cells/ml. In order to achieve inducible expression based on the GAL4_EcR-UAS (GE) system, 50 μl of the cell suspension were mixed with 20 μl of V39, V41, V42, V43, or V120 in a 0.5-ml reaction tube, respectively. In order to achieve inducible expression based on the Cre_ER^{T2}-loxP system, 50 μl of the cell suspension were mixed with 20 μl of V32, V35, V36, or V37 in a 0.5-ml reaction tube, respectively. The mixture was incubated for 5 min at room temperature. Afterwards, the mixture was seeded into a 96-well plate. 72 h after transduction, virus-containing medium was aspirated and replaced with normal growth medium. The created cell lines *H4_39*, *H4_41*, *H4_42*, *H4_43*, *H4_120, H4_32, H4_35, H4_36,* and *H4_37* were expanded and maintained as described in chapter 3.4.2.

All following viral transductions were performed according to the transduction protocol described above. The created cell lines *H4_39* and H4_32 were transduced with V46 or V33, respectively, resulting in cell lines *H4_39-46* and *H4_32-33*. The cell lines *H4_41*, *H4_42*, *H4_43*, *H4_120* and *H4_39-46* were transduced with V100, resulting in cell lines *H4_100-41*, *H4_100-42*, *H4_100-43*, *H4_100-120* and *H4_100-39-46.* The cell lines *H4_32-33, H4_35, H4_36,* and *H4_37* were transduced with V102, resulting in cell lines *H4_102-32-33, H4_102-35, H4_102-36,* and *H4_102-37. H4_100-42* was transduced with V42 a second time generating cell line *H4_100-42$_2$*. *H4_100-39-46* was transduced with V46, generating cell line *H4_100-39-46$_2$*, which was then transduced with V39, generating cell line *H4_100-39$_2$-46$_2$*. The later on commonly used cell lines were renamed according to Table 3-6.

Table 3-6: List of H4 cell lines

This table summarizes the inducible H4 cell lines created in this study.

Old Name	New Name
H4_100-41	H4_GE-SV
H4_100-42$_2$	H4_GE-S
H4_100-43	H4_GE-V
H4_100-120	H4_mC_GE-S
H4_100-39$_2$-46$_2$	H4_GE-V1S+SV2
H4_102-35	H4_CE^{T2}-SV
H4_102-36	H4_ CE^{T2}-S
H4_102-37	H4_ CE^{T2}-V
H4_100-32-33	H4_ CE^{T2}-V1S+SV2

3.8.2 LUHMES Cells

3.8.2.1 Optimization of the LUHMES Transduction Protocol

In order to obtain as many positively transduced LUHMES cells as possible we tested the transduction efficiency of viruses V99 and V43 (see Table 3-5) using different protocols. For all protocols LUHMES cells were handled as described in chapter 3.4.3.

Protocol A$_{LUHMES}$:

LUHMES cells were diluted to a concentration of 50,000 cells/ml. 2 ml of the cell suspension were transferred to one well of a 6-well plate. 20 μl of V43 were added. The composition was mixed by rocking the plate gently and incubated at 37°C in a humidified 95% air/5% CO_2 atmosphere. 24 h after transduction, medium was aspirated and replaced by 2 ml complete growth medium supplemented with 20 μl of V99. 24 h later, virus medium was discarded and the LUHMES cells were passaged into a T75 flask. 72 h later, cells were seeded into 6-well plates at a concentration of 50,000 cells/ml.

Protocol B$_{\text{LUHMES}}$:

LUHMES cells were diluted to a concentration of 500,000 cells/ml. 200 µl of the cell suspension were mixed with 20 µl V43 in a 0.5-ml reaction tube and incubated for 2 min at room temperature. The mixture was transferred to one well of a 6-well plate. 1.8 ml of complete growth medium were added and mixed with the cell-virus suspension by rocking the plate gently and incubated at 37°C, 5% CO_2. 48 h later, virus medium was discarded and the LUHMES cells were passaged into a T75 flask. Upon reaching a confluency of 80% the cells were transduced with V99 as described above.

Protocol C$_{\text{LUHMES}}$:

LUHMES cells were diluted to a concentration of 1,000,000 cells/ml. 100 µl of the cell suspension were mixed with 20 µl V43 in a 0.5-ml reaction tube and incubated for 5 min at room temperature. The mixture was transferred to one well of a 6-well plate. 1.9 ml of complete growth medium were added and mixed with the cell-virus suspension by rocking the plate gently and incubated at 37°C, 5% CO_2. 72 h later, virus medium was discarded and the LUHMES cells were passaged into a fresh 6-well plate. Upon reaching a confluency of 80% the cells were passaged into a T75 flask. Upon reaching a confluency of 80% the cells were transduced with V99 as described above. 72 h later, virus medium was discarded and the LUHMES cells were passaged into a T75 flask. Upon reaching a confluency of 80% the cells were seeded into 6 well plates at a concentration of 50,000 cells/ml.

For all protocols, cell nuclei were stained with Hoechst33342 (0.5 µg/ml; Invitrogen, H1399) 72 h later, and pictures were taken using a fluorescence microscope (Olympus, Hamburg). The fraction of fluorescing cells was determined manually using the *ImageJ* software.

3.8.2.2 Creation of Stable Inducible LUHMES Cell Lines

LUHMES cells were diluted to a concentration of 1,000,000 cells/ml. 100 µl of the cell suspension were mixed with 20 µl of V100 in a 0.5-ml reaction tube and incubated for 5 min at room temperature. The mixture was pipetted into one well of a 6-well plate. 1.9 ml of complete growth medium were added and mixed with the cell-virus suspension by rocking the plate gently and incubated at 37°C in a humidified 95% air/5% CO_2 atmosphere for 2 h.

Table 3-7: List of LUHMES cell lines

This table summarizes the inducible LUHMES cell lines created in this study.

Old Name	New Name
LUHMES_100$_4$-41$_4$	LUHMES_GE-SV
LUHMES_100$_4$-42$_4$	LUHMES_GE-S
LUHMES_100$_4$-43$_4$	LUHMES_GE-V
LUHMES_100$_4$-120$_4$	LUHMES_mC_GE-S
LUHMES_100$_4$-39$_4$-46$_4$	LUHMES_GE-V1S+SV2

72 h later, virus medium was discarded and the generated LUHMES_100 cells were passaged into a T75 flask. Cells were maintained until they reached a confluency of 80%. Transduction was repeated for three times.

Afterwards the generated *LUHMES_100$_4$* cells were transduced four times as described above with V39, V41, V42, V43, or V120, respectively. *LUHMES_100$_4$-39$_4$* cells were then transduced four times as described above with V46, generating cell line *LUHMES_100$_4$-39$_4$-46$_4$*. The generated cell lines were renamed according to Table 3-7.

3.9   Induction of Transgene Expression

Tebufenozide (Santa Cruz, sc-280110) was diluted in DMSO to a final concentration of 100 mM. Based on this solution, 1,000-fold stock solutions were made with concentrations ranging from 100 nM to 100 mM. To induce transgene expression, cells were incubated with 100 pM to 100 μM tebufenozide and a final DMSO concentration of 0.1%.

(z)-4-OH-tamoxifen (Abcam, ab141943) was diluted in DMSO to a final concentration of 100 mM. Based on this solution, 1,000-fold stock solutions were created with concentrations ranging from 100 nM to 100 mM. To induce transgene expression, cells were incubated with 100 pM to 100 μM 4-OH-tamoxifen and a final DMSO concentration of 0.1%.

3.10 BCA Assay

To determine the protein concentrations of the cell lysates for western blot, sucrose gradient, or fluorescence correlation spectroscopy we used a BCA assay. In this assay, the protein solution was incubated with a mixture of bicinchoninic acid and copper(II) sulfate ($CuSO_2$). In the presence of protein, Cu^{2+} is reduced to Cu^+ which is subsequently chelated by two molecules of bicinchoninic acid. This results in a green to purple color change which is proportional to the amount of protein over a broad range of protein concentrations and can be quantified by measuring absorbance at $\sim$560 nm[273].

In order to perform this assay, the cell lysates were diluted to an expected concentration of 0.2 to 1 mg/ml in 25 µl and transferred into the wells of a 96-well plate in quadruplicates. Bicinchoninic acid solution (BCA; Sigma, B9643) and $CuSO_2$ (Sigma, C2284) were mixed 50:1 and 200 µl of the BCA/$CuSO_2$ solution were pipetted to each well.

For the calibration curve, bovine serum albumin (BSA, 1 mg/ml) was diluted in lysis buffer to concentrations of 0.8 mg/ml, 0.6 mg/ml, 0.4 mg/ml, 0.2 mg/ml, and 0 mg/ml in duplicates in a 96-well plate with a final volume of 25 µl each.

The plate was then incubated at 37°C for 30 min. Subsequently, absorbance at 560 nm was analyzed using a FLUOStar OPTIMA Microplate Reader (BMG Labtech). Protein concentration was determined in reference to the fitted standard curve using the provided software (BMG Labtech).

3.11 Western Blot

3.11.1 Cell Lysis for Western Blot

Cells were maintained, enzymatically dissociated and centrifuged as described in chapter 3.4. Afterwards the cells were resuspended in 1 ml of precooled DPBS (4°C) and transferred to a 1.5-ml reaction tube. Cells were centrifuged at 4°C and 16,100 rcf for 10 min (Eppendorf centrifuge 5415 R). The supernatant was discarded and cell pellets were resuspended in 40-80 µl precooled (4°C) lysis buffer (25 mM Tris, 50 mM NaCl, 0.5% Na-deoxycholate, 0.5% Triton X-100, pH=8.0; prior to use, protease inhibitor (Roche Applied Science, 04693124001) was added) per 1,000,000 cells. Cells were incubated at 4°C and 1,000 rpm on a Thermomixer Comfort (Eppendorf, Hamburg) for 30 min and afterwards centrifuged at 4°C and 16,100 rcf for 10 min. Supernatant was transferred to a precooled 1.5-ml Protein LoBind reaction tube (VWR, 525-0133) and protein concentration was determined by BCA assay.

3.11.2 Preparation of the Polyacrylamide Gels

15% polyacrylamide separating gels were prepared by mixing 1.875 ml Lower Tris 4x (181.7 mg/ml Tris Base (Carl Roth, 4855.2), 0.4% sodium dodecyl sulfate (SDS, Carl Roth, CN30.3), pH 8.8), 1.8 ml H_2O, and 3.75 ml Rotiphorese® Gel 30 (Carl Roth, 3029.1). 6.25 µl tetramethylethylenediamine (TEMED) (Carl Roth, 2367.3) and 62.5 µl 10% ammonium persulfate (APS) (Carl Roth, 9592.2) were added and all components were mixed by inverting the 50-ml tube gently. The mixture was cast between clean glass plates for SDS-PAGE. To get rid of air bubbles, 400 µl of isopropanol were pipetted on top of the separating gel mixture. Subsequently, the gel was incubated for 15 min at room temperature to polymerize. Afterwards, isopropanol was discarded and the stacking gel was prepared by mixing 0.85 ml Upper Tris 4x (60.6 mg/ml Tris Base, 0.4% SDS, pH 6.6), 2.45 ml H_2O, and 462.5 µl Rotiphorese® Gel 30 in a 50-ml centrifugation tube. 3.75 µl TEMED and 37.5 µl 10% APS were added and all components were mixed by inverting the 50-ml tube gently. The mixture was cast on top of the separating gel and a gel comb was inserted carefully into the stacking gel without producing air bubbles to create 15 pockets. The gel was incubated at 4°C overnight to polymerize.

3.11.3   Sample Preparation

For western blot analysis cell lysates were diluted to a concentration of 2.08 mg/ml. 24 µl of the samples were mixed with 6 µl 5x Lämmli sample buffer (10% SDS (w/V), 250 mM Tris (pH 6.8), 1 mg/ml bromophenol blue, 0.5 M DTT, 50% glycerol (V/V)) and incubated at 95°C for 5-7 min. This results in a reduction of preformed disulfide bonds to thiols by DTT and the breakup of non-covalent interactions by SDS, thus destroying the proteins' secondary structure and enabling a separation according to molecular weight in the following electrophoresis. 30 µl of each sample and Lämmli buffer mixture were pipetted into separate pockets of the polyacrylamide gel, so that 50 µg of protein per mixture were used for PAGE. To determine the size of occurring western blot bands, 5 µl of PageRuler™ Prestained Protein Ladder (Thermo Fisher Scientific, 26616) were pipetted into one pocket of the polyacrylamide gel.

3.11.4   Electrophoresis

For electrophoresis the gel comb was removed and the gels including glass plates were inserted into a PAGE running chamber filled with 1x running buffer (3 mg/ml Tris Base, 14.4 mg/ml glycine (Carl Roth, 3790.3), 1 mg/ml SDS). After samples and ladder had been loaded to the gel, a voltage of 80 V was applied until samples reached the bottom of the stacking gel (approximately 30 min). Afterwards a voltage of 120 V was applied until the green marker (10 kDa) of the protein ladder reached the bottom of the separating gel (approximately 60 min).

Afterwards, running buffer was discarded and the gels were removed from the running chamber. The glass plates were removed, separating and stacking gel were separated and stacking gel was discarded. Until further processing, the separating gel was incubated in blotting buffer (3.032 mg/ml Tris Base, 14.4 mg/ml glycine, 20% methanol).

3.11.5   Blotting

In order to transfer the proteins from the polyacrylamide gel to a polyvinylidene fluoride (PVDF) blotting membrane (Millipore, IPVH00010), four pieces of Whatman blotting paper (9 cm x 7 cm; Hartenstein, GB40) were incubated in blotting buffer until they were fully soaked. For activation, the PVDF membrane (9 cm x 7 cm) was incubated in methanol (Hartenstein, CM20) for 5 min at RT. Two Whatman blotting papers were put into a blotting chamber on top of each other and the PVDF membrane was carefully put on top without inclusion of air bubbles. The

separating gel was carefully put on top of the membrane without inclusion of any air bubbles. Two Whatman papers were put on top, and the whole "sandwich" was carefully compressed to ensure close contact between all parts of it. To transfer proteins from the polyacrylamide gel to the PVDF membrane, a current of 50 mA per gel was applied for 2 h. Afterwards, the membrane was subjected to labeling with Ponceau S solution or antibody detection.

3.11.6 Ponceau S Staining

For Ponceau S staining the membrane was incubated in Ponceau S solution (Carl Roth, 5938.1) for 2-3 min. Afterwards Ponceau S solution was removed and the membrane was washed with desalted water until protein bands appeared with a good signal-to-noise ratio.

3.11.7 Antibody Labeling

After blotting, the membranes were blocked in 5% milk (AppliChem, A0830) in TBS-T (0.01 M Tris-HCl (VWR, 1.08219.1000), 0.15 M NaCl, 0.2% Tween® 20 (AppliChem, A1389)) for 1 h. Afterwards, the membranes were incubated overnight with primary antibodies (anti-αSyn (15G7[274], 4B12 (monoclonal; Hiss, SIG-39730-200)), anti-phospho-αSyn(pSyn; Abcam, ab59264), anti-GFP (Abcam, Ab290), anti-GAPDH (Abcam, ab9485), anti-tubulin (Sigma, T4026), anti-actin (Sigma, A2066)) diluted in 5% milk in TBS-T supplemented with 0.02% NaN$_3$ according to Table 3-8.

After washing the membranes four times with TBS-T for 5 min, they were incubated with a secondary antibody (rabbit-anti-rat IgG (H&L) (alkaline phosphatase (AP)-conjugated) (Biomol GmbH, 712-405-002), goat-anti-rabbit IgG (AP-conjugated) (JacksonImmoResearch, 111-055-003), goat-anti-mouse IgG (AP-conjugated) (Cell Signaling Technology, 7056)), goat-anti-rabbit (horseradish peroxidase (HRP)-conjugated) (Cell Signaling Technology, 7074), horse-anti-mouse (HRP-conjugated) (Cell Signaling Technology, 7076)) diluted in 5% milk in TBS-T according to Table 3-8 for 1 h. After washing the membranes four times with TBS-T for 5 min membranes were prepared for signal detection.

Table 3-8: List of antibodies

This table summarizes the primary and corresponding secondary antibodies used for western blot analyses.

Primary Antibody		Corresponding Secondary Antibody	
Type	**Dilution**	**Type**	**Dilution**
15G7 (anti-αSyn)	1:2000-1:2500	rabbit-anti-rat (AP-conjugated)	1:2000
4B12 (anti-αSyn)	1:1000-1:5000	goat-anti-mouse (AP-conjugated)	1:5000
		horse-anti-mouse (HRP-conjugated)	1:5000
pSyn (anti-phospho-αSyn)	1:1000	goat-anti-rabbit (AP-conjugated)	1:5000
		goat-anti-rabbit (HRP-conjugated)	1:5000
anti-GFP	1:10000	goat-anti-rabbit (AP-conjugated)	1:5000
		goat-anti-rabbit (HRP-conjugated)	1:5000
anti-GAPDH	1:3000	goat-anti-rabbit (AP-conjugated)	1:5000
		goat-anti-rabbit (HRP-conjugated)	1:5000
anti-β-tubulin	1:500	goat-anti-mouse (AP-conjugated)	1:5000
		horse-anti-mouse (HRP-conjugated)	1:5000
anti-actin	1:200	goat-anti-rabbit (AP-conjugated)	1:5000
		goat-anti-rabbit (HRP-conjugated)	1:5000

3.11.8 Detection

All secondary antibodies used in this study were either conjugated with alkaline phosphatase (AP) and signal was detected using CDP-Star (Roche Applied Science, 12041677001), or with horseradish peroxidase (HRP) and signal was detected using the Clarity™ Western ECL Substrate (BioRad, 1705060). The CDP-Star solution contains dioxetane which is dephosphorylated by AP to metastable dioxetane phenolate anion which emits light at a wavelength of 466 nm upon its decomposition (see CDP-Star manual for more detailed information). The HRP catalyses the oxidation of luminol 3-aminophtalate dianion which is accompanied by light emission. The ECL substrate includes an enhancer which increases longevity and intensity of the luminescence reaction (see Clarity™ Western ECL Substrate Instruction Manual for more detailed information). The chemiluminescence can be detected with suitable camera systems.

For detection of AP-conjugated antibodies, the membranes were washed with AP buffer (0.1 M Tris, 0.1 M NaCl, pH 9.5) for 5 min at room temperature. Afterwards the membranes were dried with paper towels and the chemiluminescence reaction was started by incubating the membranes with 5 drops of CDP-Star (Roche Applied Science, 12041677001) in a plastic cover for 2 min.

For detection of HRP-conjugated antibodies, the membranes were dried using paper towels. Per membrane, 500 µl of Clarity™ Western ECL Substrate (Bio-Rad, #1705060) were pipetted onto the membrane and incubated in a plastic cover for 2 min before signal detection.

Chemiluminescence signals were detected with the ChemiLux camera system and the ChemoStar software (Intas, Göttingen)

3.12 Sucrose Gradient Centrifugation

3.12.1 Cell Lysis for Sucrose Gradient Centrifugation

Cells were maintained, enzymatically dissociated and centrifuged as described above. Afterwards the cells were resuspended in 1 ml of precooled DPBS (4°C) and transferred to a 1.5-ml reaction tube. Cells were centrifuged at 4°C and 16,100 rcf for 10 min (Eppendorf centrifuge 5415 R). Supernatant was discarded and cell pellets were resuspended in 40 µl SC lysis buffer (50 mM Tris (pH 7.4), 175 mM NaCl, 0.1% NP-40, 1x protease inhibitor (Roche Applied Science, 04693124001)). The cell suspension was repeatedly pipetted up and down and incubated on ice for 15 min. Afterwards, cell suspension was pipetted up and down again and incubated on ice for additional 15 min. Next, the suspension was centrifuged at 17,000 rcf and 4°C for 1 minute. The supernatant was transferred to a precooled 1.5-ml Protein LoBind reaction tube (VWR, 525-0133) and protein concentration was determined by BCA assay.

3.12.2 Sample Preparation and Centrifugation

50-200 µg of total protein were adjusted to a volume of 200 µl in 50 mM Tris (pH 7.4), 175 mM NaCl, and 0.1 % NP-40 and used for sucrose gradient centrifugation. Centrifuge tubes were filled with buffer A (50 mM Tris-HCl (pH 7.5), 0.1 % NP-40, 0-60 % Sucrose) in layers in the given order: 200 µl 60 % sucrose, 400 µl 50 % sucrose, 400 µl 40 % sucrose, 400 µl 30 % sucrose, 400 µl 20 % sucrose, 400 µl 10 % sucrose, 200 µl sample without sucrose (Figure 3-1). The samples were ultracentrifuged at 4°C and 40,000 rpm in an SW60 rotor (Beckmann Coulter) for 70 min (Sorvall WX Ultra 90, Thermo Scientific). After centrifugation, 12 fractions of 200 µl each were collected from top to bottom.
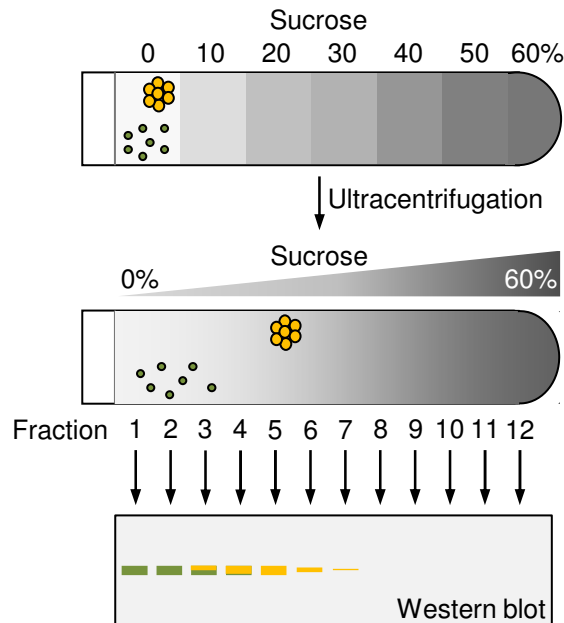
Figure 3-1: Schematic representation of sucrose gradient centrifugation

The sample is loaded on top of layers with increasing sucrose concentration. During ultracentrifugation αSyn species migrate according to their density and are finally detected by western blot analysis (figure modified from Dr. rer. biol. hum. Felix Schmidt, LMU Munich).

3.12.3 TCA Precipitation

200 µl of the fractions were added to 800 µl of 12.5% trichloroacetic acid (TCA). Afterwards samples were inverted and incubated at 20°C overnight. After centrifugation at 20,000 rcf and 4°C for 15 min, supernatant was discarded and pellets were washed by adding 1 ml acetone (-20°C). The samples were inverted repeatedly and centrifuged at 4°C and 20,000 rcf for 15 min. Supernatant was discarded and pellet was allowed to dry at room temperature for 5 min. 30 µl of 5x Lämmli sample buffer were added and samples were shaken for 10 min at 30°C and 1,400 rpm. Afterwards, they were incubated at 96°C for 5 min, vortexed briefly and spun down.

3.12.4 SDS-PAGE and Western Blot

After TCA precipitation samples were subjected to SDS-PAGE and western blot analysis. 12.5% polyacrylamide gels were prepared according to chapter 3.11.1. Samples were loaded onto the gel with the topmost fraction to the left and the fraction from the bottom to the right (Figure 3-1).

3.13 Confocal Single Particle Spectroscopy

Single particle spectroscopy represents a powerful tool to characterize αSyn aggregation on single particle level using fluorescently labeled αSyn both for *in vitro* studies and for the investigation of cell lysates.

3.13.1 Measurement Setup

Single particle spectroscopy was performed using an Insight™ Reader (Evotec-Technologies, Hamburg). The measurement setup resembles a confocal microscope (Figure 3-2). Laser light is emitted by an argon-ion laser at a wavelength of 488 nm and by a helium-neon laser at a wavelength of 633 nm. Light of both wavelengths is reflected at the first dichroic mirror and focused into the sample volume approximately 150 μm above the glass bottom of a 384-well plate (Evotec-Technologies/Perkin Elmer, Hamburg) via a 40x water immersion objective (Olympus, Hamburg) with high numerical aperture (1.2). Due to Brownian movement, fluorescently labeled particles in the sample solution will pass the laser focus (comprising a volume of approximately 1 fl) and emit photons upon excitation by the laser light. Since this fluorescence light is emitted in all directions, a part of it passes the objective and follows the way of the exciting laser light retrogradely until it passes the first dichroic mirror and is reflected by the second dichroic mirror. In order to reduce background signals, the light has to pass a pinhole with a diameter of 70 μm. The pinhole is inserted at a position corresponding to the intermediate image of a conventional optical microscope. Afterwards, light is separated according to its wavelength by the third dichroic mirror. Thus, light of two different wavelengths is detected separately by two single-photon avalanche detectors enabling the separate detection and analysis of a fluorescence signal in two channels in parallel. As readout, fluctuation of fluorescence intensity over time can be observed. Using mathematical evaluation tools, information on certain particle characteristics such as concentration, diffusion time and particle brightness can be extracted. This allows the conclusion of particle size and thus enables the distinction between monomeric and oligomeric protein assemblies.

Measurements can be performed using a stationary focus or the beam scanner unit in which oscillating mirrors move the laser focus horizontally through the sample solution. Scanning the sample increases the probability for the detection of rare particles. Thus, while the optimal particle concentration for a stationary focus lies in the low nanomolar range (0.1-50 nM), the detection limit is decreased to attomolar particle concentrations using the beam scanner[275].
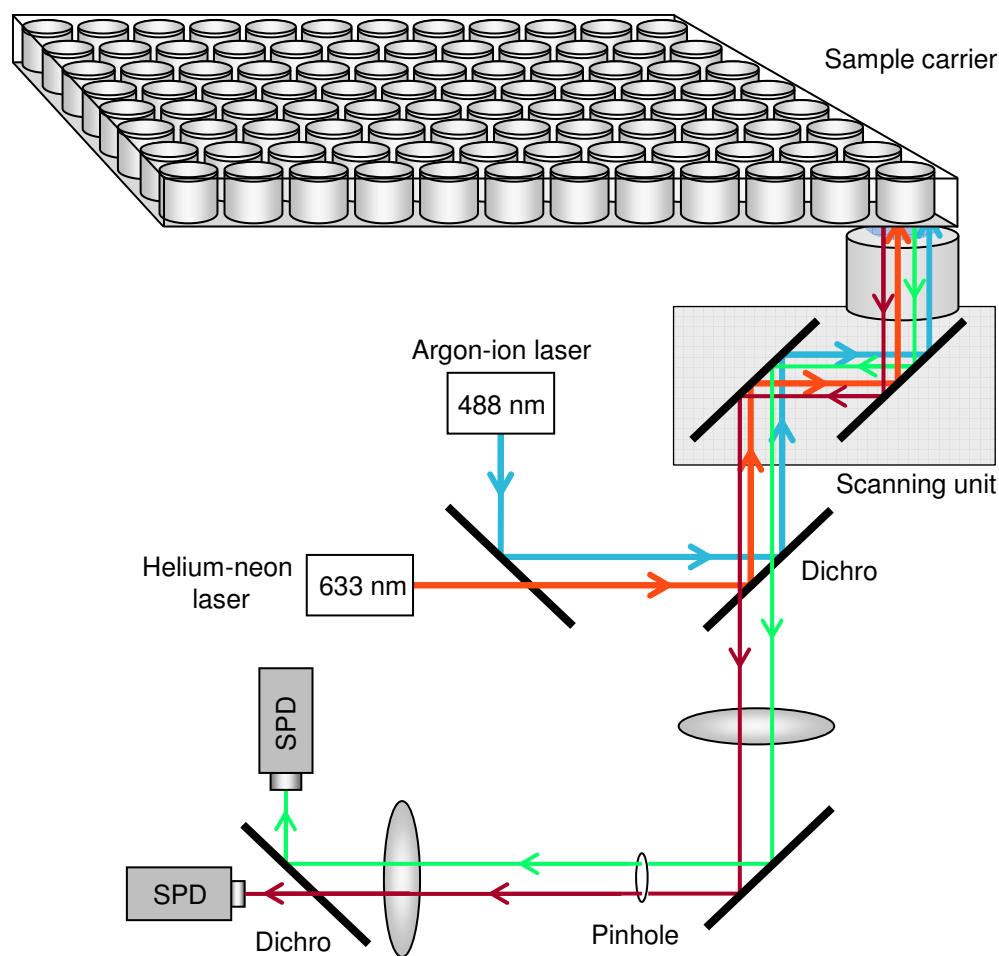
Figure 3-2: Measurement setup of the Insight[TM] Reader

Schematic representation of the Insight[TM] Reader. Laser light from two lasers (488 nm and 633 nm) is focused into the sample volume via dichroic mirrors and a beam scanning unit. Emitted photons pass the objective retrogradely and are guided via dichroic mirrors and a pinhole to be detected separately in two single-photon avalanche diodes[205,275]. SPD: single photon detector.

3.13.2 Adjustment

Lasers were turned on 30 min before the experiments to ensure constant laser power during the measurement. Afterwards, laser power was adjusted to 200 µW for the argon-ion laser (488 nm).

In order to adjust the device for the measurement, the correct positioning of the focus was manually controlled by detection of reflections in the glass bottom using a camera. The focus volume and shape were monitored by fluorescence intensity and diffusion time of a defined calibration solution containing freely diffusing fluorescence dyes (Alexa 488 and Alexa 647) with

known properties. Critical parameters for the adjustment of the optimal focus conditions were counts per particle (CPP) and diffusion time (T_{diff}) of individual fluorescence molecules. CPP represents a measure for the brightness of individual fluorescence molecules independent of their concentration. T_{diff} is a measure for the focus spot size. Positioning of laser focus, pinhole, and sample carrier was controlled via the included FCS+Plus_Control software (Evotech, Hamburg).

Each single measurement was performed for 10-15 seconds at room temperature. In scanned measurements samples were scanned in a length of 100 µm with a frequency of 50 Hz of the mobile focus (beam scanner) and a displacement of 2,000 µm of the sample carrier.

3.13.3 Data Analysis

The setup described above allows to determine fluctuations of fluorescence intensity over time. Using mathematical evaluation tools like fluorescence correlation spectroscopy[276-278] (FCS) or fluorescence intensity distribution analysis[279,280] (FIDA) further information concerning particle number, concentration, brightness, and diffusion time can be obtained. Scanning for intensely fluorescent targets[202,203] (SIFT) represents an approach to maximize sensitivity for slowly diffusing bright particle species like aggregates of fluorescently labeled proteins[275].

3.13.3.1 Correlation Analysis

Autocorrelation analysis (Figure 3-3, A) relies on the characterization of the fluctuation of a fluorescence signal over time. Thus, this analysis method can only be applied to measurements with stationary focus. For autocorrelation the FCSPP Evaluation 2.0 Software (Evotec Technologies) was used. For this type of data evaluation, time is subdivided into so called *bins* of usually 50 ns and the fluorescence signal is converted into a binary signal (0 = no fluorescence signal detected; 1 = fluorescence signal detected) resulting in a row of numbers 0 and 1. Using the autocorrelation function the values for all bins which are separated by defined time gaps of multiples of 50 ns (correlation times; 50 ns, 100 ns, 150 ns, …) are multiplied with each other. The products for each correlation time are then summed up and normalized against the overall signal.
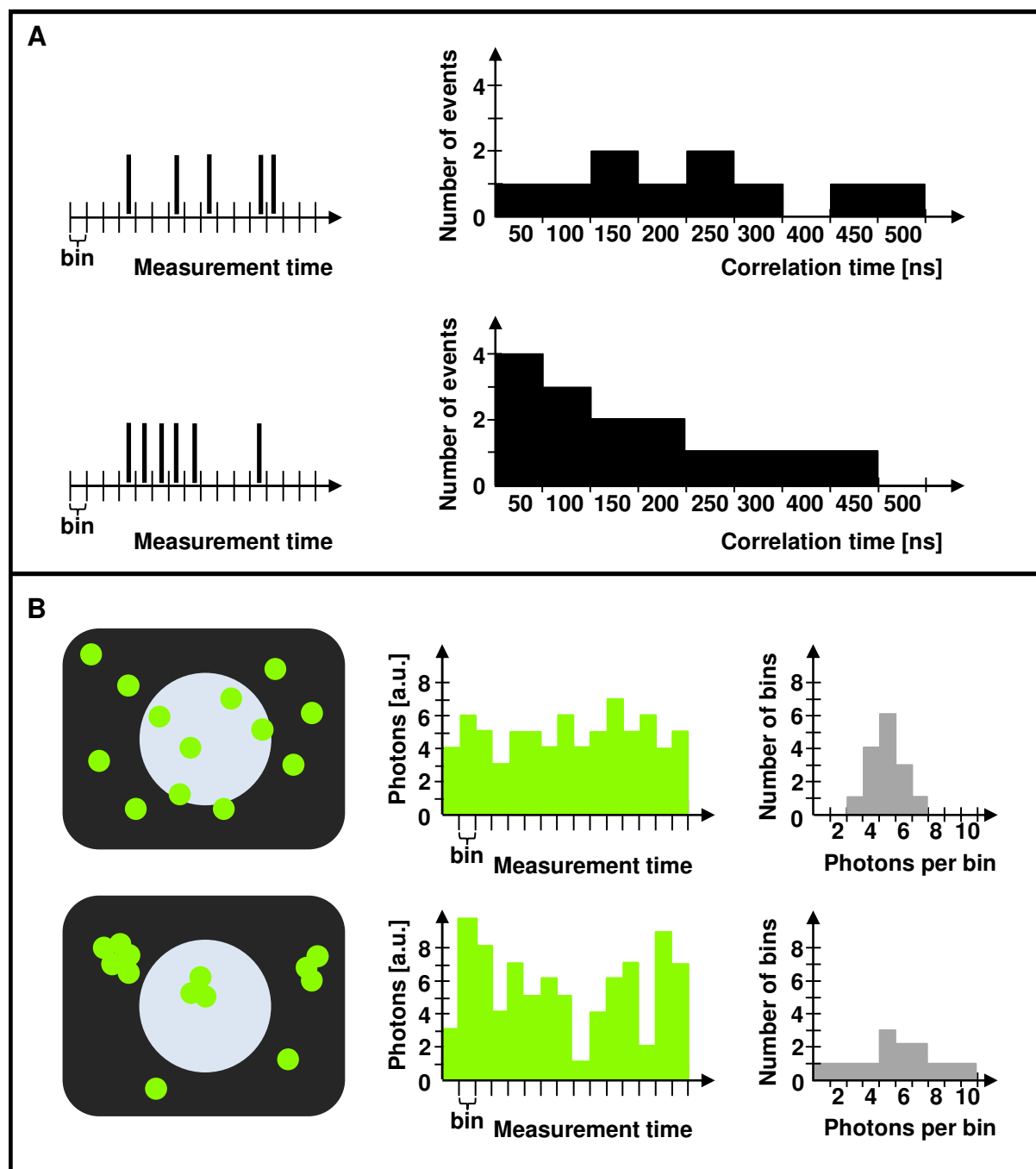
Figure 3-3: FCS and FIDA analysis

Figure 3-3: FCS and FIDA analysis

This figure shows the basic principle of fluorescence correlation spectroscopy (FCS) and fluorescence intensity distribution analysis (FIDA) in a simplified manner.

A) For FCS, time is subdivided into bins of typically 50 ns and signals are evaluated in a binary manner. The number of events occurring for distinct correlation times can be visualized using a correlation histogram. When a fluorescently labeled particle passes the laser focus, this results in a burst lasting for several bins (lower panel, left). This leads to higher values of the autocorrelation function (visualized by an increased number of events in the correlation histogram (lower panel, right)) for shorter correlation times. As a result, the diffusion time of the average particle can be deduced from the shape of the autocorrelation function.

B) For FIDA, time is subdivided into bins of typically 40 µs. The number of photons per bin is recorded (middle column) and can be plotted as intensity distribution histogram (right column). For monomeric protein solutions (upper row) the number of photons per bin is quite constant, resulting in a sharp peak in the intensity distribution histogram. For solutions with protein aggregates of variable size the number of photons per bin will be more variable, resulting in a broader peak in the intensity distribution histogram. Thus, the shape of the intensity distribution histogram provides insight into the aggregate composition of the protein solution.

Whenever a fluorescent particle passes the focus it creates a fluorescence burst lasting for several bins according to its time in focus. This results in highest autocorrelation values for neighboring bins (i.e., time gaps which are shorter than the particle's duration of stay in the focus). The autocorrelation function is mathematically fitted in an iterative process from the correlation distribution and the fit quality is estimated using Chi-square. The mean diffusion time (T_{diff}) and thus the particle size of the average particle can finally be deduced from the autocorrelation function.

Different further parameters like mean particle brightness (CPP) and mean number of particles in the laser focus (N) can be inferred: The mean number of photons over measurement time (given in kHz) is directly deduced from the measurement and accounts for the total fluorescence intensity (I_{tot}). CPP is calculated by dividing total fluorescence intensity by the number of particles (I_{tot}/N). Using the FCSPP Evaluation Software different species of molecules can also be detected using a multi component fit. Here, a relative amount of particles (in %) and a corresponding T_{diff} are assigned to each component.

The cross-correlation represents an analysis for measurements with fluorescence signals in more than one channel. This enables the quantitative analysis of intermolecular aggregation processes. To this end, the detected signal intensity in one channel is correlated to the signal intensity in the second channel for all correlation times. Hence, particle species showing

coinciding signals in both channels can easily be distinguished from particles showing a fluorescence signal in only one channel.

Given that I_{tot} remains stable over the measurement, parameters such as concentration, diffusion time (T_{diff}), and specific brightness of the particle species showing fluorescence signals in both channels can be determined. A typical experiment for this application is the investigation of receptor-ligand binding using different fluorescently labeled binding partners[276-278].

3.13.3.2 Fluorescence Intensity Distribution Analysis (FIDA)

For fluorescence intensity distribution analysis (FIDA, Figure 3-3 B) the number of photons in consecutive time intervals of defined length (so called bins, typically 40 µs) is detected and statistically analyzed using the Evaluation 2.0 Software (Evotec Technologies). The number of detected photons per bin is illustrated in an intensity distribution histogram and can be statistically analyzed via a FIDA multi component fit. Here, a model-based fitting procedure is applied to infer the brightness (q_n [kHz]) and the concentration (c_n) of one to four particle types from the total fluorescence intensity of the sample (I_{tot}) depending on the expected amount of different kinds of particles[275].

Since fluorescence intensity is the primary measure for FIDA, this kind of analysis is independent of diffusion time and can thus be applied both for scanned and unscanned measurements. Moreover, the measurement of fluorescence intensity renders FIDA more sensitive towards small aggregates than FCS (since fluorescence intensity increases approximately linearly with the number of fluorescently labeled particles within one aggregate, whereas diffusion time only increases with the third root of particle diameter). However, it provides no information on diffusion time.

3.13.3.3 Scanning for Intensely Fluorescent Targets (SIFT)

Using a stationary focus has limitations when it comes to the detection of rare and large (and thus slowly diffusing) particles at low concentrations. Since FIDA is independent of measuring diffusion time, the measurement efficiency for such solutions can be increased by scanning for intensely fluorescent targets (SIFT)[202,203] where the focus scans through the solution (Figure 3-4 A) using the Insight™ Reader's scanning unit (Figure 3-2)[279,280].

Thus, aggregation and co-aggregation processes can easily be analyzed qualitatively in color-coded intensity distribution histograms that can be evaluated further using SIFT analysis via the 2D-SIFT Software (Evotec Technologies)[202] (Figure 3-4 B). For quantification the histogram can be subdivided into several segments and a threshold – evaluated in samples without aggregates – can be determined to exclude the signal from low intensity bins[202,203,205,281]. Since the signal of equally intensely fluorescing particles is approximately uniformly distributed over the same number of bins, the number of "highly intense bins" correlates with the number and concentration of intensely fluorescent target molecules.

All in all, FIDA is highly sensitive for rare, large particles but provides no information on the diffusion time since the mean time a particle is located in the focus is no longer determined by its properties but by the scanning velocity.

3.13.4 Cell Lysis for Fluorescence Correlation Spectroscopy

Cells were maintained, enzymatically dissociated and centrifuged as described above. Afterwards the cells were resuspended in 1 ml of precooled DPBS (4°C) and transferred to a 1.5-ml reaction tube. Cells were centrifuged at 4°C and 16,100 rcf for 10 min (Eppendorf centrifuge 5415 R) and supernatant was discarded. Afterwards, cell lysis was performed as described previously[282]. Briefly, cell pellets were resuspended in 200 µl of RIPA buffer (50 mM Tris-HCl, pH 7.6, 1% NP-40, 150 mM NaCl, 1 mM EDTA) and incubated on ice for 10 min. Afterwards, samples were homogenized by pipetting ten times through a yellow needle and subsequently centrifuged for 10 min at 16,100 rcf and 4°C. The supernatant was transferred to new precooled 1.5-ml reaction tubes and frozen at -80°C.
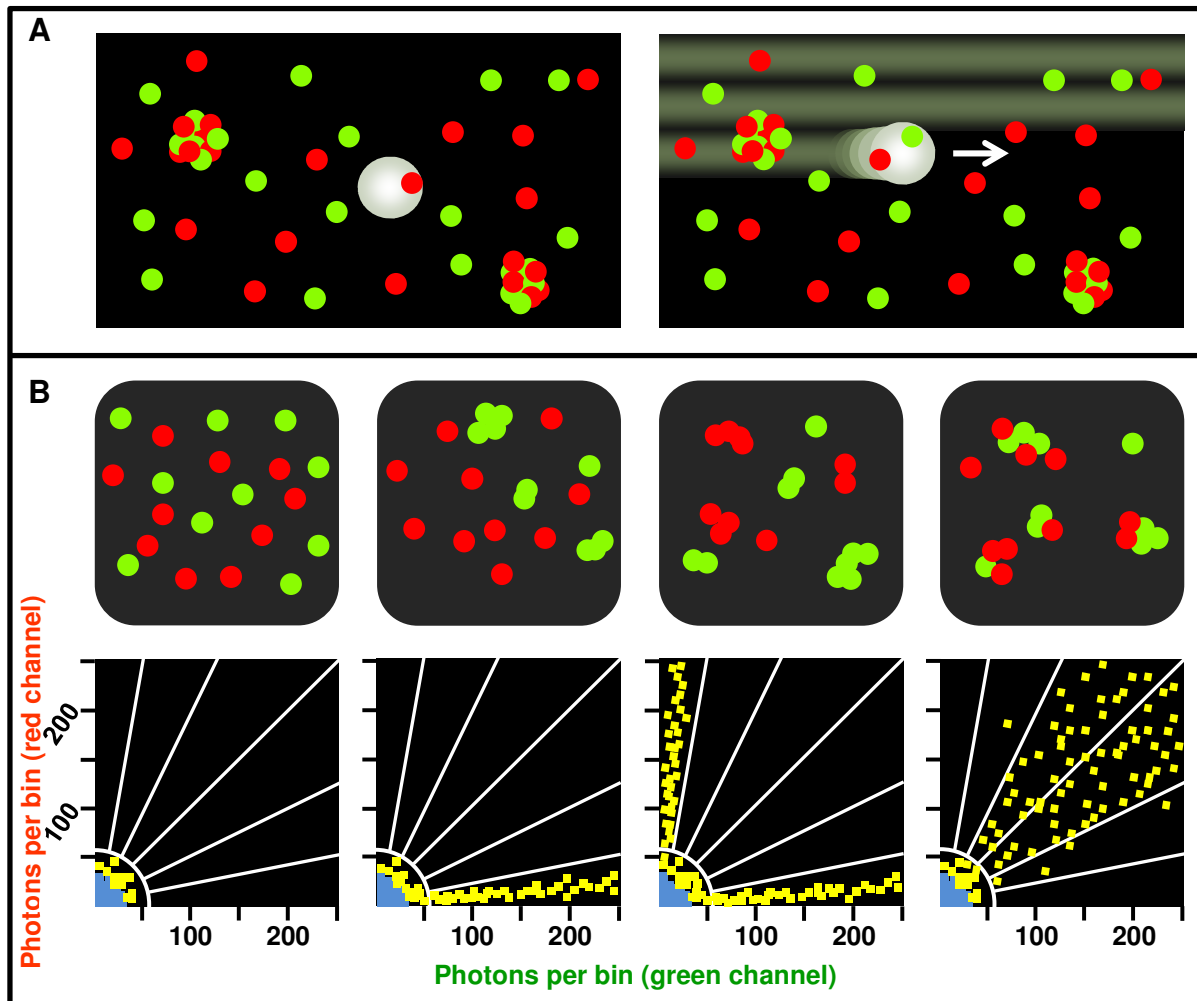
Figure 3-4: SIFT analysis

The figure shows the main principles of SIFT in a simplified manner.

A) Using a stationary focus the detection of large particles is limited by their slow Brownian movement (left) and can be improved by moving the laser focus through the sample volume using the Insight[TM] Reader's beam scanning unit (right).

B) A qualitative analysis of aggregation and co-aggregation can be obtained by using two-dimensional color-coded histograms. As example, histograms for monomeric proteins (left column), monomeric "red" proteins and aggregated "green" proteins (2nd left column), aggregated "red" proteins and aggregated "green" proteins (2nd right column), and mixed aggregates of "red" and "green" proteins (right column) are shown.

3.14 High Content Screening (Opera®)

3.14.1 Cell Maintenance for High Content Screening

Cells were maintained as described above. Prior to measurement, nuclei were stained by incubating the cells for 15 min at 37°C in a humidified 95% air/5% CO_2 atmosphere with Draq5 (Thermo Fisher Scientific, 62252) diluted 1:1,000 in medium to a final concentration of 5 µM.

3.14.2 Measurement Setup of the Opera® System

High content screening was performed using the Opera® high-throughput confocal imaging platform (PerkinElmer Cellular Technologies GmbH, Hamburg, Germany). In this setup (Figure 3-5 A), laser light can be emitted at four different wavelengths: 442 nm, 488 nm, 561 nm, and 640 nm. The light passes the Nipkow unit with the primary dichroic mirror depending on the filters and can be focused on the sample carrier using four different objectives: one 20-fold air objective (20x_Air_LUCPLFLN_NA=0.45), and three different water immersion objectives: 20xW_UAPO20xW3/340_NA=0.7, 40xW_PlanAPO_40xWLSM_NA=0.9, and 60xW_UPLAPO_60x_NA=1.2. Fluorescent dyes or proteins in the sample carrier will emit photons upon excitation by laser light with corresponding wavelengths. Since this fluorescence light is emitted in all directions, a part of it passes the objective and follows the way of the exciting laser light retrogradely until it is reflected by the primary dichroic mirror. Depending on its wavelength, fluorescence can finally be detected by three different cameras. Camera 3 can detect fluorescence excited with 640 nm. Fluorescence excited with all other lasers is mirrored at the detection dichroic mirror 2 ("Detection dichro 2") and subdivided according to its wavelength at the detection dichroic mirror ("Detection dichro"). Depending on the filter settings applied, light of given wavelengths is finally detected using Camera 1 or Camera 2.
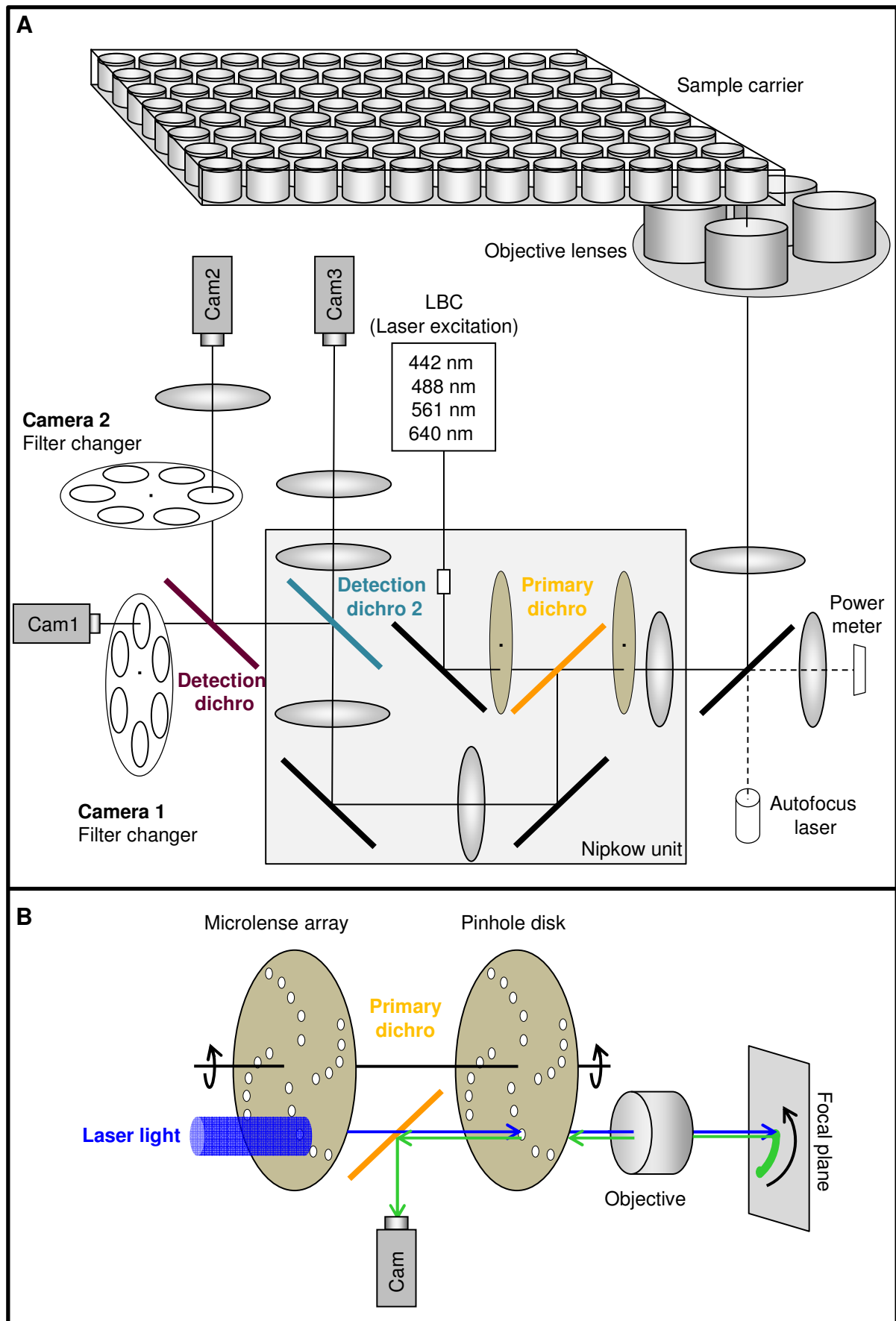
A

Sample carrier

Objective lenses

Cam2

Cam3

LBC
(Laser excitation)

442 nm
488 nm
561 nm
640 nm

Camera 2
Filter changer

**Detection
dichro 2**

**Primary
dichro**

Power
meter

Cam1

**Detection
dichro**

Autofocus
laser

Camera 1
Filter changer

Nipkow unit

B

Microlense array

Pinhole disk

**Primary
dichro**

Laser light

Focal plane

Objective

Cam

Figure 3-5: Measurement setup of the Opera®

Figure 3-5: Measurement setup of the Opera®

Schematic representation of the Opera® high-throughput confocal imaging platform and the Nipkow unit.

A) Laser light from four lasers (442 nm, 488 nm, 561 nm, and 640 nm) can be focused on the sample carrier via dichroic mirrors. Emitted photons pass the objective retrogradely and are guided via dichroic mirrors and a Nipkow unit to be detected separately using three different cameras.

B) The Nipkow disk inside the Nipkow unit consists of small holes arranged in an arched manner. Inside the Nipkow unit laser light is focused by microlenses in a disk with similar arrangement through the Nipkow disk and the objective on the sample. Emitted fluorescence is guided retrogradely through the Nipkow disk where the single holes decrease background fluorescence by excluding signals from above or below the focus plane. Due to the rotation of the Nipkow disk an arched image is recorded for each hole. The images of the different holes will finally add up to a complete image.

In order to reduce background signals, the light in a conventional confocal fluorescence microscope would normally pass a pinhole which is inserted at a position corresponding to the intermediate image of a conventional optical microscope and would thus exclude signal from fluorescent particles below or above the focus plane. In the Opera® high-throughput confocal imaging platform the confocal pinholes are replaced by a Nipkow unit (Figure 3-5 B). In this setup, the exciting laser light is focused by a microlense array before it passes the primary dichroic mirror, the pinhole disk, and the objective to finally excite fluorescent dyes or proteins in the sample. The fraction of fluorescence light that is guided retrogradely passes the pinhole disk, a spinning disk with holes arranged in an arched profile. The microlenses on the microlense array and the pinholes on the pinhole disk are arranged in a similar manner. Due to the rotation of the microlense array and the pinhole disk (with a speed of 25 revolutions per second) not a single point is detected but an arched area of the image. Due to the arrangement of the microlenses and the pinholes and the spinning of those disks, the single arched areas will add up to a complete image of the focal area.

The autofocus function enables a fully automated acquisition of fluorescence images. Here, characteristic reflections of the autofocus laser are detected when passing the bottom of the multiwell plate. Afterwards, laser light is focused on a defined height above the bottom of the multiwell plate depending on the desired image plane.

3.14.3 Adjustment

Prior to each experiment a reference image and a skew analysis have to be applied in order to compensate for systemic errors of the optics and the CCD cameras.

Uneven brightness distribution within an image was compensated for by using the "reference image" function. Using the Opera® adjustment plate, an image of free floating fluorescence dye was acquired. This should theoretically lead to evenly distributed fluorescence intensity within the image field. Practically, we observed higher intensity in the center of the image and decreasing intensity towards the edges. This effect is counteracted by the flat-field correction algorithm which (simplified) works by multiplying the recorded image with the inverted reference image.

The mechanical alignment of the CCD cameras alone is subject to variations (for example due to changes in temperature) and not sufficient to provide an adequate overlay of high resolution images obtained from more than one camera. To counteract this phenomenon the "skew analysis" function was applied. The Opera® adjustment plate provides wells with beads with different diameters for the different objectives: 10 μm for 10x, 5 μm for 20x, and 2.5 μm for 40x and 60x. Images of these beads are recorded for all excitation wavelengths and all detection cameras. Afterwards, a theoretical optimal overlay of the obtained images is calculated. This optimization is later on applied to all images of one measurement.

In order to set up an automated experiment, the kind of multiwell plate and the required objective were defined. Wavelengths and intensities of laser light as well as corresponding filters were defined depending on experimental conditions. A "plate layout" (defining the wells of a multiwell plate) and a "sublayout" (defining the area insight the wells) where images should be acquired were defined.

3.14.4 Data Acquisition

All data from automated fluorescence imaging shown in this work have been acquired using the 20x air objective.

3.14.4.1 Initial Characterization of Inducible H4 Cells

For the initial characterization of inducible H4 cells (see chapter 4.2.2) the following experimental setup was applied:

In "Exposure 1" focus height was set to -9.0 μm for the detection of Venus fluorescence in the cytoplasm. Venus fluorescence was excited using the 488-nm laser with a laser power of 7,110 μW. Fluorescence was detected using Camera 1 with an exposure time of 200 ms and twofold binning using a 520/35 filter.

In "Exposure 2" focus height was set to -13.0 μm for the detection of mCherry fluorescence in the nucleus. Fluorescence of mCherry was excited using the 561-nm laser with a laser power of 3,240 μW. Fluorescence was detected using Camera 2 with an exposure time of 7,000 ms and twofold binning using a 600/40 filter.

In "Exposure 3" focus height was set to -13.0 μm for the detection of Draq5 fluorescence in the nucleus. Fluorescence of Draq5 was excited using the 640-nm laser with a laser power of 3,830 μW. Fluorescence was detected using Camera 3 with an exposure time of 400 ms and twofold binning using a 690/50 filter.

For all three exposures, the filter of the primary dichroic mirror was 488/561/640 and the filter of the detection dichroic mirror was 568. Imaging was performed sequentially for all wells.

3.14.4.2 Fluorescence Kinetics of H4_GE Cells

For the characterization of fluorescence kinetics and fluorescence depending on tebufenozide concentration in H4_GE cells (see chapter 4.2.2.3) the following experimental setup was applied:

In "Exposure 1" focus height was set to -8.0 µm for the detection of Venus fluorescence in the cytoplasm. Venus fluorescence was excited using the 488-nm laser with a laser power of 7,110 µW. Fluorescence was detected using Camera 1 with an exposure time of 200 ms and twofold binning using a 520/35 filter.

In "Exposure 2" focus height was set to -12.0 µm for the detection of Draq5 fluorescence in the nucleus. Fluorescence of Draq5 was excited using the 640-nm laser with a laser power of 3,830 µW. Fluorescence was detected using Camera 3 with an exposure time of 120 ms and twofold binning using a 690/50 filter.

For both exposures, the filter of the primary dichroic mirror was 488/640 and the detection dichroic mirror was set to empty1. Imaging was performed sequentially for all wells.

3.14.4.3 Evaluation of the Effect of Ferric Iron and DMSO on H4_GE-V1S+SV2 and H4_GE-V Cells

In order to evaluate the effect of ferric iron and DMSO on H4_GE-V1S+SV2 and H4_GE-V cells (see chapter 4.3) the following experimental setup was applied:

In "Exposure 1" focus height was set to -8.0 µm for the detection of Venus fluorescence in the cytoplasm. Venus fluorescence was excited using the 488-nm laser with a laser power of 7,110 µW. Fluorescence was detected using Camera 1 with an exposure time of 320 ms and twofold binning using a 520/35 filter.

In "Exposure 2" focus height was set to -12.0 µm for the detection of Draq5 fluorescence in the nucleus. Fluorescence of Draq5 was excited using the 640-nm laser with a laser power of 1,500 µW. Fluorescence was detected using Camera 3 with an exposure time of 40 ms and twofold binning using a 600/40 filter.

For both exposures, the filter of the primary dichroic mirror was 488/640 and the detection dichroic mirror was set to empty1. Imaging was performed sequentially for all wells.

3.14.4.4 Initial Characterization of LUHMES_GE Cells

For the initial characterization of LUHMES_GE cells (see chapter 4.4.2.1) the following experimental setup was applied:

In "Exposure 1" focus height was set to -8.0 μm for the detection of Venus fluorescence in the cytoplasm. Venus fluorescence was excited using the 488-nm laser with a laser power of 7,110 μW. Fluorescence was detected using Camera 1 with an exposure time of 360 ms and twofold binning using a 520/35 filter.

In "Exposure 2" focus height was set to -11.0 μm for the detection of Draq5 fluorescence in the nucleus. Fluorescence of Draq5 was excited using the 640-nm laser with a laser power of 3,830 μW. Fluorescence was detected using Camera 3 with an exposure time of 120 ms and twofold binning using a 690/50 filter.

For both exposures, the filter of the primary dichroic mirror was 488/640 and the detection dichroic mirror was set to empty1. Imaging was performed sequentially for all wells.

3.14.5 Data Analysis

An automated image analysis tool was developed in order to quantify cellular Venus fluorescence using the Acapella® software (PerkinElmer Cellular Technologies GmbH).

Here, nuclei (Figure 3-6 A) and cell boundaries (Figure 3-6 B) were automatically detected based on Draq5 signal. Based on this detection, an area for the quantification of mean cellular Venus fluorescence intensity was determined (Figure 3-6 C). By setting an arbitrary threshold for the mean cellular Venus fluorescence intensity, cells were considered Venus-positive (Figure 3-6 D) or Venus-negative (Figure 3-6 E). As a final result, a table with high content data concerning different properties was obtained (Figure 3-6 F).
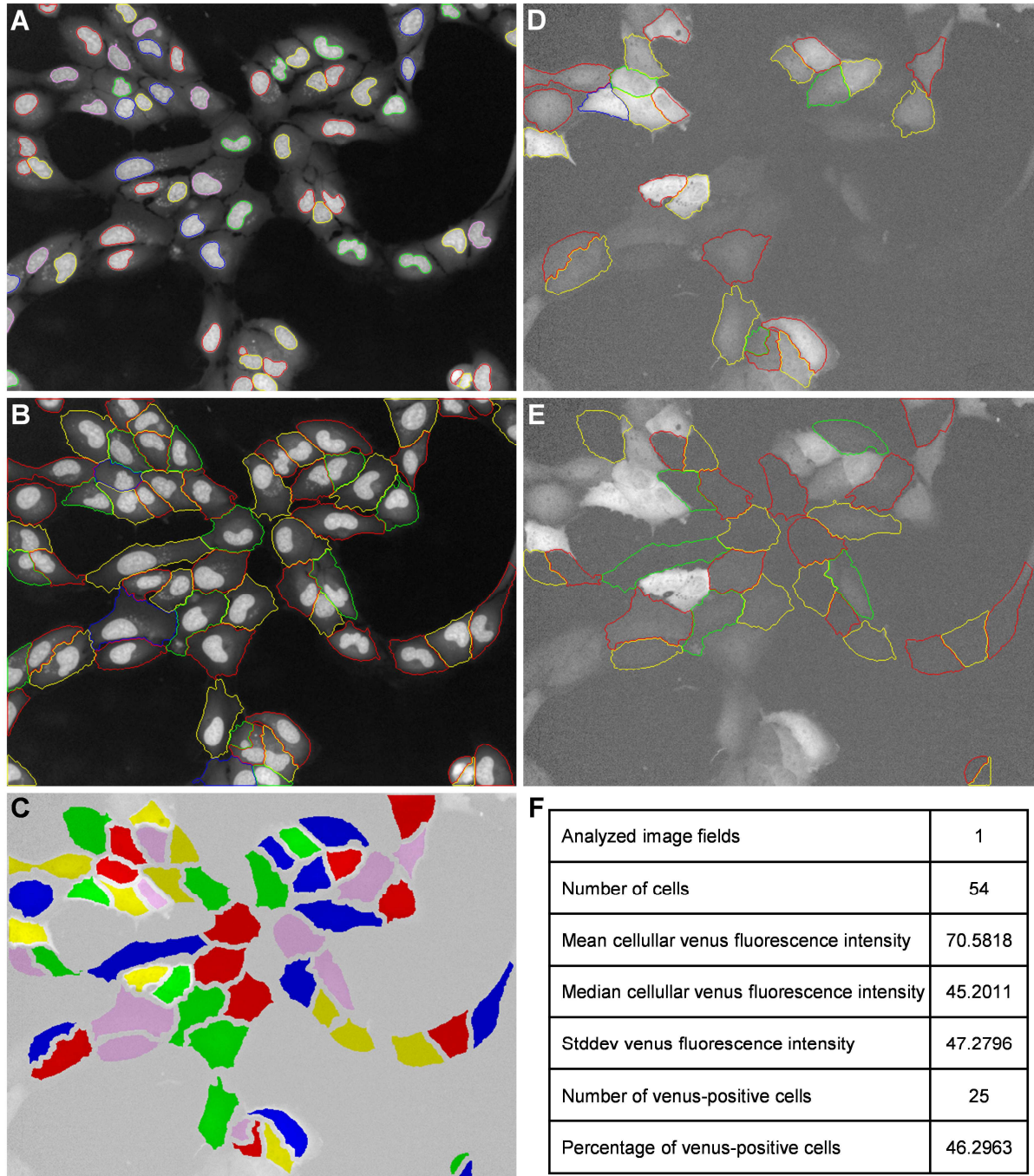
Analyzed image fields	1
Number of cells	54
Mean cellullar venus fluorescence intensity	70.5818
Median cellullar venus fluorescence intensity	45.2011
Stddev venus fluorescence intensity	47.2796
Number of venus-positive cells	25
Percentage of venus-positive cells	46.2963

Figure 3-6: Opera® data analysis

Overview of the automated image analysis using the Acapella® software.

A) Detection of nuclei based on Draq5 fluorescence.

B) Determination of cell boundaries based on Draq5 fluorescence.

C) Definition of the area to quantify mean cellular Venus fluorescence.

D) Cells considered Venus-positive based on an arbitrarily set threshold for mean cellular Venus fluorescence.

E) Cells considered Venus-negative based on an arbitrarily set threshold for mean cellular Venus fluorescence.

F) Final output table showing different sample properties.

4 Results

4.1 Testing the Project Strategy

4.1.1 Susceptibility of H4 and LUHMES Cells to Lentiviral Transduction

To test if H4 and LUHMES cells are susceptible to viral transduction, we produced a Cre driver virus, a GAL4 driver virus, a UAS-Venus receiver virus and a loxP-Venus receiver virus. H4 and LUHMES cells were expanded in 6-well plates for 48 h before incubating them in virus supernatant of Cre driver and loxP-Venus receiver or GAL4 driver and UAS-Venus receiver, respectively, for 5.5 h. Cells were imaged 24 h after addition of virus supernatant. In H4 cells, fluorescent cells for both the Cre-loxP system (Figure 4-1 A) and the GAL4-UAS system (Figure 4-1 B) were observed. For the LUHMES cells we could not detect any fluorescent cell neither for the Cre-loxP system (Figure 4-1 C) nor for the GAL4-UAS system (Figure 4-1 D). In contrast, no living LUHMES cells were observed at all. We speculated that the reason for this could be the presence of fetal bovine serum (FBS) in the virus supernatant. For this reason, we repeated the experiment and incubated LUHMES cells with purified GAL4 driver virus and UAS-GFP receiver virus (kind gift from P.H. Kuhn) without FBS at a ratio of 1:267. 48 h later, green fluorescent LUHMES cells were detectable (Figure 4-1 E). Thus, we concluded that both H4 and LUHMES cells were susceptible to lentiviral transduction, although the transduction of LUHMES cells required the usage of purified virus.
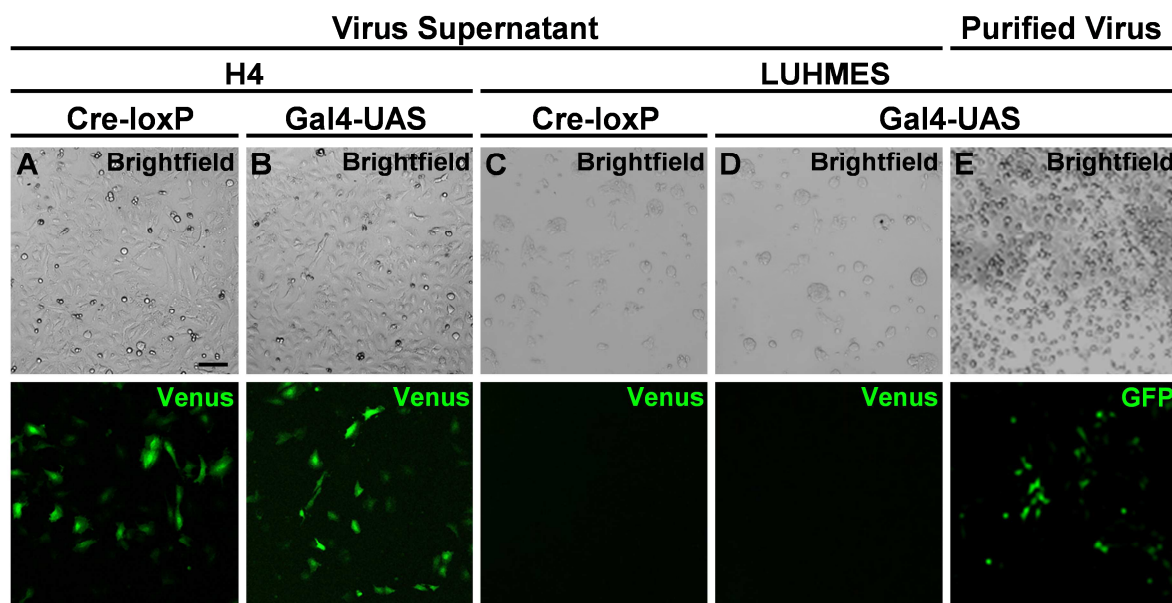
Figure 4-1: Susceptibility of H4 and LUHMES cells to lentiviral transduction

H4 and LUHMES cells were incubated with virus supernatant (A-D) or purified virus (E) of Cre driver and loxP-Venus receiver virus or GAL4 driver and UAS-Venus receiver virus, respectively. For all cells, brightfield (upper row) and fluorescence images (lower row) were taken.

A) H4 cells showed green fluorescence 24 h after transduction using the Cre-loxP system. Scale bar in A is 100 μm and is valid for all panels.

B) H4 cells showed green fluorescence 24 h after transduction using the GAL4-UAS system.

C, D) No viable LUHMES cells after incubation with virus supernatant.

E) LUHMES cells tolerated incubation with purified virus and displayed green fluorescence after 24 h incubation with purified GAL4 driver and UAS-GFP receiver virus.

4.1.2 Incomplete Separation of Hemi-Venus Constructs Using a P2A Sequence

In order to ensure equimolar expression in the BiFC system, we decided to couple the hemi-Venus constructs via a P2A sequence. To test this system, the αSyn-hemi-Venus constructs were connected via a P2A sequence (SV2-P2A-V1S). As negative control, SV2 was connected with V1 (i.e., the N-terminal Venus fragment lacking αSyn) via a P2A sequence (SV2-P2A-V1) (Figure 4-2 A). HEK293T cells were transiently transfected with both constructs and subjected to fluorescence microscopy 48 h after transfection. Surprisingly, we observed green fluorescence in both SV2-P2A-V1S-transfected cells and the negative control (Figure 4-2 A). Since no background has been described for the αSyn-hemi-GFP system when co-transfecting H4 cells with GFP$_{N-terminus}$-αSyn and GFP$_{C-terminus}$[213], we speculated that this background signal is due to an incomplete separation mediated by the P2A sequence.
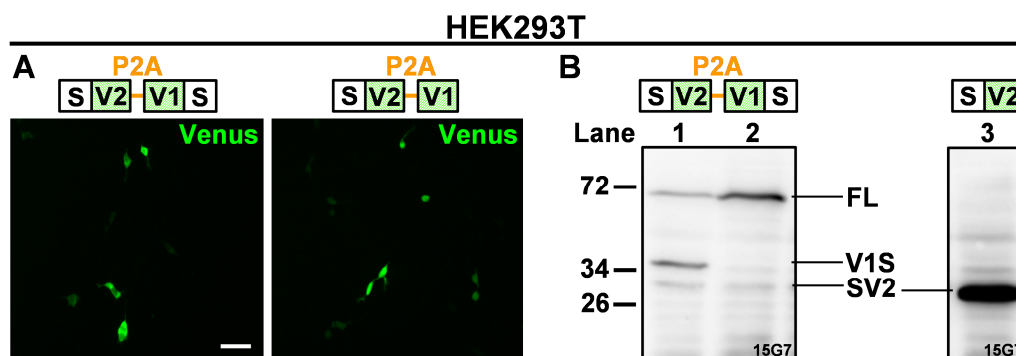
Figure 4-2: Incomplete separation of hemi-Venus fusion proteins connected by a P2A sequence

HEK293T cells were transiently transfected with SV2-P2A-V1S or a negative control lacking αSyn linked to V1 (SV2-P2A-V1) and subjected to fluorescence microscopy and western blot analysis.

A) Both cells transfected with SV2-P2A-V1S (positive control) and cells transfected with the negative control SV2-P2A-V1 showed green fluorescence. Scale bar: 100 µm.

B) Western blot of cells transfected with SV2-P2A-V1S shows incomplete separation of the two hemi-Venus constructs for two individual transfections (lane 1, 2). Lane 3: control with cells transfected with SV2. FL: full-length SV2-P2A-V1S construct.

To test this hypothesis, we transfected HEK293T cells with the SV2-P2A-V1S constructs in duplicates and harvested the cells 48 h after transfection for western blot analysis. For both transfections we observed incomplete separation of the full-length construct (Figure 4-2 B, FL). Therefore, we discarded the P2A system and decided to use separate viruses for the transduction with the V1S and the SV2 construct, respectively.

4.1.3 Background Fluorescence upon Transduction of Cells with V1 and SV2

We wondered if the incomplete P2A sequence mediated separation of the hemi-Venus constructs was the only explanation for the background signal in the cells that had been transfected with the negative control construct (lacking αSyn linked to V1; Figure 4-2 B). For the αSyn-hemi-GFP system no background signal has been described for a negative control where H4 cells had been co-transfected with GFP_{N-terminus}-αSyn and GFP_{C-terminus}[213]. Still, background fluorescence and an improvable signal-to-noise ratio are commonly observed in BiFC systems (including systems where a split-Venus strategy is applied)[251].
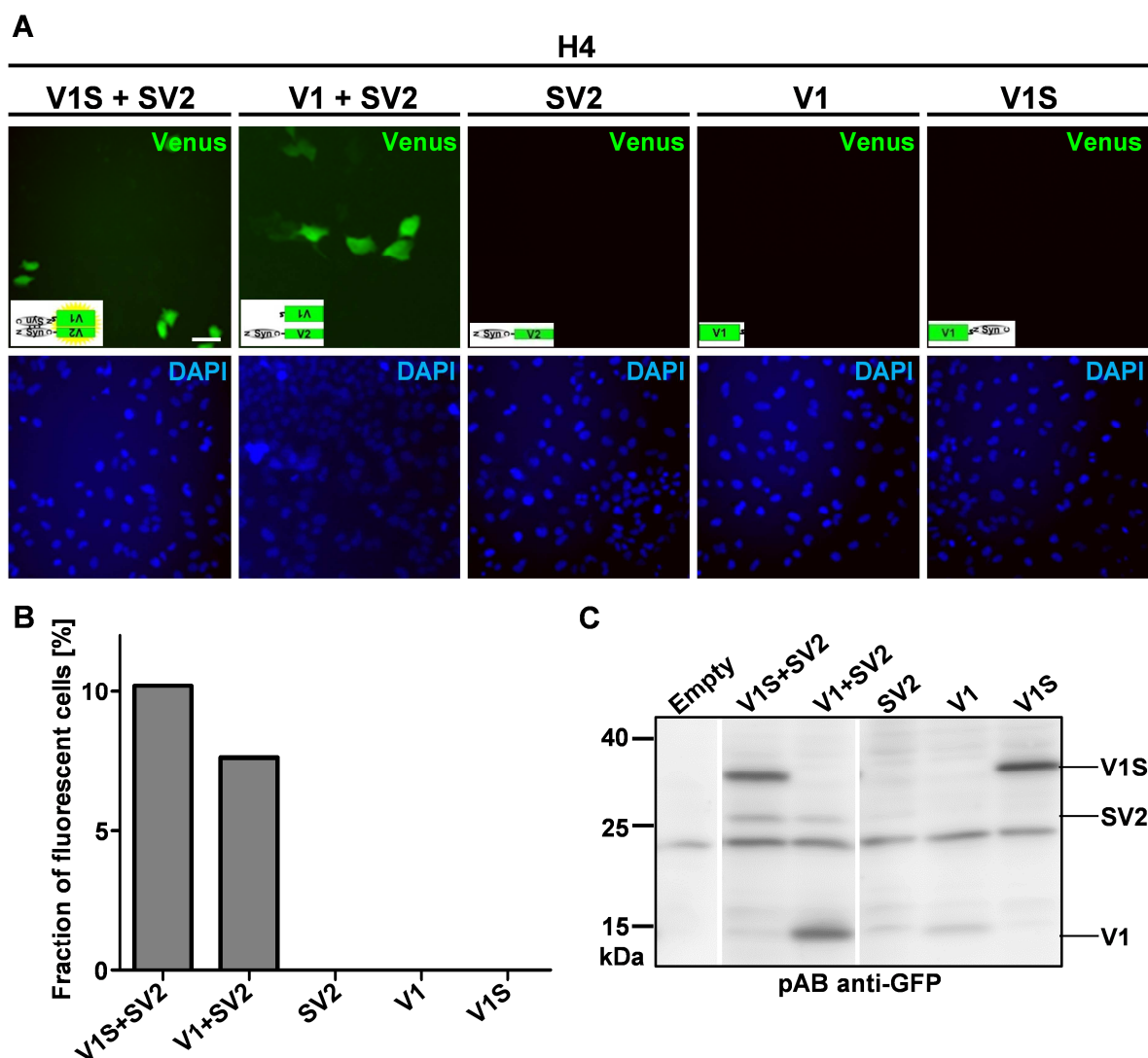
A

B

C

Figure 4-3: Background fluorescence due to self-complementation of hemi-Venus fragments

H4 cells were transduced with constitutively active GAL4 driver virus and UAS-GOI receiver viruses carrying V1, V1S, and SV2 as annotated.

A) Fluorescence images of transduced cells, nuclei were stained with DAPI. Co-transduction with both the positive control (V1S and SV2) and the negative control (V1 + SV2) led to green fluorescence. No green fluorescent cells were observed upon transduction with SV2, V1, or V1S alone.

B) The fraction of positive cells was approximately 10% for transduction with V1S + SV2, approximately 7% for transduction with V1 + SV2, and exactly 0% for transduction with SV2, V1, or V1S alone.

C) Western blot showing expression of the corresponding constructs on protein level; no massive increase in signal intensity of V1 (lane 3) compared to V1S (lane 2) was observed.

To our surprise, we did not find any literature concerning the signal-to-noise ratio of the αSyn-split-Venus system to the beginning of this thesis. Since this system is commonly used, we considered that the signal-to-noise ratio for the αSyn-split-Venus system would be an important issue to investigate.

To do so, we transduced H4 cells with purified viruses of constitutive GAL4 driver and UAS-V1 receiver, with UAS-V1S receiver, with UAS-SV2 receiver, with a combination of UAS-V1S receiver and UAS-SV2 receiver (positive control), or a combination of UAS-V1 receiver and UAS-SV2 receiver (negative control), respectively. 48 h after transduction cells were subjected to fluorescence microscopy or harvested for western blot analysis.

In the positive control (V1S + SV2) about 10% of cells showed green fluorescence (Figure 4-3 A, B, left column). To our surprise, we also observed green fluorescence in the negative control (V1 + SV2, Figure 4-3 A, B, second column) with a fraction of about 7% of positive cells. As expected, no fluorescent cells were observed when cells were transduced with any of the constructs V1, V1S, or SV2 alone (Figure 4-3 A, B, right three columns).

The observed background signal in the negative control might be explained by a massive overexpression of V1 compared to V1S. To exclude this possibility, we performed western blot analysis and did not observe a visible increase in signal intensity for V1 compared to V1S (Figure 4-3 C).

Thus, we found noteworthy self-complementation of Venus fragments without αSyn oligomerization as driving force resulting in background fluorescence in cells transfected with a combination of V1 and SV2.

4.1.4   No Increase in the Signal-to-Noise Ratio upon Insertion of Point Mutations into V1 and V2

Background fluorescence and an unfavorable signal-to-noise ratio are common problems in BiFC assays[251]. It has been described that one possibility of increasing the signal-to-noise ratio is the insertion of point mutations at the interface of Venus fragment interaction[251] since the complementation of the two Venus fragments appears to be at least partly driven by hydrophobic interactions of the side chains[283]. Thus, in order to decrease self-association tendencies, hydrophobic amino acids could be replaced by neutral amino acids[283,284]. For Venus, several of these point mutations have been described[283,285,286]. We inserted two such promising single amino acid exchanges – I152L[283] and L201V[285] – in V1 and V2, respectively[287].
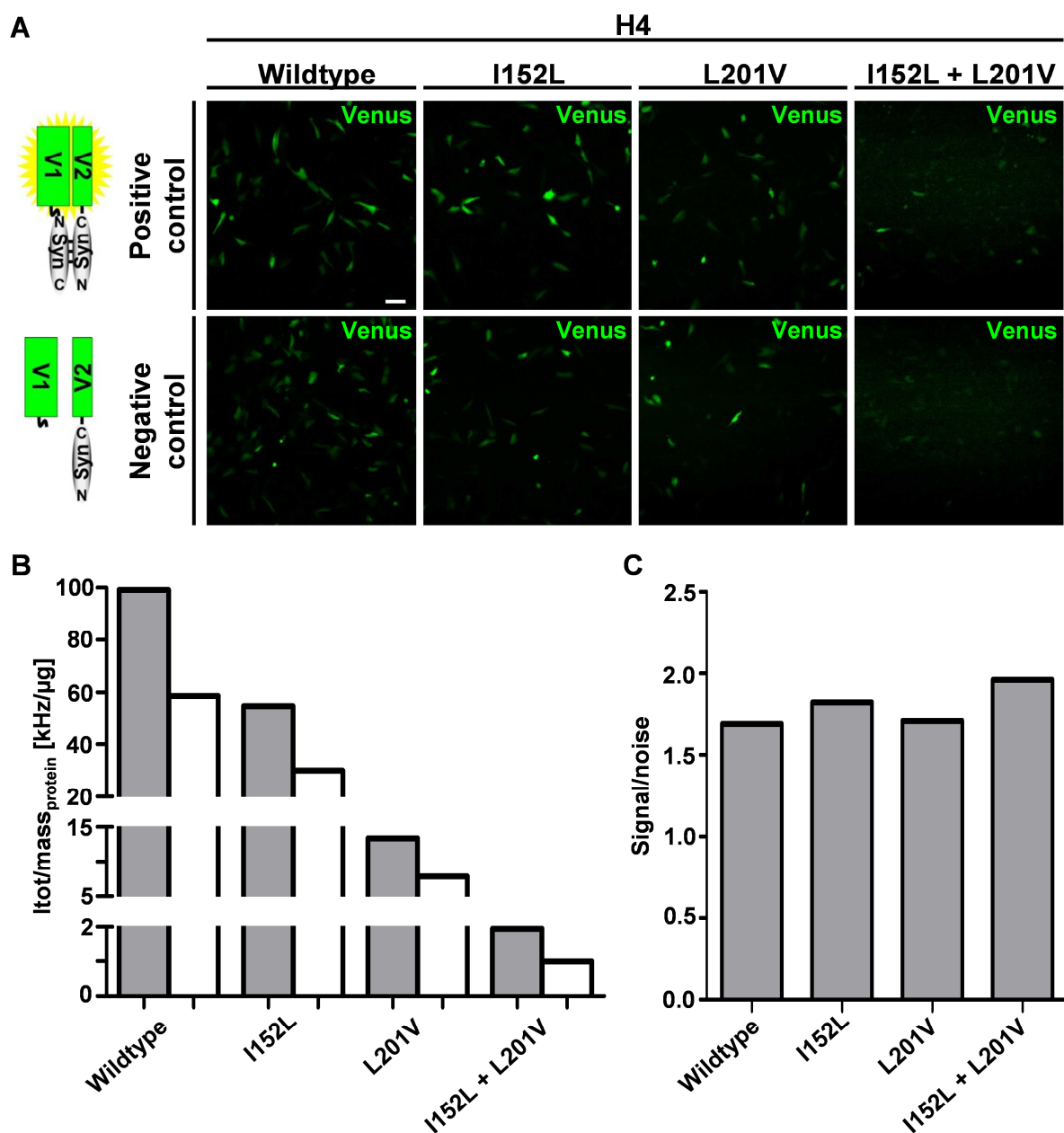
Figure 4-4: No effect of point mutations in V1 and V2 on signal-to-noise ratio

H4 cells were transiently transfected with V1S + SV2 as positive control or V1 + SV2 as negative control with or without the point mutations I152L (in V1) and L201V (in V2) to test their effect on the signal-to-noise ratio.

A) Fluorescence images showing decreased fluorescence intensity for both the I152L and the L201V mutation and both the positive and the negative control. Scale bar: 100 μm.

B) Quantification of total fluorescence intensity per protein amount using the Insight™ Reader. Fluorescence intensity decreased for both I152L and L201V mutation for both the positive and the negative control.

C) Signal-to-noise ratio was determined from signal intensities shown in B) and not considerably affected by insertion of both point mutations.

Bars in B) and C) show mean of 1-2 independent experiments.

H4 cells were transiently transfected with V1S + SV2 as positive control or V1 + SV2 as negative control carrying different combinations of V1$_{wt}$, V1$_{I152L}$, V2$_{wt}$, and V2$_{L201V}$. 48 h after transfection cells were subjected to fluorescence microscopy and cell lysates were analyzed using single particle spectroscopy. For both the positive and negative control highest total fluorescence intensity was observed for wildtype, i.e., the combination V1$_{wt}$ + V2$_{wt}$ (Figure 4-4 A, B, left column). Compared to wildtype, total fluorescence intensity was decreased for I152L, i.e., the combination V1$_{I152L}$ + V2$_{wt}$ (Figure 4-4 A, B, second column). The fluorescence intensity decreased even more for L201V, i.e., the combination V1$_{wt}$ + V2$_{L201V}$ (Figure 4-4 A, B, third column), and was lowest for the combination of both mutations, V1$_{I152L}$ + V2$_{L201V}$ (Figure 4-4 A, B, right column). Unfortunately, we did not observe a noteworthy increase in signal-to-noise ratio due to either of the point mutations or a combination of both of them (Figure 4-4 C).

Thus, since the mutations did not critically increase the signal-to-noise ratio and since we obtained the highest total fluorescence intensity when using the combination V1$_{wt}$ + V2$_{wt}$, we decided to do our further studies using these constructs.

4.1.5 Decreased Fluorescence Intensity in Cells Transfected with V1S and SV2 upon Incubation with Known Modulators of αSyn Aggregation

The main advantage of the BiFC system is that it allows the real-time observation of αSyn oligomerization in living cells. Thus, it might be a useful tool for high-throughput screenings for αSyn anti-aggregative compounds. In order to test if the BiFC system – despite the self-complementation of the Venus fragments in the absence of αSyn – is suitable for such experiments, H4 cells were transiently transfected with αSyn BiFC plasmids and treated with anle138b, anle138c, baicalein, or DMSO as control. Anle138b, anle138c, and baicalein have been shown to inhibit αSyn aggregation *in vitro*[56,145,192,288-290] and anle138b has also shown beneficial effects in various animal models of PD[192,291,292]. 48 h after transfection, cells were subjected to fluorescence microscopy, and fluorescence intensity of cell lysates was determined using single particle spectroscopy.

Fluorescence intensity was decreased following treatment with anle138b, anle138c, or baicalein compared to DMSO control, suggesting inhibited aggregation of αSyn (Figure 4-5). Moreover, fluorescence intensity was increased upon treatment with DMSO compared to the untreated control (Figure 4-5). This is well in line with *in vitro* findings where incubation of recombinant αSyn with DMSO increased aggregation[145].
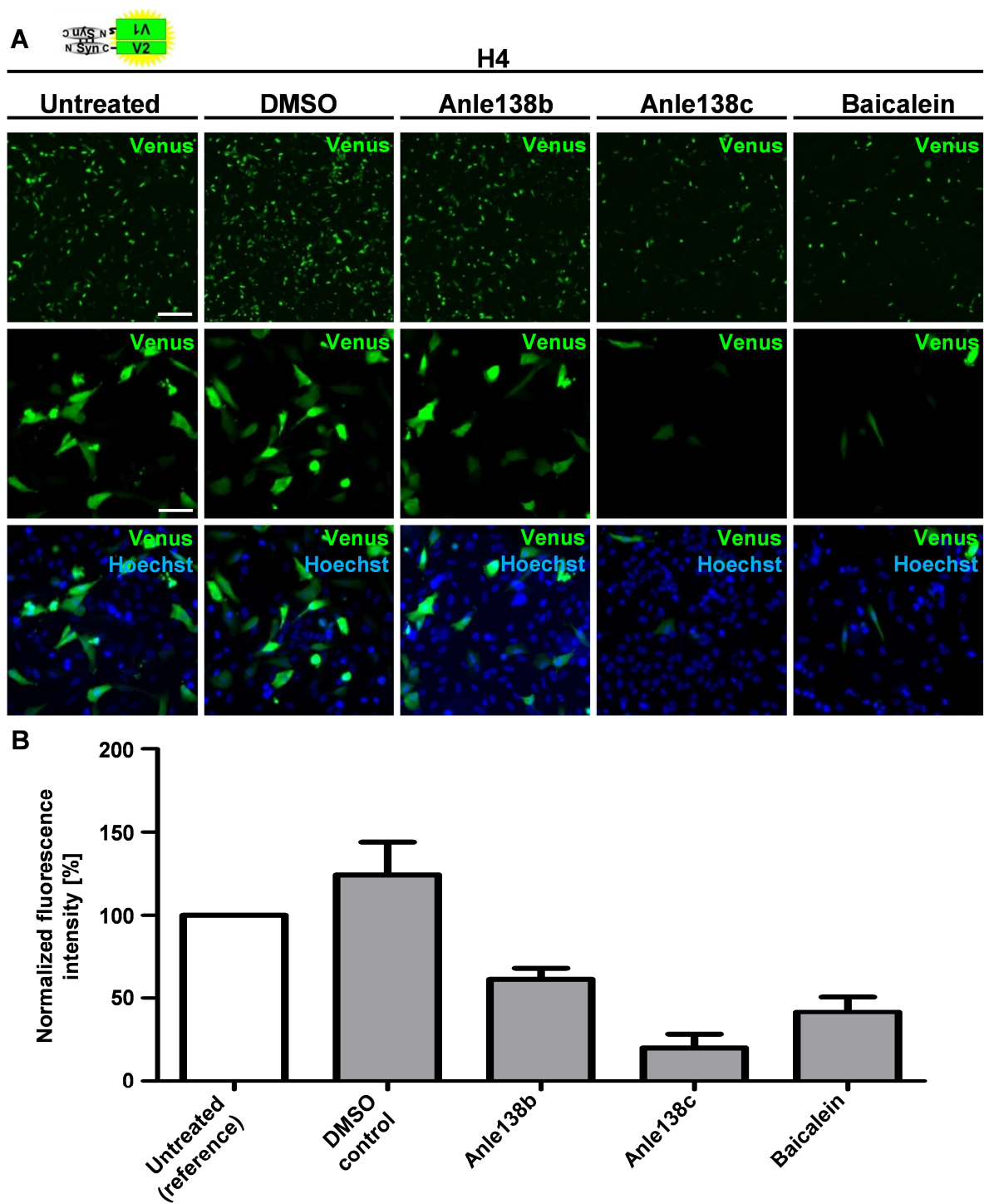
Figure 4-5: Reduced fluorescence intensity in the BiFC system as result of aggregation inhibitors

Figure 4-5: Reduced fluorescence intensity in the BiFC system as result of aggregation inhibitors

H4 cells were transiently transfected with the BiFC plasmids and left untreated or were incubated with DMSO (control), anle138b, anle138c, or baicalein.

A) Fluorescence images showed a decrease in fluorescence intensity upon treatment with anle138b, anle138c, and baicalein compared to treatment with DMSO. Nuclei were stained with Hoechst33342. Scale bar in top left panel is 500 µm and valid for images in the first row. Scale bar in the left panel of the second row is 100 µm and valid for images in the second and third row.

B) Cell lysates were analyzed using single particle spectroscopy. Total fluorescence intensity was increased in DMSO-treated cells compared to untreated cells and decreased upon treatment with anle138b, anle138c, or baicalein compared to DMSO-treated cells.

Thus, the BiFC system is suitable to detect anti-aggregative compounds (like anle138b, anle138c, and baicalein) as well as substances that increase αSyn aggregation (like DMSO) and therefore might represent a valuable tool for high-throughput screening assays. Obviously, additional experiments will be needed to carefully evaluate hits from primary screens since false positive results cannot be excluded.

4.2 Establishment and Characterization of Inducibly αSyn Overexpressing H4 Cell Lines

4.2.1 Transgene Expression in 98% of H4 Cells for at Least 18 Days after Lentiviral Transduction

In the next step, we produced and purified the required lentiviruses to prepare stable cell lines. In order to obtain as many lentivirally transduced H4 cells as possible, an optimized transduction protocol was established. To this end, cells were incubated with viruses that carry a constitutive GAL4 driver (V99, see Table 3-5) and the UAS-SV receiver (V41, see Table 3-5) following 4 different protocols. 72 h after transduction cells were imaged and Venus-positive cells were counted using *ImageJ*. For protocol A we obtained approximately 20% of Venus-positive cells (Figure 4-6 A), protocol B led to approximately 39% of Venus-positive cells (Figure 4-6 A). Using protocol C we counted ~80% of Venus-positive cells (Figure 4-6 A) and using protocol D we obtained 98% of Venus-positive cells (Figure 4-6 A, B, C). Following protocol D, the fraction of positive cells remained quite stable for at least 18 days after transduction. 23 days after transduction we observed a decrease in the fraction of positive cells (95%) which was not significant (p=0.36).

As a consequence, stable cell lines were created following protocol D. This resulted in the following cell lines with inducible expression based on the GE system:

- H4_GE-S: inducible overexpression of αSyn (transduction with V100 and V42)
- H4_mC_GE-S: constitutive expression of mCherry coupled to a nuclear localization sequence (NLS) resulting in red fluorescence in the nucleus of positively transduced cells and inducible overexpression of αSyn (transduction with V100 and V120)
- H4_GE-V: inducible overexpression of Venus (transduction with V100 and V43)
- H4_GE-SV: inducible overexpression of αSyn coupled to Venus (transduction with V100 and V41)
- H4_GE-V1S+SV2: inducible overexpression of the N-terminal part of Venus coupled to αSyn (V1S) and of αSyn coupled to the C-terminal part of Venus (SV2) (transduction with V100, V39, and V46)
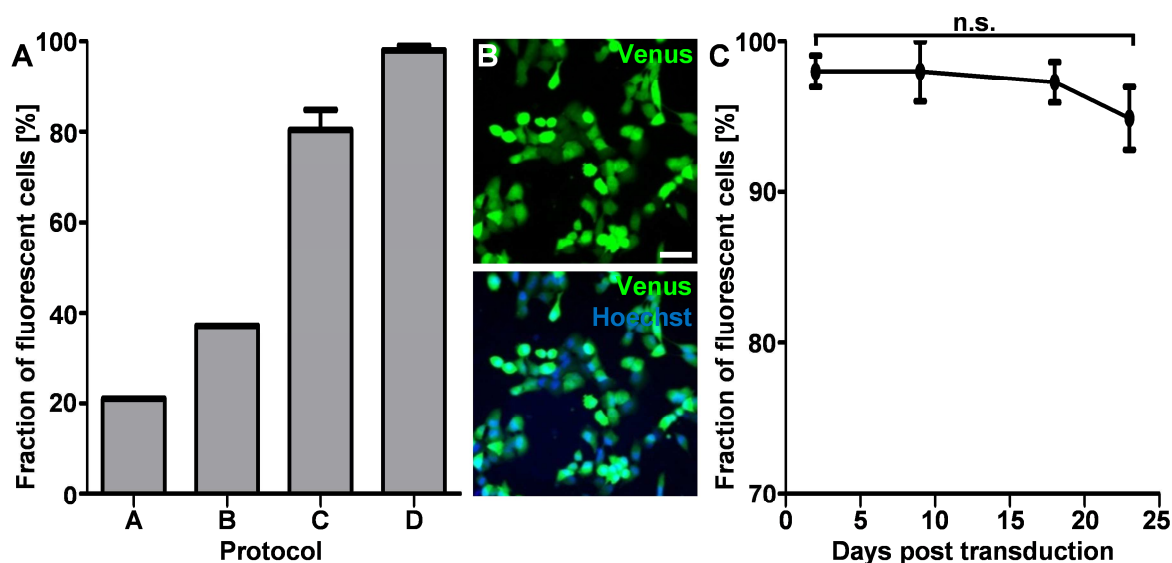
Figure 4-6: Stable and highly efficient transduction of H4 cells following protocol D

H4 cells were transduced with the constitutive GAL4 driver virus (V99) and the UAS-SV receiver virus (V41) according to protocols A-D (see chapter 3.8.1.1).

A) Quantification of the fraction of Venus-positive cells.

B) Representative images obtained for protocol D. Nuclei were stained with Hoechst33342. Scale bar is 100 μm and valid for both panels.

C) The fraction of positive cells was not significantly changed for 23 h after transduction (Fisher's exact test, n.s.: not significant (i.e. p>0.05)).

Data points represent mean of 3 to 4 wells; error bars show SEM; at least 300 cells were counted.

The following cell lines with inducible expression based on the CE^{T2} system were created:

- H4_CE^{T2}-S: inducible overexpression of αSyn (transduction with V102 and V36)

- H4_CE^{T2}-V: inducible overexpression of Venus (transduction with V102 and V37)

- H4_CE^{T2}-SV: inducible overexpression of αSyn coupled to Venus (transduction with V102 and V35)

- H4_CE^{T2}-V1S+SV2: inducible overexpression of the N-terminal part of Venus coupled to αSyn (V1S) and of αSyn coupled to the C-terminal part of Venus (SV2) (transduction with V102, V32, and V33)

Afterwards, cells were expanded and frozen in liquid nitrogen in "STOCK vials". Afterwards, one "STOCK vial" was unfrozen, cells were expanded to five T75 flasks and frozen in ten "WORK vials". For each experiment one "WORK vial" was unfrozen and cells were discarded after the experiment in order to obtain reproducible cell populations and to avoid effects of gene silencing.

4.2.2 Characterization of the Inducibly αSyn Overexpressing H4 Cell Lines

4.2.2.1 Expression of Fluorescence Proteins in H4_mC_GE-S, H4_GE-V, H4_GE-SV, and H4_GE-V1S+SV2

In order to test the generated cell lines, we incubated them with 10 μM tebufenozide or 0.1% DMSO as control for 48 h and analyzed the cells using the Opera® reader. To determine the factorial increase in transgene expression upon incubation with tebufenozide, the background signal from H4 cells was subtracted from the signal of the corresponding inducible H4_GE cells after treatment with tebufenozide or DMSO.

As expected, we observed no green fluorescence in H4 cells, H4_GE-S cells, or H4_mC_GE-S cells treated with DMSO (Figure 4-7 A, C) or tebufenozide (Figure 4-7 B, C). The fraction of Venus-positive cells was automatically determined using the Acapella® software and was below 1% for these cell lines independent of DMSO or tebufenozide treatment. We found approximately 99% mCherry-positive cells in the H4_mC_GE-S cell line independent of tebufenozide or DMSO treatment, while the fraction of mCherry-positive cells was approximately 0% in all other cell lines as expected. Thus, 99% of H4_mC_GE-S cells were transduced successfully with the mCherry-NLS-UAS-αSyn receiver virus (V120) (Figure 4-7 D).

For H4_GE-V cells we observed increased background fluorescence upon treatment with DMSO compared to untreated H4 cells (Figure 4-7, C). Following incubation with tebufenozide, fluorescence intensity increased dramatically from approximately 33 to 616 counts, suggesting an 18.6-fold increase in transgene expression following tebufenozide treatment (Figure 4-7 B, C). The fraction of Venus-positive cells increased from 87% to 99% upon treatment with tebufenozide (Figure 4-7 D).

For H4_GE-SV cells, background fluorescence intensity following treatment with DMSO was slightly lower than in H4_GE-V cells but still higher than in untreated H4 cells (Figure 4-7 A, C). Following induction of expression by tebufenozide, the fluorescence intensity increased by the factor 6.8 from approximately 29 to 198 counts (Figure 4-7 B, C). The fraction of Venus-positive cells increased from 77% to 94% upon treatment with tebufenozide (Figure 4-7 D).

For DMSO-treated H4_GE-V1S+SV2 cells, background fluorescence was in the range of unmodified H4 cells (Figure 4-7 A, C). Upon incubation with tebufenozide, fluorescence intensity increased slightly from approximately 2.6 to 15.1 counts, suggesting an 5.8-fold increase in transgene expression upon tebufenozide treatment (Figure 4-7 B, C). The fraction of Venus-positive cells increased from 0% to 37% upon treatment with tebufenozide (Figure 4-7 D).
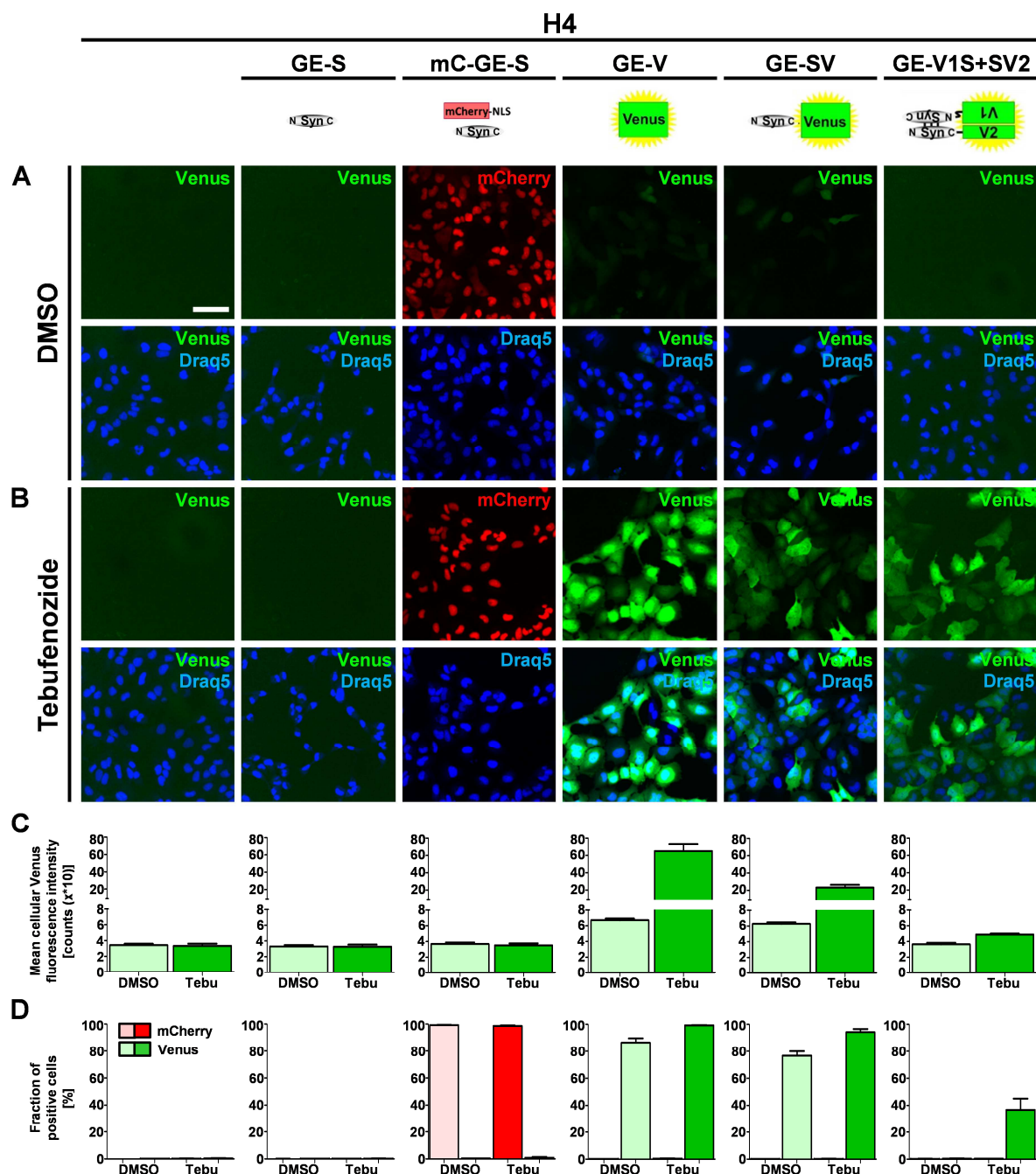
Figure 4-7: Induction of transgene expression in H4_GE cells

The generated H4_GE cell lines were incubated with 0.1% DMSO or 10 µM tebufenozide for 48 h.

A) Representative fluorescence images of cells incubated with 0.1% DMSO. Nuclei were stained with Draq5. Scale bar is 100 µm and valid for all panels in A and B.

B) Representative fluorescence images of cells incubated with 10 µM tebufenozide.

C) Quantification of the mean cellular Venus fluorescence intensity of H4 cells upon incubation with DMSO or tebufenozide using the Acapella® software.

D) Quantification of the fraction of Venus or mCherry-positive H4 cells upon incubation with DMSO or tebufenozide using the Acapella® software. Quantification was performed by setting an arbitrary threshold for Venus fluorescence intensity.

Columns in C and D show mean of 3 independent experiments; error bars show SEM; Tebu: tebufenozide.

4.2.2.2 Expression of Fluorescent Proteins in H4_CE^T2-SV, H4_CE^T2-S, H4_CE^T2-V, and H4_CE^T2-V1S+SV2

4.2.2.2.1 Determination of the Optimal Concentration of 4-OH-Tamoxifen for Transgene Induction

Since we had no experience concerning the induction of transgene expression using 4-OH-tamoxifen in cell culture, we incubated H4_CE^T2-V cells with different concentrations of 4-OH-tamoxifen ranging from 100 pM to 100 μM or DMSO as control for 72 h in order to determine its optimal concentration. Subsequently, fluorescence intensity and the number of cells were determined using the Opera® high-throughput imaging setup. We found the highest fluorescence intensity (Figure 4-8 A, B) without obvious adverse effects on cell shape and cell survival (Figure 4-8 A, C) to be obtained upon incubation with 10 μM 4-OH-tamoxifen.

4.2.2.2.2 Less Efficient Induction of Transgene Expression in H4_CE^T2 Cells Compared to H4_GE Cells

As for H4_GE cell lines, the H4_CE^T2 cell lines were incubated with 10 μM 4-OH-tamoxifen or DMSO as control for 48 h and analyzed using the Opera® reader. As described in chapter 4.4.2.1, the background signal from H4 cells was subtracted from the signal of the corresponding inducible H4_CE^T2 cell lines after treatment with 4-OH-tamoxifen or DMSO for the determination of the factorial increase in transgene expression upon incubation with 4-OH-tamoxifen.

As expected, we observed no fluorescence in H4 cells and H4_CE^T2-S cells with a fraction of Venus-positive cells below 1% independent of treatment with 4-OH-tamoxifen or DMSO (Figure 4-9 A-D).

For H4_CE^T2-V cells we observed increased background fluorescence upon treatment with DMSO compared to untreated H4 cells (Figure 4-9 C). Following incubation with 4-OH-tamoxifen, fluorescence intensity increased by a factor of 2.9 (Figure 4-9 B, C). The fraction of Venus-positive cells increased from 12.1% to 35.6% upon treatment with 4-OH-tamoxifen (Figure 4-9 D).
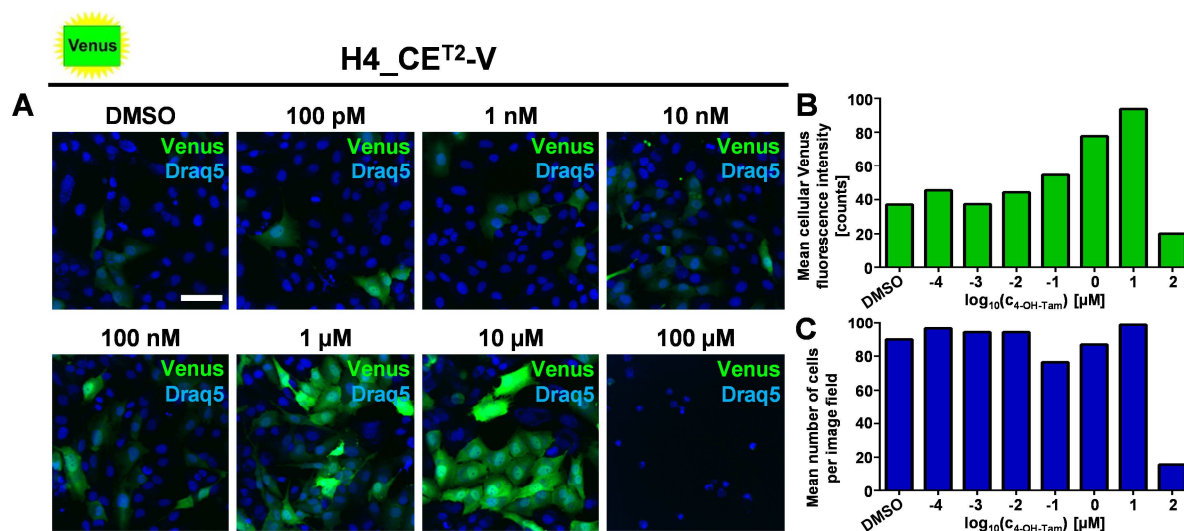
Figure 4-8: Maximum transgene induction in H4_CE^{T2} cells achieved by 10 µM 4-OH-tamoxifen

H4_CE^{T2}-V cells were incubated with different concentrations of 4-OH-tamoxifen ranging from 100 pM to 100 µM or DMSO as control for 72 h to determine the optimal concentration.

A) Fluorescence images showed increasing fluorescence with increasing concentration of 4-OH-tamoxifen up to a concentration of 10 µM. Nuclei were stained with Draq5. Scale bar is 100 µm and valid for all panels.

B) Quantification of fluorescence intensity using the Opera® system. A maximum in fluorescence intensity was observed upon incubation with 10 µM 4-OH-tamoxifen.

C) Quantification of cell number using the Opera® system. Incubation with 100 µM 4-OH-tamoxifen led to decreased cell number whereas all other concentrations showed no adverse effect on cell number.

For H4_CE^{T2}-SV cells, background fluorescence intensity following treatment with DMSO was slightly lower than in H4_ CE^{T2}-V cells but still elevated compared to H4 cells (Figure 4-9 A, C). Following induction of expression by 4-OH-tamoxifen, fluorescence intensity increased by a factor of 2.4 (Figure 4-9 B, C). The fraction of Venus-positive cells increased from 10.2% to 27.9% upon treatment with 4-OH-tamoxifen (Figure 4-9 D).

For H4_CE^{T2}-V1S+SV2 cells fluorescence intensity was in the range of untreated H4 cells and the fraction of Venus-positive cells was below 1% independent of treatment with 4-OH-tamoxifen (Figure 4-9 A-D).

Since we obtained a stronger increase in transgene expression upon treatment with tebufenozide in the H4_GE cells compared to 4-OH-tamoxifen treatment in the H4_CE^{T2} cells, we continued with the GE-based system for the characterization of expression kinetics.
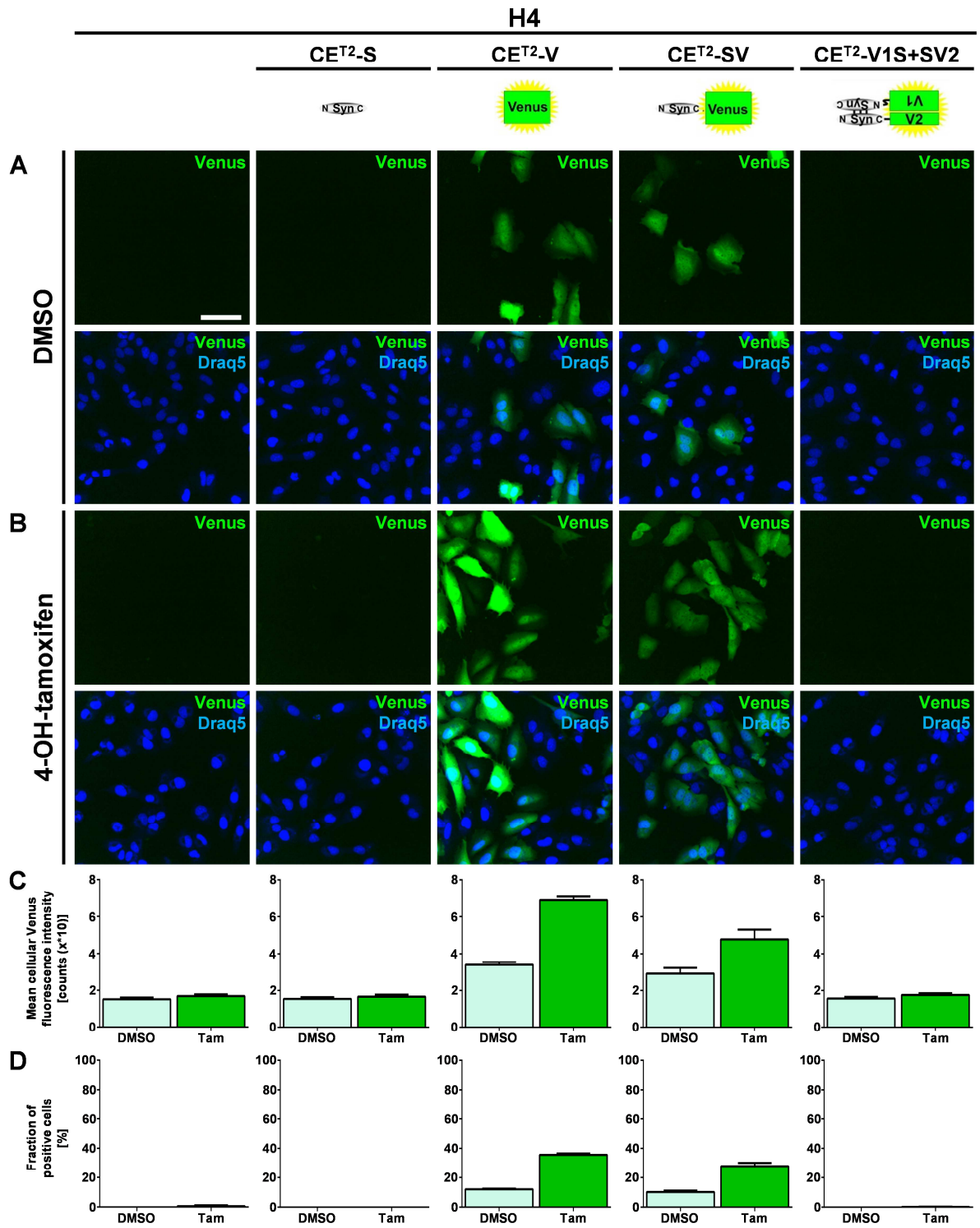
Figure 4-9: Induction of transgene expression in H4_CE^{T2} cells

Figure 4-9: Induction of transgene expression in H4_CE^T2 cells

The generated H4_CE^T2 cell lines were incubated with 0.1% DMSO or 10 μM 4-OH-tamoxifen for 48 h.

   A) Representative fluorescence images of cells incubated with 0.1% DMSO. Nuclei were stained with Draq5. Scale bar is 100 μm and valid for all panels in A and B.
   B) Representative fluorescence images of cells incubated with 10 μM 4-OH-tamoxifen.
   C) Quantification of the mean cellular Venus fluorescence intensity of H4 cells upon incubation with DMSO or 4-OH-tamoxifen using the Acapella® software. Bars show mean of 3 independent experiments; error bars show SEM; Tam: 4-OH-tamoxifen.
   D) Quantification of the fraction of Venus-positive H4 cells upon incubation with DMSO or 4-OH-tamoxifen using the Acapella® software. Quantification was performed by setting an arbitrary threshold for Venus fluorescence intensity. Bars show mean of 3 independent experiments; error bars show SEM; Tam: 4-OH-tamoxifen.

4.2.2.3 Expression Characteristics of H4_GE Cells – Cellular Fluorescence

In order to characterize the created cell lines regarding their transgene expression over time and as a function of tebufenozide concentration, all cell lines were incubated for up to 8 days post induction (DPI) with different tebufenozide concentrations ranging from 100 pM to 100 μM or DMSO as control, respectively.

No increase in mean cellular Venus fluorescence was observed in H4, H4_GE-S, or H4_mC_GE-S cells (Figure 4-10 A). In line with this, the fraction of positive cells remained 0% for all time points and tebufenozide concentrations evaluated in H4, H4_GE-S, or H4_mC_GE-S cells (Figure 4-10 B). Accordingly, no influence of tebufenozide concentration on fluorescence intensity could be observed in these cell lines (Figure 4-10 A, B, and visualized for day 5 in C).

On the contrary, the fluorescence signal increased in a tebufenozide concentration-dependent manner from day 0 on in H4_GE-V, H4_GE-SV, and H4_GE-V1S+SV2 cells (Figure 4-10 A).

In H4_GE-V cells, maximum fluorescence was obtained upon incubation with 1 μM tebufenozide on DPI 5 (Figure 4-10 A, C) with an increase from approximately 37.9 counts (for DMSO-treated cells on DPI 0) to 3,439.0 counts (all values are indicated after subtraction of background signal), equivalent to a 90.8-fold increase in fluorescence intensity following tebufenozide treatment. The fraction of positive cells increased from approximately 63% on DPI 0 (due to background fluorescence) to 100% 3-7 DPI for cells treated with 1 μM or 10 μM tebufenozide, while a maximum of about 89% of DMSO-treated cells were considered Venus-positive on DPI 5.

For H4_GE-SV cells, maximum fluorescence was obtained upon incubation with 10 µM tebufenozide on DPI 6 (Figure 4-10 A) with an increase from approximately 34.6 counts (for DMSO-treated cells at day 0) to 3,350.6 counts, equivalent to a 96.9-fold increase in fluorescence intensity following tebufenozide treatment. The fraction of positive cells increased from approximately 55% on DPI 0 (due to background fluorescence) to 100% 4-7 DPI for cells treated with 10 µM tebufenozide, while a maximum of approximately 88% of DMSO-treated cells was Venus-positive on DPI 5 (Figure 4-10 B).

In H4_GE-V1S+SV2 cells fluorescence intensity increased more slowly than in H4_GE-V and H4_GE-SV cells and reached its maximum on DPI 6 upon incubation with 10 µM tebufenozide (Figure 4-10 A) with an increase from approximately 0.4 counts (for DMSO-treated cells at DPI 0) to 520.5 counts, equivalent to an 1,240.7-fold increase in fluorescence intensity following tebufenozide treatment. The fraction of positive cells increased from approximately 1% on DPI 0 to 99% on DPI 5 and 6 for cells treated with 10 µM tebufenozide, while a maximum of approximately 15% of DMSO-treated cells was Venus-positive on DPI 5 (Figure 4-10 B).

For H4_GE-V, H4_GE-SV, and H4_GE-V1S+SV2 cells, fluorescence intensity increased with increasing tebufenozide concentrations in the range of 100 pM to 10 µM and decreased when cells were incubated with 100 µM tebufenozide (Figure 4-10 C).

For all cell lines the number of cells increased until DPI 4 or 5. No obvious effect on cell number was observed for all tebufenozide concentrations except for treatment with 100 µM tebufenozide where the number of cells was decreased in all cell lines.
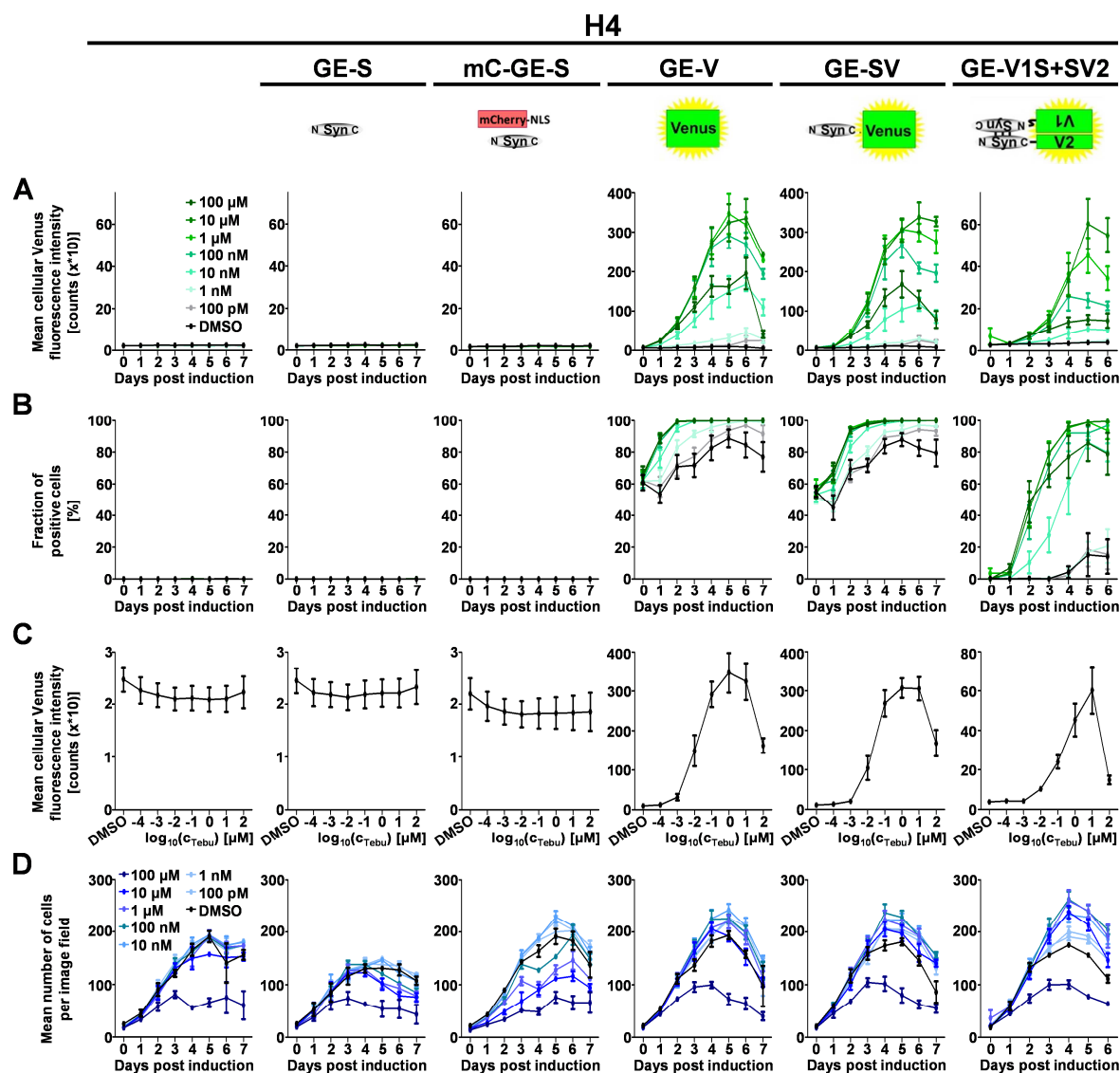
Figure 4-10: Expression characteristics of H4_GE cells – cellular fluorescence

H4 cell lines were incubated for up to 8 days with DMSO or with different tebufenozide concentrations ranging from 100 pM to 100 µM and imaged using the Opera® system. Quantification was performed using the Acapella® software.

A) Quantification of the mean cellular Venus fluorescence intensity of H4 cells upon incubation with DMSO or different concentrations of tebufenozide (color-coded).

B) Quantification of the fraction of Venus-positive H4 cells.

C) Quantification of the mean cellular Venus fluorescence intensity of H4 cells in dependence of the tebufenozide concentration using the dataset from A) at DPI 5.

D) Quantification of the number of cells per image field.

Data points show mean of 3-6 independent experiments; error bars show SEM.

4.2.2.4 Expression Characteristics of H4_GE Cells – Protein Amount Depending on Tebufenozide Concentration

In order to further characterize the cell lines regarding their transgene expression properties in dependence of the tebufenozide concentration, the cells were incubated for 4 days with different tebufenozide concentrations ranging from 10 nM to 10 µM or with DMSO as control, respectively. After 4 days cells were harvested, lysed and subjected to western blot analyses.

As expected, we observed no transgene expression in H4 cells (Figure 4-11 A).

For all transgene-expressing cell lines we observed very little background expression upon incubation with DMSO. In all cases, protein amounts increased with increasing tebufenozide concentration up to 1 or 10 µM (Figure 4-11 B, C).

Cell lines H4_GE-S, H4_mC_GE-S, and H4_GE-V showed the highest transgene expression after incubation with 10 µM tebufenozide, whereas maximum transgene expression in H4_GE-SV and H4_GE-V1S+SV2 was observed upon incubation with 1 µM tebufenozide. According to the quantification of western blot signal intensity we obtained a maximum increase in transgene expression compared to DMSO by a factor of 19.7 in H4_GE-S, 45.9 in H4_mC_GE-S, 5.1 in H4_GE-V, 7.0 in H4_GE-SV, and 10.0 in H4_GE-V1S+SV2 for SV2 expression. Concerning the expression of V1S in H4_GE-V1S+SV2 the factorial increase in transgene expression could not be evaluated since no background signal for treatment with DMSO was detected.
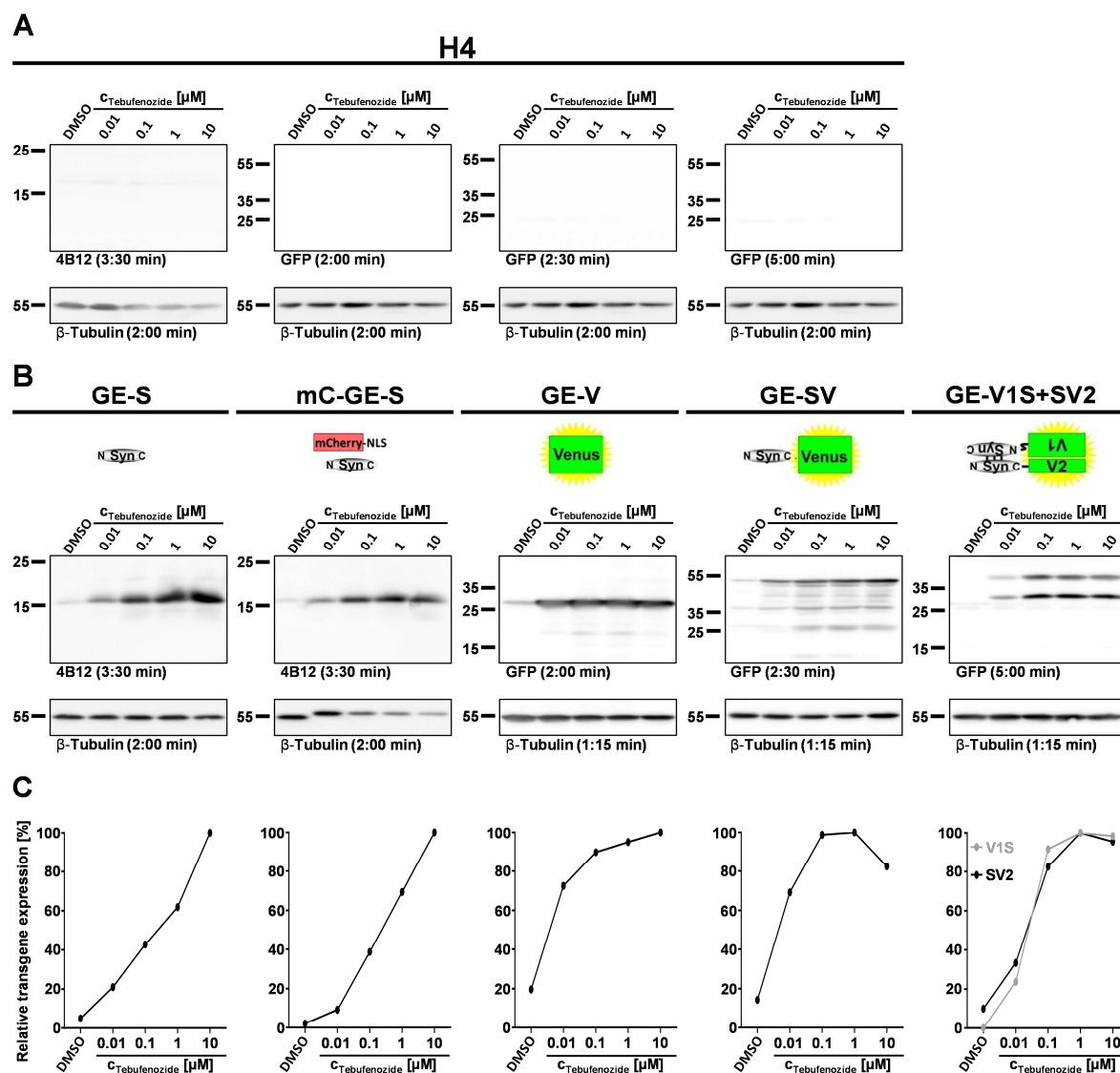
Figure 4-11: Expression characteristics of H4_GE cells – protein amount depending on tebufenozide concentration

H4 cell lines were incubated for 4 days with DMSO or different tebufenozide concentrations ranging from 10 nM to 10 µM. For all samples, expression of housekeeper β-tubulin was used as reference.

A) Control western blots of H4 cells were treated like the western blots of the corresponding samples and showed no expression of αSyn, Venus, SV, V1S, or SV2.

B) In all transgene expressing cell lines signal intensity increased with increasing tebufenozide concentration up to 1 µM or 10 µM for inducible transgenes.

C) Quantification of western blot signal intensity was performed using *ImageJ*. Signal intensity of transgenes was normalized to housekeeper signal (β-tubulin).

4.2.2.5 Expression Characteristics of H4_GE Cells – Kinetics of Protein Amount

In order to further characterize the cell lines regarding their expression kinetics according to protein levels, the cells were incubated for up to 5 days with 10 µM tebufenozide since 10 µM reached the highest transgene expression in most cell lines (see Figure 4-10 and Figure 4-11). Cells were harvested, lysed and subjected to western blot analyses on DPI 0, 1, 2, 3, 4, and 5.

As expected, no transgene expression was observed in H4 cells (Figure 4-12 A).

For all transgene expressing cell lines we observed very little background expression in the absence of tebufenozide (DPI 0). For all transgene expressing cells lines we observed an increase in protein amounts over time (Figure 4-12 B, C).

According to the quantification of western blot signal intensity we obtained a maximum increase in protein amount by a factor of 27.8 in H4_GE-S, 16.7 in H4_mC_GE-S, and 90.3 in H4_GE-V. For H4_GE-SV and H4_GE-V1S+SV2 the factorial increase in protein amounts could not be evaluated since no background signal was observed on DPI 0.
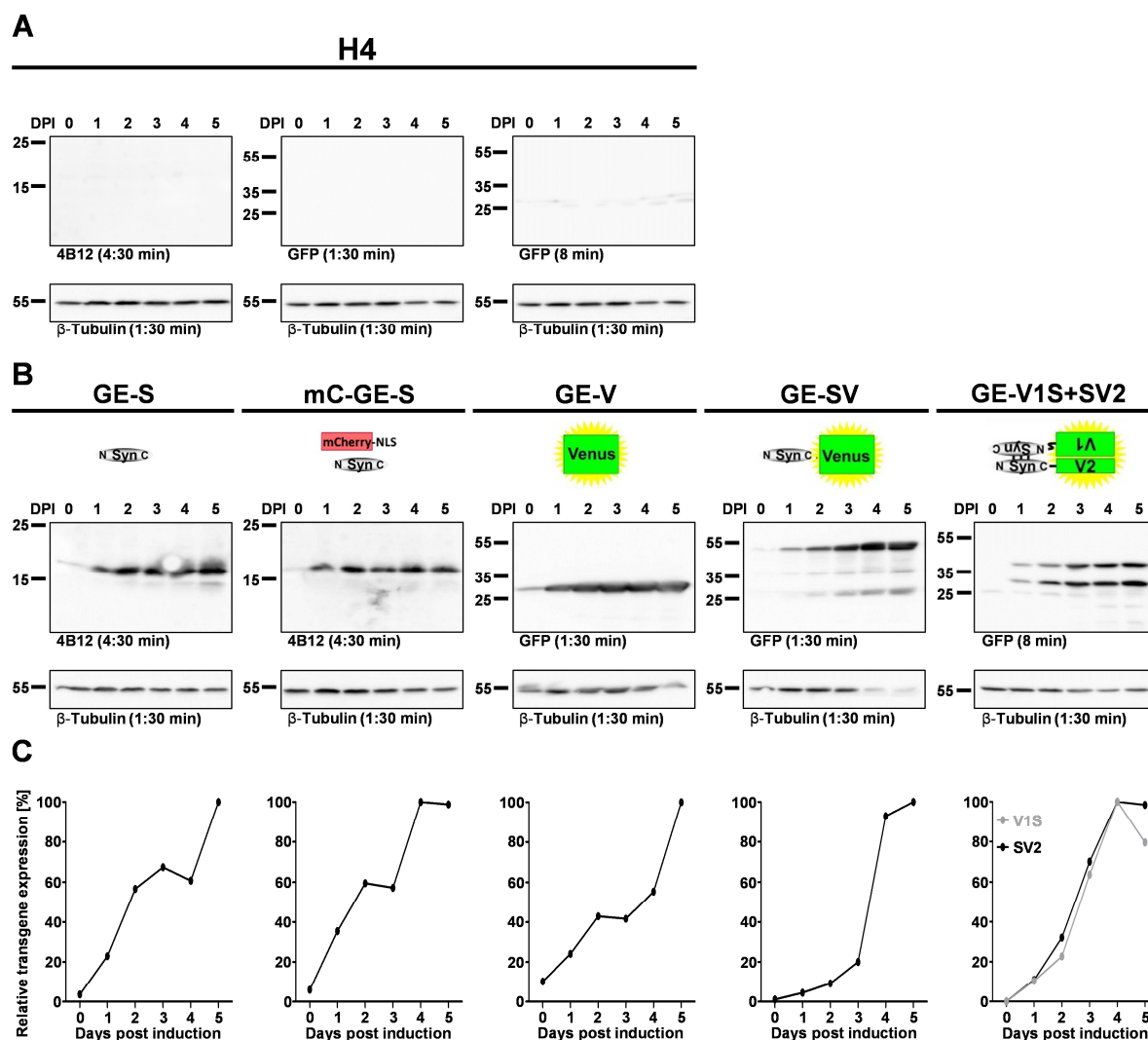
Figure 4-12: Expression characteristics of H4_GE cells – kinetics of protein amount

H4 cell lines were incubated with 10 µM tebufenozide for 0 to 5 days. For all samples, expression of housekeeper β-tubulin was used as reference.

A) Control western blots of H4 cells were treated like the western blots of the corresponding samples and showed no expression of αSyn, Venus, SV, V1S, or SV2.

B) In all transgene expressing cell lines signal intensity increased over time for inducible transgenes.

C) Quantification of western blot signal intensity was performed using *ImageJ*. Signal intensity of transgenes was normalized to housekeeper signal (β-tubulin).

4.3 Increased αSyn Aggregation upon Incubation with DMSO and Ferric Iron

DMSO and FeCl$_3$ have been shown to increase αSyn aggregation *in vitro*[144,145]. In order to investigate the effect of DMSO and ferric iron on αSyn aggregation in the H4_GE cell model, H4_GE-V1S+SV2 and H4_GE-V cells were incubated with different combinations of DMSO (ranging from 0.1% to 1.0%) and FeCl$_3$ concentrations (ranging from 0 µM to 1 mM) for 3 days. Transgene expression was induced with 10 µM tebufenozide in H4_GE-V1S+SV2 cells and with 10 nM tebufenozide in H4_GE-V cells for three days in order to reach comparable fluorescence intensities. After 3 days, cellular fluorescence intensity was determined using the Opera® setup.

We found an increase in fluorescence intensity with increasing DMSO and FeCl$_3$ concentrations in H4_GE-V1S+SV2 cells (Figure 4-13, A left) but not in H4_GE-V cells (Figure 4-13, A right). The increase in fluorescence intensity was most prominent for incubation with FeCl$_3$ compared to other tri-, di-, or monovalent metal ions (Figure 4-13, B).

To test if the observed increase in fluorescence intensity in the BiFC assay is due to αSyn aggregation, we also analyzed the effect of DMSO and ferric iron on protein amount of cells overexpressing variants of αSyn (H4_GE-S, H4_GE-SV, and H4_GE-V1S+SV2) compared to H4_GE-V cells overexpressing Venus. Since we observed many dead and rounded cells among both H4_GE-V1S+SV2 and H4_GE-V cells upon incubation with 1% DMSO and iron precipitation upon incubation with 1 mM FeCl$_3$, we chose the conditions 0.75% DMSO and 100 µM FeCl$_3$ versus 0.1% DMSO and 0 µM FeCl$_3$. Allcell lines were incubated for 3 days, then harvested and lysed. We observed an increase in protein amount in H4_GE-S, H4_GE-SV, and H4_GE-V1S+SV2 upon treatment with 0.75% DMSO and 100 µM FeCl$_3$ compared to incubation with 0.1% DMSO, while there was no striking effect on Venus protein amount in H4_GE-V cells (Figure 4-14 A).

Additionally, H4_GE-V1S+SV2 cells and H4_GE-V cells were analyzed using sucrose gradient centrifugation. For H4_GE-V1S+SV2 cells we observed higher molecular αSyn species (occurring in fractions with higher sucrose concentrations) when cells were treated with 0.75% DMSO and 100 µM FeCl$_3$ (Figure 4-14 B, left top) compared to cells treated with 0.1% DMSO (Figure 4-14 B, left bottom). In contrast, we found no difference between both treatments in H4_GE-V cells (Figure 4-14 B, right).

Taken together, this suggests that incubation with high concentrations of DMSO and FeCl$_3$ increases aggregation of αSyn in inducibly αSyn-overexpressing H4_GE cells.
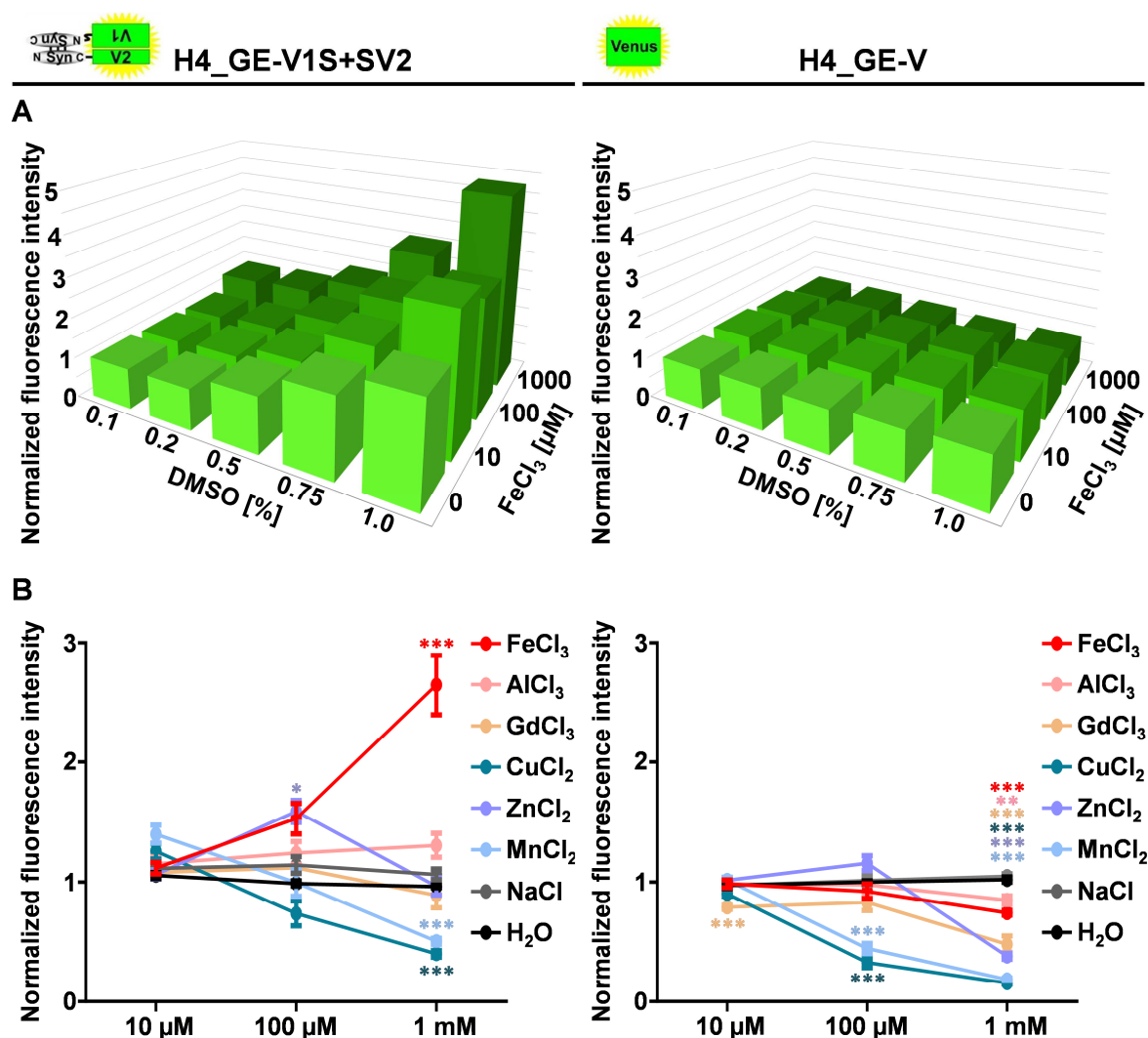
Figure 4-13: Increased fluorescence intensity in H4_GE-V1S+SV2 cells upon incubation with DMSO and FeCl$_3$

H4_GE-V1S+SV2 and H4_GE-V cells were incubated with 10 µM or 10 nM tebufenozide, respectively, and different concentrations of DMSO and tri-, di-, or monovalent ions for 3 days.

  A) Mean cellular Venus fluorescence intensity was increased upon incubation with higher DMSO and FeCl$_3$ concentrations in H4_GE-V1S+SV2 cells (left), but not in H4_GE-V cells (right). Bars show mean of three independent experiments.

  B) Fluorescence intensity increased upon incubation with FeCl$_3$ compared to other trivalent (AlCl$_3$, GdCl$_3$), divalent (CuCl$_2$, ZnCl$_2$, MnCl$_2$), or monovalent (NaCl) ions. All cells were co-incubated with 1% DMSO. Data points show mean of 8 to 9 independent experiments; error bars show SEM. *: p'<0.05; **: p'<0.01; ***: p'<0.001 (Student's t-test, Bonferroni corrected for multi-testing).
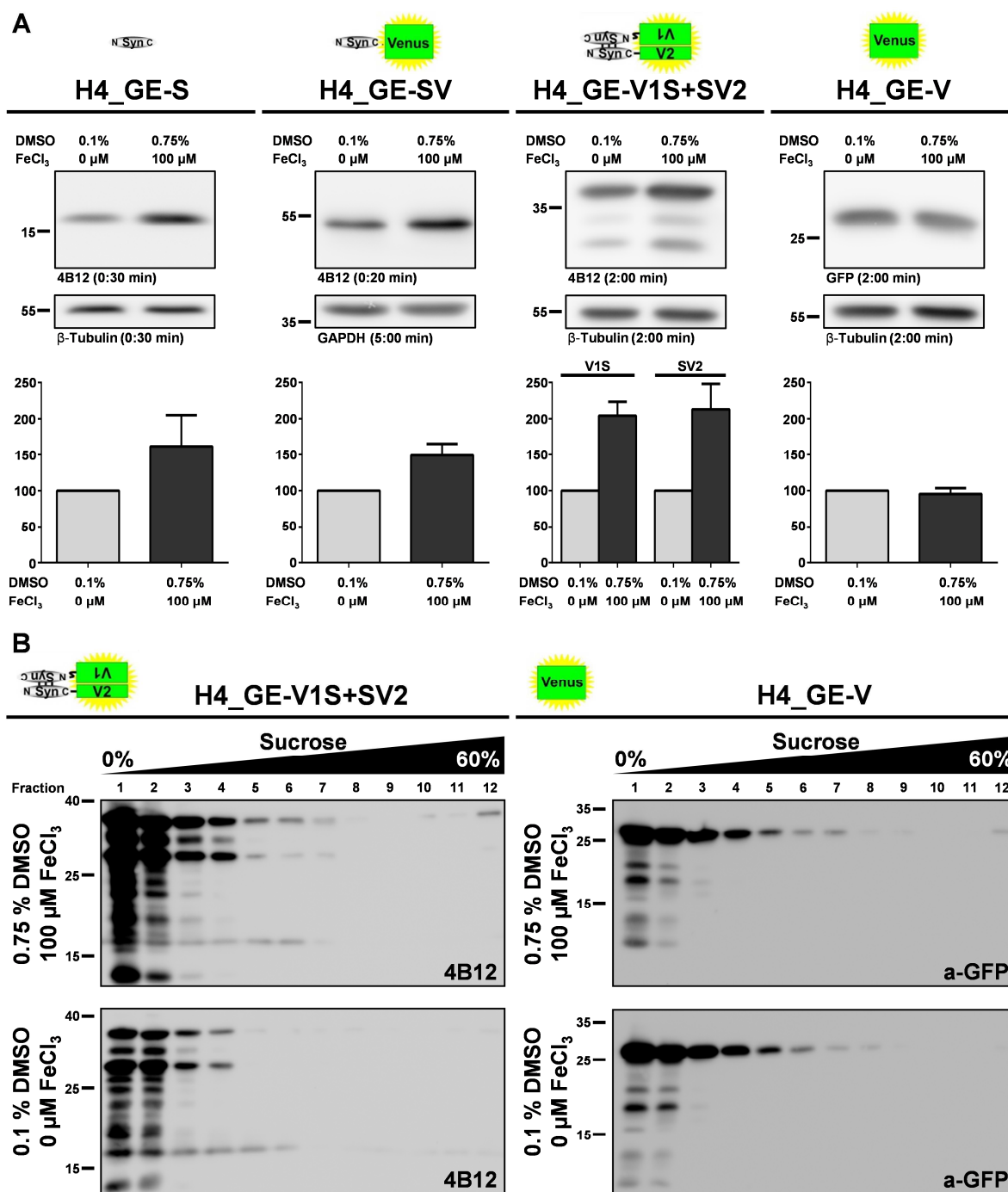
Figure 4-14: Increased protein amount and aggregation in αSyn-overexpressing H4_GE cells upon incubation with DMSO and FeCl$_3$

Figure 4-14: Increased protein amount and aggregation in αSyn-overexpressing H4_GE cells upon incubation with DMSO and FeCl₃

H4_GE-V1S+SV2 and H4_GE-V cells were incubated with 10 µM or 10 nM tebufenozide, respectively, and different concentrations of DMSO and FeCl$_3$ for 3 days.

    A) Protein amounts increased in cell lines overexpressing variants of αSyn but not in cells overexpressing Venus alone upon incubation with 0.75% DMSO and 100 µM FeCl$_3$. For quantification signals were normalized to housekeeper. Signals from samples treated with 0.1% DMSO were set to 100%. Bars show mean of 3 to 4 independent experiments and error bars show SEM.

    B) Western blots from cell lysates after sucrose gradient centrifugation of H4_GE-V1S+SV2 (left) and H4_GE-V cells (right) incubated with 0.75% DMSO and 100 µM FeCl$_3$ (top) or 0.1% DMSO and 0 µM FeCl$_3$ (bottom).

4.4 Establishment and Characterization of Inducibly αSyn Overexpressing LUHMES Cells

4.4.1 Transgene Expression in 75% of LUHMES Cells After Lentiviral Transduction

In order to obtain as many transgene expressing LUHMES cells as possible we first tried to apply the same protocol that was used for the establishment of the stable H4 cell lines (Figure 4-6 A, protocol D). Since all LUHMES cells were dead 24 h after transduction, we next tested three different transduction protocols to create stable LUHMES cell lines (see chapter 3.8.2.1). For this, LUHMES cells were transduced with the constitutive GAL4 driver virus (V99) and the UAS-Venus receiver virus (V43). After imaging the fraction of Venus-positive cells was determined manually using *ImageJ* (Figure 4-15). Using protocol A a fraction of 36% of Venus-positive cells was obtained (Figure 4-15 A). Protocol B led to a fraction of 63% (Figure 4-15 A, B) and protocol C to a fraction of 75% of Venus-positive cells (Figure 4-15 A).

As for the inducible H4 cells, we next created the following inducible LUHMES cell lines following protocol C:

- LUHMES_GE-S: showing inducible overexpression of αSyn (transduction with V100 and V42)
- LUHMES_mC_GE-S: showing constitutive expression of mCherry coupled to a nuclear localization sequence (NLS), resulting in red fluorescence in the nucleus of positively transduced cells, and inducible overexpression of αSyn (transduction with V100 and V120)
- LUHMES_GE-V: showing inducible overexpression of Venus (transduction with V100 and V43)
- LUHMES_GE-SV: showing inducible overexpression of αSyn coupled to Venus (transduction with V100 and V41)
- LUHMES_GE-V1S+SV2: showing inducible expression of the N-terminal part of Venus coupled to αSyn (V1S) and of αSyn coupled to the C-terminal part of Venus (SV2) (transduction with V100, V39, and V46)

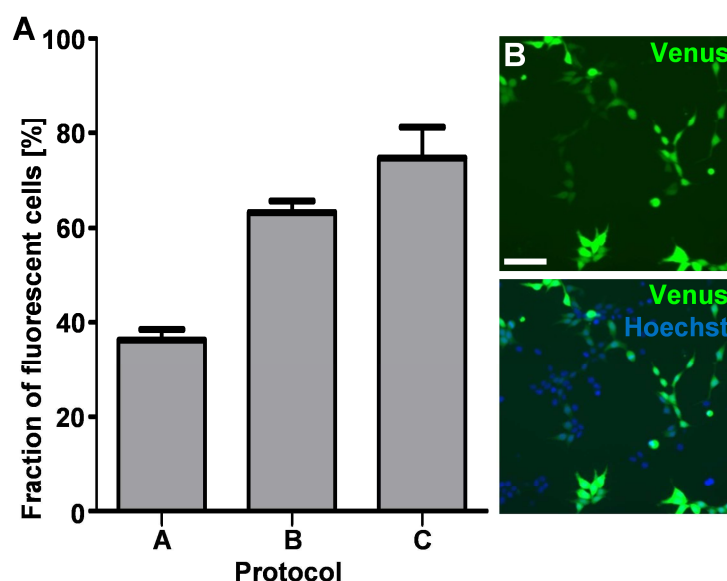Each LUHMES cell line was transduced four times with each virus.

Figure 4-15: Highly efficient transduction of LUHMES cells following protocol C

LUHMES cells were transduced with the constitutive GAL4 driver virus (V99) and the UAS-Venus receiver virus (V43) according to protocols A-C (see chapter 3.8.2.1). Nuclei were stained with Hoechst33342.

A) Quantification of the fraction of Venus-positive cells. Columns show mean of 4 to 5 wells. Error bars show SEM. At least 380 cells were counted for each protocol.

B) Representative images obtained for protocol B. Scale bar is 100 µm and valid for both panels.

4.4.2 Characterization of the Inducibly αSyn-Overexpressing LUHMES Cells

4.4.2.1 Increased Transgene Expression upon Incubation with Tebufenozide in all LUHMES_GE Cell Lines

LUHMES cell lines were incubated with differentiation medium for 48 h. Afterwards, cells were incubated with differentiation medium supplemented with DMSO or 10 µM tebufenozide for 4 days.

As expected, no effect of tebufenozide neither on fluorescence (Figure 4-16 A-C) nor on protein expression (Figure 4-16 D) was observed in LUHMES cells.
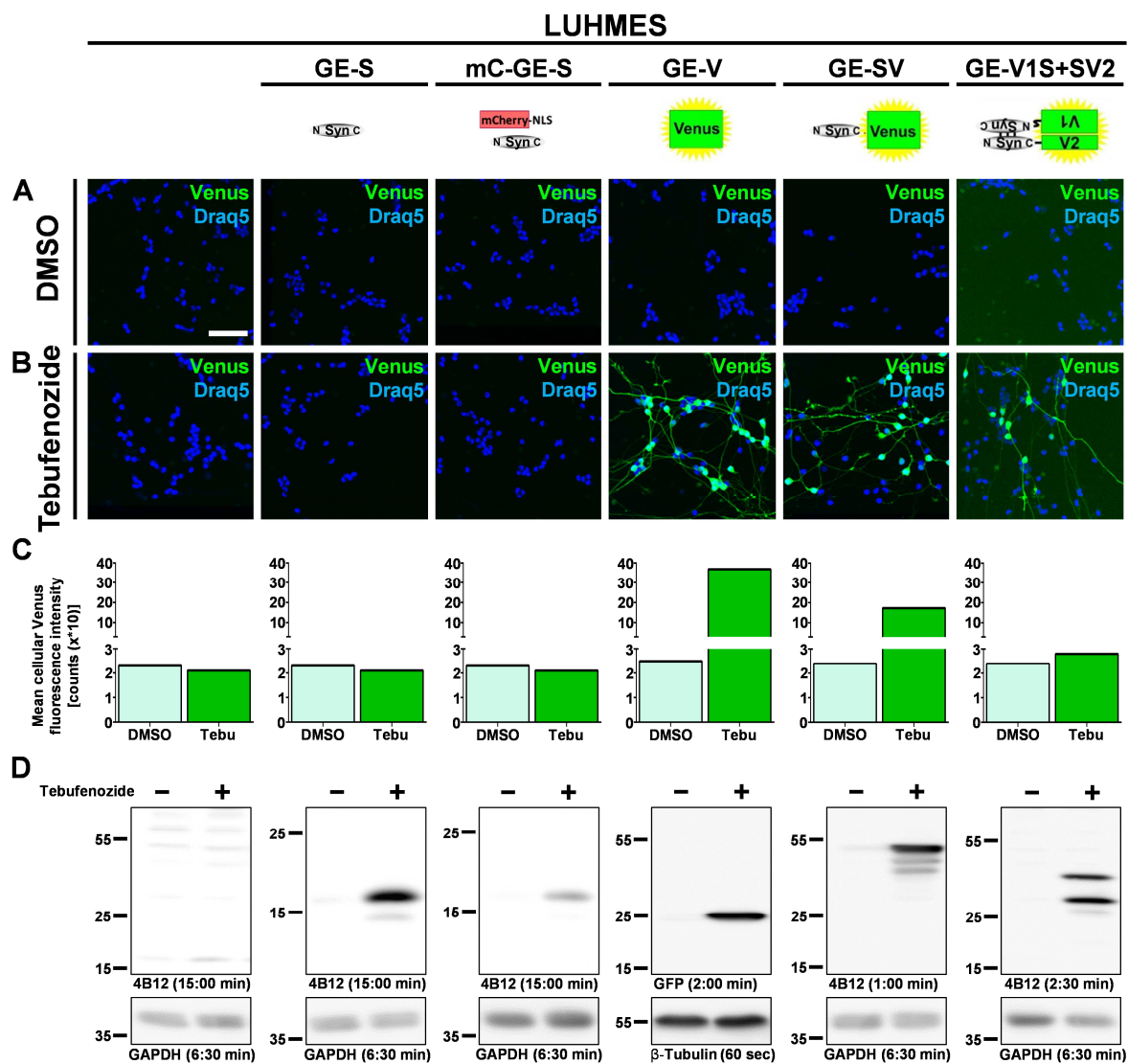
Figure 4-16: Induction of transgene expression in LUHMES_GE cells

LUHMES cell lines were incubated with differentiation medium for 48 h. Afterwards cells were incubated with differentiation medium supplemented with DMSO or 10 µM tebufenozide for 4 days.

A) Fluorescence images of cells incubated with 0.1% DMSO. Nuclei were stained with Draq5. Scale bar is 100 µm and valid for all panels in A and B.

B) Fluorescence images of cells incubated with 10 µM tebufenozide.

C) Quantification of the mean cellular Venus fluorescence intensity of LUHMES cells upon incubation with DMSO or tebufenozide using the Acapella® software. Tebu: tebufenozide.

D) Western blot analysis of protein levels in LUHMES cells upon incubation with tebufenozide or DMSO. All LUHMES_GE cell lines showed an increase in protein levels upon incubation with tebufenozide.

Data were obtained from one single experiment.

For LUHMES_GE-S and LUHMES_mC_GE-S cells, tebufenozide showed no effect on fluorescence intensity (Figure 4-16 A-C). While LUHMES_GE-S cells showed a faint αSyn band in the western blot in the absence of tebufenozide (Figure 4-16 D), no background expression could be detected in LUHMES_mC_GE-S cells (Figure 4-16 D). In both cell lines expression of αSyn increased upon incubation with tebufenozide.

Both in LUHMES_GE-V and LUHMES_GE-SV cells we observed neither background fluorescence (Figure 4-16 A) nor protein expression (Figure 4-16 D) upon treatment with DMSO, but fluorescence quantification revealed a faint increase in mean cellular Venus fluorescence (Figure 4-16 C). Transgene expression increased dramatically upon incubation with tebufenozide (Figure 4-16 B-D).

For LUHMES_GE-V1S+SV2 cells we detected no background expression of V1S or SV2 (Figure 4-16 A, C, D). Upon incubation with tebufenozide, fluorescence increased only slightly (Figure 4-16 B, C), whereas protein expression was markedly increased (Figure 4-16 D).

5 Discussion

5.1 Development of Stable Inducible Cell Lines – Original Strategy, Problems and Troubleshooting

5.1.1 Development of Viruses for the Overexpression of Various αSyn Constructs Using the GE System or the CE[T2] System

This thesis presents the development of H4 and LUHMES cells that stably and inducibly overexpress different constructs, namely: wt αSyn (S), the YFP variant Venus (V), αSyn coupled to Venus (SV), the N-terminal part of Venus coupled to αSyn (V1S), and αSyn coupled to the C-terminal part of Venus (SV2), where the co-expression of V1S and SV2 can be used for a bimolecular fluorescence complementation assay (BiFC). BiFC systems have been widely used to study protein-protein interactions in general[207,293] and oligomerization of αSyn in particular[213,294].

In order to stably insert the expression machinery into host cells, we produced lentiviruses to deliver both the expression driver (GAL4_EcR and Cre_ER[T2], respectively) and the receiver (UAS-GOI and loxP-GOI, respectively) for the inducible system. We decided to use the GAL4_EcR-UAS (GE) system and the Cre_ER[T2]-loxP (CE[T2]) system for inducible expression in our cell lines since differentiation of LUHMES cells relies on a Tet-OFF system. For this reason, we had to concentrate on inducible systems that do not use tetracycline as agonist or antagonist in order to be able to induce expression independent of differentiation. Both the GE and the CE[T2] system were kindly provided by the Lichtenthaler group.

The GAL4-UAS system has been used extensively for tissue-specific transgene expression in *Drosophila melanogaster* and zebrafish[254,295,296]. In these model systems, GAL4 is typically expressed under control of a tissue-specific promoter in order to achieve tissue-specific transgene expression. The GOI is expressed under the control of a minimal promoter which is controlled by a UAS. Thus, expression of the GOI depends on binding of GAL4 to the UAS. The existence of various driver lines expressing GAL4 in specific tissues and various receiver lines expressing different GOIs enables the creation of transgenic animals by breeding of distinct driver and receiver lines. This results in the expression of the GOI in a distinct tissue due to mendelian recombination.

In 2007, Esengil *et al.*[255] developed an inducible expression system based on the GAL4-UAS system. For this system, the DNA-binding and homodimerization domains of GAL4 (a yeast transcription factor) was coupled to a modified subset of the activation domain of the herpes

simplex virus regulatory protein VP16 and the ligand binding domain of the ecdysone receptor (EcR) of *Bombyx mori*. Ecdysone is an insect steroid hormone without known effects on vertebrate cells[256-258]. In this system, incubation with an ecdysone agonist, called tebufenozide, leads to translocation of GAL4-EcR from the cytoplasm into the nucleus[255]. Consequently, expression of a transgene located downstream of a UAS is induced.

The Cre-loxP system[259,297,298] from bacteriophage P1 is widely used for tissue-specific gene knockdown or gene expression and especially popular for studies in mice, where a great variety of Cre driver lines is available. It consists of the enzyme Cre recombinase which catalyzes recombination of DNA between specific recognition sequences called loxP sites. Similar to the GAL4-UAS system, the Cre recombinase can be expressed under the control of a tissue-specific promoter for tissue-specific gene expression or knockout. For gene knockout the GOI is surrounded by two loxP sites, i.e., it is floxed, and located downstream of a constitutively active promoter. In cells that express Cre recombinase the GOI and one of the loxP sites will be excised resulting in knockdown of the expression of the GOI.

For expression of a specific GOI it is located downstream of a constitutively active promoter and a floxed spacer gene carrying a termination codon. In the absence of Cre recombinase the GOI will not be expressed due to the termination codon. In Cre recombinase-expressing cells the spacer gene will be excised resulting in expression of the GOI[299].

For tissue and time-specific transgene expression, Cre recombinase was coupled to a mutated ligand-binding domain of the estrogen receptor (ER^{T2}) which showed highest binding affinity not for estrogen but for tamoxifen[260]. Upon binding of tamoxifen to ER^{T2}, Cre_ER^{T2} is translocated to the nucleus where Cre recombinase interacts with the loxP sites[300]. For time-specific expression mice can be injected intraperitoneally (i.p.) with tamoxifen. Interestingly, this is also possible for embryonic gene expression when pregnant animals are treated with tamoxifen[301]. Time-specific gene knockout or expression is of special interest for the investigation of developmental processes or proteins with lethal phenotypes at early developmental stages.

In vivo, tamoxifen is metabolized to several products with 4-OH-tamoxifen displaying greater affinity for the estradiol receptor than tamoxifen and showing the most potent antiestrogenic effect[302-304]. Thus, for cell culture experiments, the addition of 4-OH-tamoxifen is preferable, yet hampered by its low stability. Recently, endoxifen has been proposed as a potential alternative compound[305].

After cloning of the desired constructs, we created lentiviruses for both the GE system and the CE^{T2} system. Next, we established a protocol for an effective transduction of H4 cells resulting in

long-term stable gene expression (Figure 4-6). Inducible H4 cell lines relying on both induction systems (H4_GE cells and H4_CE[T2] cells) were created. After testing both systems we concentrated on the GE system since we obtained higher transgene inducibility in pilot experiments (18.6-fold vs. 2.9-fold for Venus, and 6.8-fold vs. 2.4-fold for Syn-Venus) (Figure 4-7, Figure 4-9). Moreover, this system holds the benefit that transgene expression can be turned on and off again, whereas the CE[T2] system cannot be turned off once the floxed gene has been excised. However, lentiviruses for both expression systems were developed and will immediately be available for further studies, allowing the production of inducible αSyn overexpression models in short time. Possible applications include the production of diverse cell lines to study different synucleinopathies. Exemplarily, αSyn deposition was observed in astroglial cells in patients suffering from dementia with Lewy bodies (DLB). Moreover, oligodendroglial cells could represent an interesting model for multiple system atrophy (MSA), where glial cytoplasmic inclusions (GCIs or Papp-Lantos bodies) represent the histopathological hallmark[306]. We have recently started a collaboration to test different strategies against αSyn-mediated toxicity individually and in combination in several cell culture and animal models. For this, we created an inducible oligodendroglial cell line based on MO3.13 cells using the GE system.

Moreover, the system for the development of stable cell lines that inducibly overexpress a certain protein of interst upon incubation with a chemical agonist could easily be adjusted for the investigation of other disease-associated proteins or peptides like tau[307] or amyloid-beta[308] and other cell lines.

Apart from cell culture applications, especially the loxP-GOI receiver virus might be interesting for the inoculation of animals expressing Cre or Cre_ER[T2] in dopaminergic neurons or for primary neuron cultures from such animals. To a lesser extent, this might also be true for the UAS-GOI receiver in GAL4 expressing animal models.

5.1.2 Individual Insertion of V1S and SV2 by Separate Lentiviruses

Ideally, equimolar expression of the V1S and SV2 construct for the BiFC assay would be desirable. Therefore, we decided to couple the V1S and SV2 constructs in a first attempt via a 2A sequence since 2A sequences have been shown to display quite stoichiometric expression of the upstream and downstream transgene, whereas IRES sequences typically show a decreased expression of the downstream transgene[264]. When two genes are linked via a 2A sequence both genes and the embedded 2A sequence are transcribed as one mRNA. During translation in the ribosome the 2A sequence causes a tilt in the nascent polypeptide chain which leads to ribosomal skipping of a peptide bond[267]. This should result in the occurrence of two separate proteins from one mRNA both of which carry a short peptide tag resulting from the 2A sequence[265].

Several 2A sequences from different organisms have been established. Here, we decided to use a P2A sequence from teschovirus-1 since it showed the best separation properties in different model systems including HEK293T, HT1080, and HeLa cells compared to other 2A sequences. Importantly, Kim *et al.*[265] observed very low amounts of "uncleaved" protein in HEK293T cells when using a P2A sequence. Unfortunately, in our hands and in an experimental setup where we transiently transfected HEK293T cells with SV2-P2A-V1S we observed incomplete separation of V1S and SV2 in the western blot (Figure 4-2) with great inter experimental variation in separation efficiency. This controversial observation might be due to different amounts of expressed protein or an influence of the flanking proteins on P2A-mediated cleavage efficiency itself. Consequently, we discarded the P2A sequence and transduced the cells with lentiviruses carrying V1S or SV2 individually.

5.1.3 No Improvement of Signal-to-Noise Ratio by the Insertion of Point Mutations into V1 and V2

Self-assembly of Venus fragments and resulting background fluorescence is commonly observed in BiFC assays. At the beginning of this thesis, no study had evaluated the signal-to-noise ratio of an αSyn-hemi-Venus-based BIFC (to the best of our knowledge). However, while the present work was in progress, Eckermann *et al.*[99] postulated a signal-to-noise ratio in an αSyn-hemi-Venus BiFC of approximately 2-10, whereas we observed a signal-to-noise ratio in the range of 1.5 (Figure 4-4). However, the signal-to-noise ratio might depend greatly on the strength of transgene expression and on the cell culture model used, with H4 cells displaying a particularly low signal-to-noise ratio[99].

In order to improve the signal-to-noise ratio in Venus-based BiFCs several point mutations have been described mainly located at the interface of the Venus fragments[251]. The rational is a replacement of hydrophobic amino acids with neutral amino acids in order to reduce self-complementation tendencies due to hydrophobic interactions.

For the C-terminal Venus fragment, Nakagawa *et al*. observed a maximum increase in the signal-to-noise ratio of 4.2-fold for the mutation L201V upon transfection into mouse C3H10T1/2 cells whereas the mutation L207V yielded a 3.0-fold increase[285]. For the N-terminal Venus fragment, Kodama *et al*.[283] described an increase in the signal-to-noise ratio of approximately 4-fold for the mutations V150L and I152L upon transfection of COS-1 cells. Here, the N-terminal Venus fragment was coupled to the bZIP domain of c-Jun (bJun) and the C-terminal Venus fragment was coupled to the bZIP domain of c-Fos (bFos). For the negative control, the C-terminal Venus fragment was coupled to a mutant version of bFos (ΔbFon). For both mutations an increase in signal-to-noise ratio has also been described by Lin *et al*.[286], and an 8.6-fold increase has been described for V150A[285]. Since the overall fluorescence intensity was markedly reduced when inserting the mutation of V150L compared to I152L[283] we decided to test the mutation I152L in our BiFC system.

We inserted the point mutations I152L into V1[283] and L201V into V2[285] and transiently transfected H4 cells with different combinations of $V1_{wt}(S)$, $SV2_{wt}$, $V1_{I152L}(S)$, and $SV2_{L201V}$. 48 h after transfection, cells were imaged or harvested and cell lysates were analyzed using the Insight™ Reader. While we observed a decrease in total fluorescence intensity when using mutated Venus fragments compared to wt Venus, signal-to-noise ratio was not dramatically affected (Figure 4-4).

Thus, in our hand in this experimental setup, the insertion of point mutations I152L and L201V into the Venus fragments showed no noteworthy effect on signal-to-noise ratio which is in contrast to the observations by Nakagawa *et al*.[285], Kodama *et al*[283]., and Lin *et al*.[286]. This might be due to different amounts of expressed protein or to the usage of different cell lines since it has been described that the signal-to-noise ratio of BiFC assays is affected by the applied cell line[99]. Moreover, expression levels and the subcellular localization of the protein connected to the Venus fragments might affect the amount of their self-complementation tendencies.

5.2 Characterization of H4 Cells

5.2.1 Highly Efficient and Stable Lentiviral Transduction in H4 Cells

In order to obtain a high fraction of transgene expressing H4 cells, we tested different transduction protocols using a constitutive GAL4 driver virus and the UAS-SV receiver virus. In the best case – for protocol D – we obtained approximately 98% transgene expressing cells 72 h after transduction. We monitored the cells until 23 days after transduction and observed no significant change in the fraction of Venus-positive cells. However, we observed a trend towards a decrease in transgene expressing cells at day 23 which might be due to epigenetic events resulting in gene silencing[309]. This effect might depend on the promoter employed: Following lentiviral transduction, Oberbek *et al.* observed a decrease of GFP-positive Chinese hamster ovary (CHO) cells using a human cytomegalovirus (CMV) major immediate early promoter/enhance after 2 to 3 weeks, whereas the fraction of positive cells was stable when applying a human elongation factor-1α (EF-1α) promoter[262].

In order to minimize interexperimental variations of cellular characteristics we applied a strategy where we obtained 300 batches of cells with theoretically identical properties for all cell lines. Since a new batch is used for every single experiment, a stable transgene expression over a time-course of 23 days appears to be sufficient. Indeed, for the experiments presented in this work, cells were in culture for less than 13 days.

After production of stable H4_GE cell lines following protocol D, we obtained almost 100% of transgene expressing cells for all cell lines that express fluorescence proteins (H4_mC_GE-S (Figure 4-7 D), H4_GE-V, H4_GE-SV, and H4_GE-V1S+SV2 (Figure 4-10 B)). Thus, it is likely that we also obtained a very high fraction of αSyn-expressing cells in the H4_GE-S cell line, although this has not been shown yet. Immunohistochemical stainings using αSyn-specific antibodies will have to be performed in order to determine the fraction of αSyn-overexpressing cells in the H4_GE-S cell line.

5.2.2 Induction of Transgene Expression in a Time- and Tebufenozide Concentration-Dependent Manner

In order to characterize the cell lines concerning their transgene expression, we used the Opera® system and western blot analyses. The Opera® system is a fully automated confocal fluorescence microscope. In order to quantify fluorescence intensities we developed a script for the Acapella® evaluation software. This software enables – among other readouts – the determination of the mean cellular fluorescence intensity, the fraction of positive cells (by using an arbitrary threshold for fluorescence intensity), and the number of cells.

We incubated the different cell lines with different tebufenozide concentrations ranging from 100 pM to 100 µM for 8 days and imaged the cells every 24 h (Figure 4-10). We found that mean cellular fluorescence intensity showed a maximum at day 5 or 6. This corresponds to the data obtained from the western blot evaluation of expression kinetics (Figure 4-12). Interestingly, the fluorescence intensity and the fraction of positive cells increased more slowly in the H4_GE-V1S+SV2 cells compared to H4_GE-V or H4_GE-SV cells, while protein amounts increased in a comparable fashion. This might be due to the fact that a detectable fluorescence signal in the BiFC system requires not only expression of a fluorescence protein but also nucleation of αSyn aggregation. This is further supported by investigation of the expression kinetics of H4_GE-V1S+SV2 cells. While they showed a rather exponential increase in fluorescence intensity over time (Figure 4-10 A) protein amounts of V1S and SV2 increased rather linearly (Figure 4-12 B, C).

Furthermore, we found that fluorescence intensity was dependent on tebufenozide concentration. These data are in line with our investigation of protein amounts increasing with tebufenozide concentration using western blot analysis (Figure 4-11). Our results correspond to the expression kinetics in zebrafish embryos published by Esengil *et al.*[255] where transgene expression increased in a tebufenozide-dependent manner upon incubation with 1 nM to 10 µM tebufenozide. The decreased fluorescence intensity observed when incubating cells with 100 µM tebufenozide can most likely be explained by precipitation of tebufenozide.

For H4_GE-S, H4_mC_GE-S, H4_GE-V, and H4_GE-SV cell lines we found low background expression in the absence of tebufenozide by fluorescence microscopy (Figure 4-7 A, B), quantification of fluorescence intensity (Figure 4-7 C and Figure 4-10 A) and western blot analysis (Figure 4-11 and Figure 4-12). For H4_GE-V1S+SV2 almost no background expression could be observed compared to untreated H4 cells.

The dynamic range and the increase in transgene expression are important aspects for inducible cell lines. The results we obtained for induction of transgene expression showed great variation and are summarized in Table 5-1.

For all cell lines the number of cells increased until day 4 or 5 after induction (Figure 4-10). The following decrease in cell number is probably due to the experimental setup where we seeded the cells at a concentration of 50,000/ml on day 0 and incubated them without splitting them or changing the medium until the end of the experiment. Thus, it is likely that cell growth was hampered by a depletion of nutrients and an increasing pH.

After our cell lines had been established, Moussaud *et al.* published a paper in which they described the development of a comparable model for inducible expression of αSyn in H4 cells[206]. For their model, they stably inserted the different αSyn constructs using the Flp-FRT recombinase in combination with a tetracycline-driven bidirectional expression system, thus enabling the inducible transgene expression via a Tet-Off system. In this system, presence of tetracycline inhibits the expression of the transgene, whereas removal of tetracycline induces transgene expression.

In their study, two kinds of protein fragment complementation assays are used to investigate αSyn aggregation: Like in the thesis presented here, their first model uses a fluorescence readout and relies on complementation of hemi-Venus constructs (V1S and SV2). The second model requires a bioluminescence readout. Here, αSyn is coupled to the C-terminal or N-terminal part of *Gaussia princeps* luciferase (SL1 and SL2). Upon aggregation of αSyn the luciferase parts complement. In the presence of luciferin and ATP, luciferase catalysis a multistep reaction resulting in the emission of light. The luminescence intensity should be approximately proportional to αSyn aggregation. For both systems they used Leucine zipper-linked protein complementation (V1Lz and LzV2, or LzL1 and LzL2, respectively) as positive control. Additionally, they produced H4 cells which inducibly overexpressed wt αSyn.

Table 5-1: Relative increase in transgene expression

This table summarizes the relative increase in transgene expression according to change in fluorescence intensity or protein amount. WB: western blot

		Fold increase in fluorescence (Figure 4-10)	Fold increase in WB signal (Figure 4-11)	Fold increase in WB signal (Figure 4-12)
H4_GE-S		-	19.7	27.8
H4_mC_GE-S		-	45.9	16.7
H4_GE-V		90.8	5.1	90.3
H4_GE-SV		96.9	7.0	no background
H4_GE-V1S+SV2	V1S	1,240.7	no background	no background
	SV2		no background	10.0

A reliable comparison of the characteristics of the cell lines produced by Moussaud *et al.* and ours would require the investigation of both kinds of cell lines in parallel under equal conditions and is difficult from published data alone. However, the strategy applied by Moussaud *et al.* holds two fundamental disadvantages compared to our strategy: First, the stable insertion of the induction system relies on transient plasmid transfection, but a variety of established cell lines (including LUHMES cells) and primary cell lines are rather insusceptible to transient transfection with plasmids[1]. Second, the induction of transgene expression relies on presence or absence of tetracycline in a Tet-Off system. Thus, independent transgene induction cannot be achieved in model systems where a Tet-On or Tet-Off system is used for inducible expression of other proteins. This is for example the case in LUHMES cells where addition of tetracycline turns off the expression of *v-myc* and by this induces their differentiation to dopaminergic neurons[235,236].

Moussaud *et al.* observed low background transgene expression in the presence of tetracycline. Transgene expression was detectable from 16 h after removal of tetracycline on using western blot analysis. Transgene expression increased over time and reached a maximum 4 days after removal of tetracycline. Expression was not monitored from that time on[206]. In our cells, we did not investigate transgene expression before 24 h after induction. Like Moussaud *et al.* we observed low background expression and an increase in transgene expression over time, reaching a maximum 4 to 6 days after induction (Figure 4-10, Figure 4-12).

Interestingly, Moussaud *et al.* observed αSyn immunoreactivity in H4 V1S&SV2 cells which did not display Venus fluorescence suggesting the presence of monomeric αSyn[206]. This is in line

with our findings that expression of V1S and SV2 increased faster than fluorescence intensity in H4_GE-V1S+SV2 cells (Figure 4-10, Figure 4-12). One explanation is that the probability of nucleation increases with increasing amounts of αSyn and that a certain threshold of αSyn monomers might be required in order to induce a sufficient amount of oligomeric αSyn species to be detectable via BiFC.

Additionally, Moussaud *et al.* found that protein tags for the protein complementation assay (PCA) do neither interfere with the normal cellular distribution of αSyn nor with the polymerization of αSyn. Yet, αSyn half-life and oligomer stability appeared to be increased in the H4 V1S&SV2 cells which might be due to an irreversibility of Venus fragment complementation[206,209,214,310]. Moreover, using the H4 V1S&SV2 cells they performed a preliminary screening for anti-aggregative compounds using an EnVision multilabel HTS plate reader (PerkinElmer) and concluded that the fluorescent αSyn PCA can be used as high-throughput primary assay to screen large libraries[206]. This is in line with our experiments to screen for anti-aggregative compounds (Figure 4-5) and aggregation enhancers (Figure 4-13). All in all, the paper by Moussaud *et al.* further supports the relevance of BiFC-based inducible αSyn cell models as valuable tools in drug discovery for PD.

5.3 Increased αSyn Aggregation upon Incubation with DMSO and FeCl$_3$

Iron has been discussed extensively and controversially as possible risk factor for the development of PD[133,311]. Elevated levels of iron (and other metal ions) have been described in the SN of PD patients when compared to control tissue[135,137,138,312] at least in severely affected individuals[313]. High iron levels were also observed in Lewy bodies of the SN of PD patients[314] and several epidemiological studies describe a correlation between the exposure towards iron (and other heavy metals) and an increased risk for PD[311,315,316].

In order to investigate the effect of DMSO and ferric iron on αSyn aggregation in cell culture, we induced transgene expression in H4_GE-V1S+SV2 and H4_GE-V cells and incubated them with different concentrations of DMSO (ranging from 0.1% to 1.0%) and FeCl$_3$ (ranging from 0 μM to 1 mM) (Figure 4-13). DMSO concentration cannot be decreased to 0% since tebufenozide, the inducer of transgene expression, is dissolved in DMSO. In H4_GE-V1S+SV2 cells, fluorescence intensity increased considerably upon incubation with 1.0% DMSO even in the absence of FeCl$_3$, whereas incubation with different concentrations of FeCl$_3$ without additional DMSO did not markedly influence fluorescence intensity. The strongest increase in fluorescence intensity was

observed for the combination of DMSO and $FeCl_3$, reaching a maximum upon incubation with 1% DMSO and 1 mM $FeCl_3$.

In contrast, fluorescence intensity was not affected by incubation with DMSO or $FeCl_3$ in H4_GE-V cells, suggesting that the effect on fluorescence intensity observed in H4_GE-V1S+SV2 cells was not due to an effect on Venus fluorescence itself but due to an increase in complementation of the Venus fragments V1 and V2 (Figure 4-13 A). This effect appeared to be rather specific for incubation with $FeCl_3$ and was more pronounced than for incubation with other tri-, di-, or monovalent ions where only incubation with 100 µM $ZnCl_2$ resulted in slightly increased fluorescence intensity in H4_GE-V1S+SV2 cells (Figure 4-13 B).

To further validate the effect of DMSO and $FeCl_3$ on aggregation of αSyn in cell culture we analyzed the protein amount and observed an increase in αSyn protein load in H4_GE-S, H4_GE-SV, and H4_GE-V1S+SV2 cells upon treatment with 1% DMSO and 100 µM $FeCl_3$, but no change in the Venus protein load in H4_GE-V cells (Figure 4-14 A). An increase in αSyn protein load upon its aggregation has been reported before[317] and might be due to reduced degradation of aggregated αSyn.

We also performed sucrose gradient analyses from cell lysates obtained from both H4_GE-V1S+SV2 and H4_GE-V cells incubated with 0.75% DMSO and 100 µM $FeCl_3$, or 0.1% DMSO and 0 µM $FeCl_3$. We chose the parameters 0.75% DMSO and 100 µM $FeCl_3$ as high control since we observed many dead cells upon incubation with 1% DMSO and precipitation of iron upon incubation with 1 mM $FeCl_3$. We observed a shift in the αSyn signal to fractions of higher sucrose density in H4_GE-V1S+SV2 cells upon incubation with 0.75% DMSO and 100 µM $FeCl_3$ compared to incubation with 0.1% DMSO and 0 µM $FeCl_3$, suggesting increased αSyn oligomerization. This effect was not observed for Venus in H4_GE-V cells (Figure 4-14 B). However, since αSyn oligomers appear to be very sensitive to the cell lysis methods applied, especially concerning detergents, we are currently further optimizing the cell lysis conditions for sucrose gradient analysis. Thus, these results should be carefully regarded as preliminary.

Taken together, our data suggest an increase in αSyn aggregation in H4_GE cells upon incubation with DMSO and $FeCl_3$. Iron is present in the body in two oxidative states: ferrous iron (Fe^{2+}) and ferric iron (Fe^{3+}) and our results are well in line with several findings that point towards ferric iron as an important player in the course of pathology. Accordingly, a shift in the Fe^{2+}/Fe^{3+} ratio in favor of Fe^{3+} has been observed in the SN of PD patients. In line with this, a decreased amount of glutathione (GSH) – which can dimerize to glutathione disulfide (GSSG) upon oxidization and protect cellular molecules from oxidative stress by acting as electron donor for reactive oxygen species – and an increased amount of the ferric iron binding protein ferritin has been

described[312,313]. After injection of $FeCl_3$ into the SN, rats show almost erased dopamine levels in the striatum and develop a parkinsonian phenotype[318]. In line with this, an epidemiological study found an increased risk for PD among individuals with high nonheme iron and low vitamin C intake[319].

In vitro, incubation of recombinant αSyn with DMSO and with or without $FeCl_3$ leads to the formation of distinct oligomer species[145]. In this study, incubation with DMSO leads to formation of intermediate I oligomers *in vitro*. The additional incubation with $FeCl_3$ induces the formation of intermediate II oligomers[145] which are capable of inserting pores into lipid bilayers[145,171]. Moreover, ferric iron has been shown to accelerate αSyn fibrillization[131]. Interestingly, oligomerization of αSyn appears to result from direct interaction with ferric iron whereas oxidizing agents show no direct effect on αSyn oligomerization. Thus, an effect of oxidative stress on aggregation of αSyn might be mediated by oxidation of ferrous iron to ferric iron[144].

5.4 Reduced Fluorescence Intensity in the BiFC Assay upon Incubation with Known Modulators of αSyn Oligomerization

Interestingly, we also observed a slight increase in fluorescence intensity in the BiFC assay upon transient transfection of H4 cells with V1S and SV2 and incubation with DMSO. In the same experimental setup, incubation with three known inhibitors of αSyn aggregation – baicalein, anle138c, and anle138b – led to a decrease in fluorescence intensity compared to incubation with DMSO (Figure 4-5). These three substances have been shown to have antiaggregative properties *in vitro*, and anle138b has also been shown to have a beneficial effect on disease progression in a variety of models for PD and other neurodegenerative disorders[56,145,192,288-292]. We conclude that the αSyn BiFC system might represent a valuable tool for high-throughput screening assays for aggregation inhibitors of αSyn despite its poor signal-to-noise ratio. It has to be mentioned that this assay system is not specific for compounds that act directly on αSyn aggregation. In contrast, also compounds decreasing expression or increasing clearance of αSyn might appear as hits in a primary screen. Moreover, we cannot exclude the possibility of false positive results since compounds might also act on fluorescence intensity or Venus fragment complementation.

However, Venus shows a β-barrel structure which is typical for GFP-derived fluorescent proteins[250,320], and the complementation of Venus fragments relies on the interaction of β-sheets in both fragments with interaction of hydrophobic amino acids appearing to be a driving force[284,285]. This is comparable to the situation observed in the aggregation process of αSyn,

where the NAC-region (comprising amino acids 61-95, see Figure 2-2) appears to be of critical importance[95-100]. The NAC-region comprises the amino acids 61-95 of which almost 50% are hydrophobic. Indeed, Giasson *et al.*[100] found that the 12-amino-acid stretch comprising amino acids 71-82 (<u>V</u>TG<u>V</u>T<u>A</u>V<u>A</u>QKT<u>V</u>) in the NAC region is necessary and sufficient for the assembly of αSyn filaments. Notably, six of these amino acids (underlined) exhibit hydrophobic side chains. Therefore, both the complementation of Venus fragments and the aggregation of αSyn appear to be at least partly driven by the interaction of hydrophobic amino acids. For this reason, inhibitors of αSyn aggregation are not unlikely to also act on complementation of Venus fragments. Thus, excluding compounds that do not act specifically on αSyn aggregation but also on Venus fragment complementation might result in the exclusion of promising therapeutic candidates. That is why we decided not to do a control for specificity (in contrast to the leucine zipper (LZ)-hemi-Venus used by Moussaud *et al.*[206]). Still, we would expect that our strategy leads to more false positive results that will have to be extracted in secondary screenings which are independent of protein complementation. For this, cell lines inducibly overexpressing untagged αSyn in combination with western blot or sucrose gradient centrifugation analysis (Figure 4-14), immunohistochemical stainings for total or phosphorylated αSyn or αSyn oligomers using specific antibodies[321,322], and cytotoxicity assays will likely prove beneficial.

5.5   Inducible Transgene Expression in LUHMES Cells

The first step towards the creation of stable LUHMES cell lines was to test the transduction protocol that was used for the creation of stable H4 cell lines. Interestingly, LUHMES cells did not tolerate this protocol and we had to reduce the amount of virus from 1:3.5 (volume per volume) to 1:100 in order to obtain stably transgene-expressing LUHMES cells (Figure 4-15). Using protocol C we finally obtained 75% of Venus-positive cells and further used this protocol to create stable LUHMES cell lines that inducibly overexpress αSyn variants.

In order to test the inducible LUHMES cells, we first induced differentiation according to the two-step protocol by Scholz *et al.*[237]. Two days after induction of differentiation, cells were split and seeded into 384-well plates for Opera® analysis and T75 flasks for western blot analysis in differentiation medium, respectively. Cells were incubated with 10 μM tebufenozide for 4 days to induce transgene expression or DMSO as control, respectively.

After 6 days of incubation in differentiation medium LUHMES cells showed a morphological change to a neuron-like phenotype with an extensive network of neurites (Figure 4-15 B; Figure 4-16 B). Comprehensive characterization on the phenotype of differentiated LUHMES cells has

been performed before and revealed that they release dopamine and display neuronal electric properties[237,238]. For all inducible LUHMES cell lines we detected no obvious increase in background fluorescence upon incubation with DMSO compared to untreated LUHMES cells (Figure 4-16). In contrast, we observed an increase in western blot signal of the POI upon incubation with tebufenozide for all inducible LUHMES cell lines (Figure 4-16 D). Despite the clear increase in protein amount in LUHMES_GE-V1S+SV2 cells upon treatment with tebufenozide (Figure 4-16 D), we observed only a very faint increase in mean cellular fluorescence intensity (Figure 4-16 B, C). This is in line with our findings in H4_GE-V1S+SV2 cells and fits the observation by Moussaud *et al.*[206] that significant amounts of V1S and SV2 are required for a detectable BiFC signal. However, since these data were obtained from one single experiment they should be carefully regarded as proof of concept, and further evaluation of the LUHMES_GE cells concerning expression characteristics will need to be performed.

It has to be mentioned that, in our hands, the two-step differentiation protocol described by Scholz *et al.*[237] was hampered by the fact that harsh conditions had to be used for trypsinization after two days of differentiation. Unfortunately, proliferation of LUHMES cells is not immediately stopped upon incubation with differentiation medium, but cells proliferate markedly for at least two additional days. Thus, skipping the splitting step after two days of differentiation is difficult in small formats (like 384-well plates). We are currently optimizing the differentiation protocol for different formats (T75 flasks, 6-well plates, 24-well plates, 96-well plates, 384-well plates).

According to Schlachetzki *et al.*, the perfect cell line to study possible disease processes in PD would comprise "a homogeneous cell culture system that is easy to handle (…). Cells should be easy to expand in order to generate large numbers of neuronal precursor cells. Next, these cells should be easily directed towards a postmitotic state in a synchronized manner with a mature neuronal (dopaminergic) phenotype"[1]. LUHMES cells fulfill these criteria and seem to become more and more popular in PD research. In order to overexpress αSyn in LUHMES cells, different strategies have been applied so far including the stable constitutive overexpression of αSyn and the induction of αSyn overexpression by lentiviral transduction[242,243]. To the best of our knowledge, we here present the first report on LUHMES cells where overexpression of αSyn can be triggered by incubation with a chemical agonist.

Taken together, the model presented in this work shows several advantages compared to strategies where αSyn is constitutively overexpressed or where αSyn overexpression is induced by lentiviral transduction. Exemplarily, strength and kinetics of αSyn expression should be highly reproducible in our system since we have produced several homogeneous stocks of inducible H4_GE and LUHMES_GE cells that should not differ significantly between one another concerning fraction of transgene expressing cells and expression characteristics. The transgene

induction using the GE system was highly reproducible in H4_GE cells (Figure 4-10, Figure 4-11, Figure 4-12) and it is unlikely that reproducibility in LUHMES_GE cells is significantly worse. On the contrary, we would expect greater inter-experimental variation concerning the number of transduced cells and the strength of transgene expression when αSyn overexpression is induced by lentiviral transduction. Moreover, the success of lentiviral transduction critically relies on the quality of the produced lentiviruses, which itself is subject to variation between different virus productions and purifications. Furthermore, the production of lentiviruses is rather time- and money-consuming compared to purchasing the chemical agonist tebufenozide.

Several factors may contribute to the affection of dopaminergic cells in the SN in PD. Correspondingly, dopaminergic neurons show high metabolic needs due to their high density of connections to other neurons and their high-frequency autonomous firing[32,323,324]. This is accompanied by increased oxidative stress and increased calcium entry via opened L-type calcium channels (driving the rhythmic pacemaking activity) into the cell which is not well tolerated by SN neurons[32,325-327]. The effect of calcium is even more pronounced since they lack the expression of calcium binding proteins (like calbindin) which can act as calcium buffers[32]. Additionally, their large number of synapses increases the risk of being exposed to seeding species, and synaptic connections are generally thought to be "hot spots" for pathology in various types of neurons[32,104]. Using differentiated and undifferentiated LUHMES cells might be a valuable tool to unravel the role of dopamine metabolism on the pathological effect of αSyn aggregation.

Since PD represents a slowly progressing neurodegenerative disorder and a combination of genetic background and long-term exposition towards environmental risk factors at low-dose appears to be a driving force in disease progression, the use of acute cytotoxicity studies seems to be of limited use[197,328]. In this context, differentiated LUHMES cells represent a valuable tool since they allow prolonged exposure for up to 9-12 days in conventional cell culture compared to other immortalized cell lines where exposure time is usually limited by proliferation and a following increase in cell number. Recently, a protocol for 3D culturing of LUHMES cells has been published. Following this protocol, differentiated LUHMES cells showed a stable dopaminergic phenotype for up to 21 days, further strengthening the LUHMES cell model for the investigation of long-term exposure against low-dose toxicants[197].

6 Conclusions and Suggestions for Further Work

We here present the development of a system for the fast and easy creation of cell lines which inducibly overexpress the fluorescence protein Venus (V) or different variants of αSyn-140, namely human wildtype αSyn (S), αSyn coupled to Venus (SV), and αSyn coupled to the N-terminal (V1S) or C-terminal (SV2) part of Venus for a BiFC assay. The induction machinery was stably inserted into the host genome mediated by lentiviral transduction and relies on a modified GAL4-UAS system where GAL4 is coupled to an ecdysone receptor to allow inducible transgene expression (GE)[255]. Alternatively, induction was achieved by using a Cre_ER[T2]-loxP system (CE[T2]). Both induction systems were applied successfully to H4 cells, where the GE system showed stronger inducibility compared to the CE[T2] system. Transgene expression properties of H4_GE cells were characterized in detail both with regard to kinetics and dependence on tebufenozide concentration.

Iron has been discussed extensively as possible risk factor for the development of PD. Here, we observed a striking effect of $FeCl_3$ on αSyn aggregation which was not observed for other tri-, di-, or monovalent ions. The incubation of H4_GE cells with DMSO and $FeCl_3$ led to increased aggregation of αSyn demonstrated by increased fluorescence intensity in the BiFC model, increased αSyn protein load in αSyn overexpressing H4_GE cells, and by sucrose gradient centrifugation.

Moreover, the GE system was successfully implemented in LUHMES cells, and inducibility was demonstrated in a proof of concept experiment. To the best of our knowledge, this is the first report on inducible overexpression of αSyn in LUHMES cells mediated by a chemical agonist. Further experiments to characterize transgene expression are currently in progress.

It will be interesting to investigate effects of αSyn overexpression on its aggregation in combination with αSyn-mediated cytotoxicity and susceptibility to cytotoxic agents. Preparatory experiments to screen for modulators of αSyn aggregation and αSyn-mediated toxicity are currently in progress.

Moreover, using the system described herein, we have developed H4_GE cell lines that inducibly overexpress variants of αSyn carrying disease-associated mutations. Patients with SNCA mutations show distinct clinical and neuropathological phenotypes, and different mutations in αSyn lead to distinct aggregation and lipid-binding properties *in vitro*[329-334]. This suggests different pathological molecular mechanisms acting in synucleinopathies. Thus, investigating disease-associated αSyn mutations might provide information on general processes occurring in familial and sporadic PD as well as in other synucleinopathies.

Aggregation of αSyn is not a specific pathological feature of PD but in contrast occurs in a variety of disorders summarized as synucleinopathies. Yet, the location of αSyn aggregation and neuronal degeneration differs between these disorders. Exemplarily, in multiple system atrophy (MSA), αSyn aggregates mainly in oligodendrocytes with glial cytoplasmic inclusions (GCIs) or Papp-Lantos bodies being the neuropathological hallmark, and cytoplasmic aggregation of αSyn may also occur in astroglial cells in PD, dementia with Lewy bodies (DLB) or MSA[306]. The strategy presented in this work appears to be applicable to a variety of cell models and thus holds the potential to create distinct αSyn overexpression models for several different synucleinopathies.

We believe that the strategy presented in this work holds high potential for cutting edge questions in research on synucleinopathies in general and PD in particular since it is suitable for the application in a variety of established and primary cell lines for the investigation of aggregation, modulation, and toxicity of αSyn oligomers.

This could lead to the development of valuable models for PD and other synucleinopathies that help to unravel the underlying molecular pathological mechanism(s) and to develop disease-modifying therapies. In line with this, we are currently investigating a combination strategy of different treatment approaches modifying the homeostasis or aggregation of αSyn in an oligodendroglial cell model for the treatment of MSA in an *E-Rare*-funded project using the system presented in this work. For this, the induction machinery has been implemented in the oligodendroglial MO3.13 cell line.

The combination of the Venus-based BiFC assay and inducible expression appears to be especially suitable for high-throughput screenings of possible anti-aggregative compounds when combined with proper secondary readouts like sucrose gradient centrifugation and cytotoxicity assays. However, the cell models created here are not limited to the investigation of formation, modulation, and toxicity of αSyn oligomers but also enable the examination of further important effects in neurodegeneration like mitochondrial dysfunction, neurotoxicity, oxidative stress, defects in the protein degradation machinery or seeding and spreading mechanisms[1,32,335]. Thus, we hope that the system presented in this work will prove beneficial for the discovery and detailed characterization of novel drug candidates which be can be translated to clinical application in the end.

7 References

1   Schlachetzki, J. C., Saliba, S. W. & Oliveira, A. C. Studying neurodegenerative diseases in culture models. *Revista brasileira de psiquiatria* **35 Suppl 2**, S92-100, doi:10.1590/1516-4446-2013-1159 (2013).

2   Koo, E. H., Lansbury, P. T., Jr. & Kelly, J. W. Amyloid diseases: abnormal protein aggregation in neurodegeneration. *Proceedings of the National Academy of Sciences of the United States of America* **96**, 9989-9990 (1999).

3   Ross, C. A. & Poirier, M. A. Protein aggregation and neurodegenerative disease. *Nature medicine* **10 Suppl**, S10-17, doi:10.1038/nm1066 (2004).

4   Parkinson, J. An essay on the shaking palsy. 1817. *The Journal of neuropsychiatry and clinical neurosciences* **14**, 223-236; discussion 222, doi:10.1176/jnp.14.2.223 (2002).

5   Burke, R. E. & O'Malley, K. Axon degeneration in Parkinson's disease. *Experimental neurology* **246**, 72-83, doi:10.1016/j.expneurol.2012.01.011 (2013).

6   Jankovic, J. Parkinson's disease: clinical features and diagnosis. *Journal of neurology, neurosurgery, and psychiatry* **79**, 368-376, doi:10.1136/jnnp.2007.131045 (2008).

7   Sveinbjornsdottir, S. The clinical symptoms of Parkinson's disease. *Journal of neurochemistry*, doi:10.1111/jnc.13691 (2016).

8   Becker, G. *et al.* Early diagnosis of Parkinson's disease. *Journal of neurology* **249 Suppl 3**, III/40-48, doi:10.1007/s00415-002-1309-9 (2002).

9   Dauer, W. & Przedborski, S. Parkinson's disease: mechanisms and models. *Neuron* **39**, 889-909 (2003).

10   Dickson, D. W. *et al.* Evidence that incidental Lewy body disease is pre-symptomatic Parkinson's disease. *Acta neuropathologica* **115**, 437-444, doi:10.1007/s00401-008-0345-7 (2008).

11   Jellinger, K. A. Lewy body-related alpha-synucleinopathy in the aged human brain. *Journal of neural transmission* **111**, 1219-1235, doi:10.1007/s00702-004-0138-7 (2004).

12   Gowers, W. R. *A Manual of Diseases of the Nervous System*. Vol. 2 992 (London: J. & A. Churchill, 1886).

13   Nussbaum, R. L. & Ellis, C. E. Alzheimer's disease and Parkinson's disease. *The New England journal of medicine* **348**, 1356-1364, doi:10.1056/NEJM2003ra020003 (2003).

14   de Lau, L. M. & Breteler, M. M. Epidemiology of Parkinson's disease. *The Lancet. Neurology* **5**, 525-535, doi:10.1016/S1474-4422(06)70471-9 (2006).

15   de Rijk, M. C. *et al.* Prevalence of Parkinson's disease in Europe: A collaborative study of population-based cohorts. Neurologic Diseases in the Elderly Research Group. *Neurology* **54**, S21-23 (2000).

16   Pringsheim, T., Jette, N., Frolkis, A. & Steeves, T. D. The prevalence of Parkinson's disease: a systematic review and meta-analysis. *Movement disorders : official journal of the Movement Disorder Society* **29**, 1583-1590, doi:10.1002/mds.25945 (2014).

17   Kowal, S. L., Dall, T. M., Chakrabarti, R., Storm, M. V. & Jain, A. The current and projected economic burden of Parkinson's disease in the United States. *Movement disorders : official journal of the Movement Disorder Society* **28**, 311-318, doi:10.1002/mds.25292 (2013).

18   Postuma, R. B. *et al.* MDS clinical diagnostic criteria for Parkinson's disease. *Movement disorders : official journal of the Movement Disorder Society* **30**, 1591-1601, doi:10.1002/mds.26424 (2015).

19   Irvine, G. B., El-Agnaf, O. M., Shankar, G. M. & Walsh, D. M. Protein aggregation in the brain: the molecular basis for Alzheimer's and Parkinson's diseases. *Molecular medicine* **14**, 451-464, doi:10.2119/2007-00100.Irvine (2008).

20   Hughes, A. J., Ben-Shlomo, Y., Daniel, S. E. & Lees, A. J. What features improve the accuracy of clinical diagnosis in Parkinson's disease: a clinicopathologic study. *Neurology* **42**, 1142-1146 (1992).

21   Tolosa, E., Wenning, G. & Poewe, W. The diagnosis of Parkinson's disease. *The Lancet. Neurology* **5**, 75-86, doi:10.1016/s1474-4422(05)70285-4 (2006).

22   Deuschl, G. *et al.* A randomized trial of deep-brain stimulation for Parkinson's disease. *The New England journal of medicine* **355**, 896-908, doi:10.1056/NEJMoa060281 (2006).

23   Maroteaux, L., Campanelli, J. T. & Scheller, R. H. Synuclein: a neuron-specific protein localized to the nucleus and presynaptic nerve terminal. *The Journal of neuroscience : the official journal of the Society for Neuroscience* **8**, 2804-2815 (1988).

24   Schulz-Schaeffer, W. J. The synaptic pathology of alpha-synuclein aggregation in dementia with Lewy bodies, Parkinson's disease and Parkinson's disease dementia. *Acta neuropathologica* **120**, 131-143, doi:10.1007/s00401-010-0711-0 (2010).

25   George, J. M., Jin, H., Woods, W. S. & Clayton, D. F. Characterization of a novel protein regulated during the critical period for song learning in the zebra finch. *Neuron* **15**, 361-372 (1995).

26   Nakajo, S., Tsukada, K., Omata, K., Nakamura, Y. & Nakaya, K. A new brain-specific 14-kDa protein is a phosphoprotein. Its complete amino acid sequence and evidence for phosphorylation. *European journal of biochemistry / FEBS* **217**, 1057-1063 (1993).

27   Ueda, K. *et al.* Molecular cloning of cDNA encoding an unrecognized component of amyloid in Alzheimer disease. *Proceedings of the National Academy of Sciences of the United States of America* **90**, 11282-11286 (1993).

28   Jakes, R., Spillantini, M. G. & Goedert, M. Identification of two distinct synucleins from human brain. *FEBS letters* **345**, 27-32 (1994).

29   Akopian, A. N. & Wood, J. N. Peripheral nervous system-specific genes identified by subtractive cDNA cloning. *The Journal of biological chemistry* **270**, 21264-21270 (1995).

30   Ji, H. *et al.* Identification of a breast cancer-specific gene, BCSG1, by direct differential cDNA sequencing. *Cancer research* **57**, 759-764 (1997).

31   Clayton, D. F. & George, J. M. The synucleins: a family of proteins involved in synaptic function, plasticity, neurodegeneration and disease. *Trends in neurosciences* **21**, 249-254 (1998).

32   Luna, E. & Luk, K. C. Bent out of shape: alpha-Synuclein misfolding and the convergence of pathogenic pathways in Parkinson's disease. *FEBS letters* **589**, 3749-3759, doi:10.1016/j.febslet.2015.10.023 (2015).

33   Guardia-Laguarta, C. *et al.* alpha-Synuclein is localized to mitochondria-associated ER membranes. *The Journal of neuroscience : the official journal of the Society for Neuroscience* **34**, 249-259, doi:10.1523/JNEUROSCI.2507-13.2014 (2014).

34   Nakamura, K. *et al.* Direct membrane association drives mitochondrial fission by the Parkinson disease-associated protein alpha-synuclein. *The Journal of biological chemistry* **286**, 20710-20726, doi:10.1074/jbc.M110.213538 (2011).

35   Iwai, A. *et al.* The precursor protein of non-A beta component of Alzheimer's disease amyloid is a presynaptic protein of the central nervous system. *Neuron* **14**, 467-475 (1995).

36   Beyer, K. Alpha-synuclein structure, posttranslational modification and alternative splicing as aggregation enhancers. *Acta neuropathologica* **112**, 237-251, doi:10.1007/s00401-006-0104-6 (2006).

37   Chandra, S. *et al.* Double-knockout mice for alpha- and beta-synucleins: effect on synaptic functions. *Proceedings of the National Academy of Sciences of the United States of America* **101**, 14966-14971, doi:10.1073/pnas.0406283101 (2004).

38   Abeliovich, A. *et al.* Mice lacking alpha-synuclein display functional deficits in the nigrostriatal dopamine system. *Neuron* **25**, 239-252 (2000).

39   Yavich, L., Tanila, H., Vepsalainen, S. & Jakala, P. Role of alpha-synuclein in presynaptic dopamine recruitment. *The Journal of neuroscience : the official journal of the Society for Neuroscience* **24**, 11165-11170, doi:10.1523/JNEUROSCI.2559-04.2004 (2004).

40   Yavich, L., Jakala, P. & Tanila, H. Abnormal compartmentalization of norepinephrine in mouse dentate gyrus in alpha-synuclein knockout and A30P transgenic mice. *Journal of neurochemistry* **99**, 724-732, doi:10.1111/j.1471-4159.2006.04098.x (2006).

41   Scott, D. & Roy, S. alpha-Synuclein inhibits intersynaptic vesicle mobility and maintains recycling-pool homeostasis. *The Journal of neuroscience : the official journal of the Society for Neuroscience* **32**, 10129-10135, doi:10.1523/JNEUROSCI.0535-12.2012 (2012).

42   Greten-Harrison, B. *et al.* alphabetagamma-Synuclein triple knockout mice reveal age-dependent neuronal dysfunction. *Proceedings of the National Academy of Sciences of the United States of America* **107**, 19573-19578, doi:10.1073/pnas.1005005107 (2010).

43   Vargas, K. J. *et al.* Synucleins regulate the kinetics of synaptic vesicle endocytosis. *The Journal of neuroscience : the official journal of the Society for Neuroscience* **34**, 9364-9376, doi:10.1523/JNEUROSCI.4787-13.2014 (2014).

44   Gorbatyuk, O. S. *et al.* In vivo RNAi-mediated alpha-synuclein silencing induces nigrostriatal degeneration. *Molecular therapy : the journal of the American Society of Gene Therapy* **18**, 1450-1457, doi:10.1038/mt.2010.115 (2010).

45   Spillantini, M. G. *et al.* Alpha-synuclein in Lewy bodies. *Nature* **388**, 839-840, doi:10.1038/42166 (1997).

46   Maroteaux, L. & Scheller, R. H. The rat brain synucleins; family of proteins transiently associated with neuronal membrane. *Brain research. Molecular brain research* **11**, 335-343 (1991).

47   Jellinger, K. A. Neuropathological spectrum of synucleinopathies. *Movement disorders : official journal of the Movement Disorder Society* **18 Suppl 6**, S2-12, doi:10.1002/mds.10557 (2003).

48   Beyer, K. Mechanistic aspects of Parkinson's disease: alpha-synuclein and the biomembrane. *Cell Biochem Biophys* **47**, 285-299 (2007).

49   Ulmer, T. S., Bax, A., Cole, N. B. & Nussbaum, R. L. Structure and dynamics of micelle-bound human alpha-synuclein. *The Journal of biological chemistry* **280**, 9595-9603, doi:10.1074/jbc.M411805200 (2005).

50   Bussell, R., Jr. & Eliezer, D. A structural and functional role for 11-mer repeats in alpha-synuclein and other exchangeable lipid binding proteins. *Journal of molecular biology* **329**, 763-778 (2003).

51   Chandra, S., Gallardo, G., Fernandez-Chacon, R., Schluter, O. M. & Sudhof, T. C. Alpha-synuclein cooperates with CSPalpha in preventing neurodegeneration. *Cell* **123**, 383-396, doi:10.1016/j.cell.2005.09.028 (2005).

52   Fortin, D. L. *et al.* Lipid rafts mediate the synaptic localization of alpha-synuclein. *The Journal of neuroscience : the official journal of the Society for Neuroscience* **24**, 6715-6723, doi:10.1523/JNEUROSCI.1594-04.2004 (2004).

53   Jo, E. *et al.* alpha-Synuclein-synaptosomal membrane interactions: implications for fibrillogenesis. *European journal of biochemistry / FEBS* **271**, 3180-3189, doi:10.1111/j.1432-1033.2004.04250.x (2004).

54   Lee, H. J., Choi, C. & Lee, S. J. Membrane-bound alpha-synuclein has a high aggregation propensity and the ability to seed the aggregation of the cytosolic form. *The Journal of biological chemistry* **277**, 671-678, doi:10.1074/jbc.M107045200 (2002).

55   Uversky, V. N. Neuropathology, biochemistry, and biophysics of alpha-synuclein aggregation. *Journal of neurochemistry* **103**, 17-37, doi:10.1111/j.1471-4159.2007.04764.x (2007).

56   Hogen, T. *et al.* Two different binding modes of alpha-synuclein to lipid vesicles depending on its aggregation state. *Biophysical journal* **102**, 1646-1655, doi:10.1016/j.bpj.2012.01.059 (2012).

57   Cabin, D. E. *et al.* Synaptic vesicle depletion correlates with attenuated synaptic responses to prolonged repetitive stimulation in mice lacking alpha-synuclein. *The Journal of neuroscience : the official journal of the Society for Neuroscience* **22**, 8797-8807 (2002).

58   Murphy, D. D., Rueter, S. M., Trojanowski, J. Q. & Lee, V. M. Synucleins are developmentally expressed, and alpha-synuclein regulates the size of the presynaptic vesicular pool in primary hippocampal neurons. *The Journal of neuroscience : the official journal of the Society for Neuroscience* **20**, 3214-3220 (2000).

59   Ben Gedalya, T. *et al.* Alpha-synuclein and polyunsaturated fatty acids promote clathrin-mediated endocytosis and synaptic vesicle recycling. *Traffic* **10**, 218-234, doi:10.1111/j.1600-0854.2008.00853.x (2009).

60   Di Rosa, G., Puzzo, D., Sant'Angelo, A., Trinchese, F. & Arancio, O. Alpha-synuclein: between synaptic function and dysfunction. *Histology and histopathology* **18**, 1257-1266 (2003).

61   Liu, S. *et al.* alpha-Synuclein produces a long-lasting increase in neurotransmitter release. *The EMBO journal* **23**, 4506-4516, doi:10.1038/sj.emboj.7600451 (2004).

62   Al-Wandi, A. *et al.* Absence of alpha-synuclein affects dopamine metabolism and synaptic markers in the striatum of aging mice. *Neurobiology of aging* **31**, 796-804, doi:10.1016/j.neurobiolaging.2008.11.001 (2010).

63   Fortin, D. L. *et al.* Neural activity controls the synaptic accumulation of alpha-synuclein. *The Journal of neuroscience : the official journal of the Society for Neuroscience* **25**, 10913-10921, doi:10.1523/JNEUROSCI.2922-05.2005 (2005).

64   Lotharius, J. & Brundin, P. Impaired dopamine storage resulting from alpha-synuclein mutations may contribute to the pathogenesis of Parkinson's disease. *Human molecular genetics* **11**, 2395-2407 (2002).

65   Sidhu, A., Wersinger, C. & Vernier, P. Does alpha-synuclein modulate dopaminergic synaptic content and tone at the synapse? *FASEB journal : official publication of the Federation of American Societies for Experimental Biology* **18**, 637-647, doi:10.1096/fj.03-1112rev (2004).

66   Goedert, M. Alpha-synuclein and neurodegenerative diseases. *Nature reviews. Neuroscience* **2**, 492-501, doi:10.1038/35081564 (2001).

67   Jenco, J. M., Rawlingson, A., Daniels, B. & Morris, A. J. Regulation of phospholipase D2: selective inhibition of mammalian phospholipase D isoenzymes by alpha- and beta-synucleins. *Biochemistry* **37**, 4901-4909, doi:10.1021/bi972776r (1998).

68   Dev, K. K., Hofele, K., Barbieri, S., Buchman, V. L. & van der Putten, H. Part II: alpha-synuclein and its molecular pathophysiological role in neurodegenerative disease. *Neuropharmacology* **45**, 14-44 (2003).

69   Pronin, A. N., Morris, A. J., Surguchov, A. & Benovic, J. L. Synucleins are a novel class of substrates for G protein-coupled receptor kinases. *The Journal of biological chemistry* **275**, 26515-26522, doi:10.1074/jbc.M003542200 (2000).

70   Burre, J. *et al.* Alpha-synuclein promotes SNARE-complex assembly in vivo and in vitro. *Science* **329**, 1663-1667, doi:10.1126/science.1195227 (2010).

71   Nemani, V. M. *et al.* Increased expression of alpha-synuclein reduces neurotransmitter release by inhibiting synaptic vesicle reclustering after endocytosis. *Neuron* **65**, 66-79, doi:10.1016/j.neuron.2009.12.023 (2010).

72   Bertoncini, C. W. *et al.* Release of long-range tertiary interactions potentiates aggregation of natively unstructured alpha-synuclein. *Proceedings of the National Academy of Sciences of the United States of America* **102**, 1430-1435, doi:10.1073/pnas.0407146102 (2005).

73   Waxman, E. A., Mazzulli, J. R. & Giasson, B. I. Characterization of hydrophobic residue requirements for alpha-synuclein fibrillization. *Biochemistry* **48**, 9427-9436, doi:10.1021/bi900539p (2009).

74   Bodles, A. M., Guthrie, D. J., Greer, B. & Irvine, G. B. Identification of the region of non-Abeta component (NAC) of Alzheimer's disease amyloid responsible for its aggregation and toxicity. *Journal of neurochemistry* **78**, 384-395 (2001).

75   Masuda-Suzukake, M. *et al.* Prion-like spreading of pathological alpha-synuclein in brain. *Brain : a journal of neurology* **136**, 1128-1138, doi:10.1093/brain/awt037 (2013).

76   Oueslati, A., Fournier, M. & Lashuel, H. A. Role of post-translational modifications in modulating the structure, function and toxicity of alpha-synuclein: implications for Parkinson's disease pathogenesis and therapies. *Progress in brain research* **183**, 115-145, doi:10.1016/S0079-6123(10)83007-9 (2010).

77   Okochi, M. *et al.* Constitutive phosphorylation of the Parkinson's disease associated alpha-synuclein. *The Journal of biological chemistry* **275**, 390-397 (2000).

78   Specht, C. G. *et al.* Subcellular localisation of recombinant alpha- and gamma-synuclein. *Molecular and cellular neurosciences* **28**, 326-334, doi:10.1016/j.mcn.2004.09.017 (2005).

79   Zhong, S. C. *et al.* Expression and subcellular location of alpha-synuclein during mouse-embryonic development. *Cellular and molecular neurobiology* **30**, 469-482, doi:10.1007/s10571-009-9473-4 (2010).

80   Hashimoto, M. *et al.* alpha-Synuclein protects against oxidative stress via inactivation of the c-Jun N-terminal kinase stress-signaling pathway in neuronal cells. *The Journal of biological chemistry* **277**, 11465-11472, doi:10.1074/jbc.M111428200 (2002).

81   Goers, J. *et al.* Nuclear localization of alpha-synuclein and its interaction with histones. *Biochemistry* **42**, 8465-8471, doi:10.1021/bi0341152 (2003).

82   Kontopoulos, E., Parvin, J. D. & Feany, M. B. Alpha-synuclein acts in the nucleus to inhibit histone acetylation and promote neurotoxicity. *Human molecular genetics* **15**, 3012-3023, doi:10.1093/hmg/ddl243 (2006).

83   Baba, M. *et al.* Aggregation of alpha-synuclein in Lewy bodies of sporadic Parkinson's disease and dementia with Lewy bodies. *The American journal of pathology* **152**, 879-884 (1998).

84   Wakabayashi, K., Matsumoto, K., Takayama, K., Yoshimoto, M. & Takahashi, H. NACP, a presynaptic protein, immunoreactivity in Lewy bodies in Parkinson's disease. *Neuroscience letters* **239**, 45-48 (1997).

85   Hashimoto, M. & Masliah, E. Alpha-synuclein in Lewy body disease and Alzheimer's disease. *Brain pathology* **9**, 707-720 (1999).

86   Li, W. *et al.* Aggregation promoting C-terminal truncation of alpha-synuclein is a normal cellular process and is enhanced by the familial Parkinson's disease-linked mutations. *Proceedings of the National Academy of Sciences of the United States of America* **102**, 2162-2167, doi:10.1073/pnas.0406976102 (2005).

87   Anderson, J. P. *et al.* Phosphorylation of Ser-129 is the dominant pathological modification of alpha-synuclein in familial and sporadic Lewy body disease. *The Journal of biological chemistry* **281**, 29739-29752, doi:10.1074/jbc.M600933200 (2006).

88   Fujiwara, H. *et al.* alpha-Synuclein is phosphorylated in synucleinopathy lesions. *Nature cell biology* **4**, 160-164, doi:10.1038/ncb748 (2002).

89   Hasegawa, M. *et al.* Phosphorylated alpha-synuclein is ubiquitinated in alpha-synucleinopathy lesions. *The Journal of biological chemistry* **277**, 49071-49076, doi:10.1074/jbc.M208046200 (2002).

90   Takeda, A. *et al.* Abnormal accumulation of NACP/alpha-synuclein in neurodegenerative disorders. *The American journal of pathology* **152**, 367-372 (1998).

91   Giasson, B. I. *et al.* Oxidative damage linked to neurodegeneration by selective alpha-synuclein nitration in synucleinopathy lesions. *Science* **290**, 985-989 (2000).

92   Yamin, G., Uversky, V. N. & Fink, A. L. Nitration inhibits fibrillation of human alpha-synuclein in vitro by formation of soluble oligomers. *FEBS letters* **542**, 147-152 (2003).

93   Crowther, R. A., Jakes, R., Spillantini, M. G. & Goedert, M. Synthetic filaments assembled from C-terminally truncated alpha-synuclein. *FEBS letters* **436**, 309-312 (1998).

94   El-Agnaf, O. M., Jakes, R., Curran, M. D. & Wallace, A. Effects of the mutations Ala30 to Pro and Ala53 to Thr on the physical and morphological properties of alpha-synuclein protein implicated in Parkinson's disease. *FEBS letters* **440**, 67-70 (1998).

95   Serpell, L. C., Berriman, J., Jakes, R., Goedert, M. & Crowther, R. A. Fiber diffraction of synthetic alpha-synuclein filaments shows amyloid-like cross-beta conformation. *Proceedings of the National Academy of Sciences of the United States of America* **97**, 4897-4902 (2000).

96   Kahle, P. J., Haass, C., Kretzschmar, H. A. & Neumann, M. Structure/function of alpha-synuclein in health and disease: rational development of animal models for Parkinson's and related diseases. *Journal of neurochemistry* **82**, 449-457 (2002).

97   Uversky, V. N. *et al.* Biophysical properties of the synucleins and their propensities to fibrillate: inhibition of alpha-synuclein assembly by beta- and gamma-synucleins. *The Journal of biological chemistry* **277**, 11970-11978, doi:10.1074/jbc.M109541200 (2002).

98   Biere, A. L. *et al.* Parkinson's disease-associated alpha-synuclein is more fibrillogenic than beta- and gamma-synuclein and cannot cross-seed its homologs. *The Journal of biological chemistry* **275**, 34574-34579, doi:10.1074/jbc.M005514200 (2000).

99   Eckermann, K., Kugler, S. & Bahr, M. Dimerization propensities of Synucleins are not predictive for Synuclein aggregation. *Biochimica et biophysica acta* **1852**, 1658-1664, doi:10.1016/j.bbadis.2015.05.002 (2015).

100   Giasson, B. I., Murray, I. V., Trojanowski, J. Q. & Lee, V. M. A hydrophobic stretch of 12 amino acid residues in the middle of alpha-synuclein is essential for filament assembly. *The Journal of biological chemistry* **276**, 2380-2386, doi:10.1074/jbc.M008919200 (2001).

101   Braak, H. *et al.* Staging of brain pathology related to sporadic Parkinson's disease. *Neurobiology of aging* **24**, 197-211 (2003).

102   Dijkstra, A. A. *et al.* Stage-dependent nigral neuronal loss in incidental Lewy body and Parkinson's disease. *Movement disorders : official journal of the Movement Disorder Society* **29**, 1244-1251, doi:10.1002/mds.25952 (2014).

103   Mori, F. *et al.* Relationship among alpha-synuclein accumulation, dopamine synthesis, and neurodegeneration in Parkinson disease substantia nigra. *Journal of neuropathology and experimental neurology* **65**, 808-815, doi:10.1097/01.jnen.0000230520.47768.1a (2006).

104   Volpicelli-Daley, L. A. *et al.* Exogenous alpha-synuclein fibrils induce Lewy body pathology leading to synaptic dysfunction and neuron death. *Neuron* **72**, 57-71, doi:10.1016/j.neuron.2011.08.033 (2011).

105   Luk, K. C. *et al.* Intracerebral inoculation of pathological alpha-synuclein initiates a rapidly progressive neurodegenerative alpha-synucleinopathy in mice. *The Journal of experimental medicine* **209**, 975-986, doi:10.1084/jem.20112457 (2012).

106   Davie, C. A. A review of Parkinson's disease. *British medical bulletin* **86**, 109-127, doi:10.1093/bmb/ldn013 (2008).

107   Polymeropoulos, M. H. *et al.* Mutation in the alpha-synuclein gene identified in families with Parkinson's disease. *Science* **276**, 2045-2047 (1997).

108   Kruger, R. *et al.* Ala30Pro mutation in the gene encoding alpha-synuclein in Parkinson's disease. *Nature genetics* **18**, 106-108, doi:10.1038/ng0298-106 (1998).

109   Zarranz, J. J. *et al.* The new mutation, E46K, of alpha-synuclein causes Parkinson and Lewy body dementia. *Annals of neurology* **55**, 164-173, doi:10.1002/ana.10795 (2004).

110   Appel-Cresswell, S. *et al.* Alpha-synuclein p.H50Q, a novel pathogenic mutation for Parkinson's disease. *Movement disorders : official journal of the Movement Disorder Society* **28**, 811-813, doi:10.1002/mds.25421 (2013).

111   Lesage, S. *et al.* G51D alpha-synuclein mutation causes a novel parkinsonian-pyramidal syndrome. *Annals of neurology* **73**, 459-471, doi:10.1002/ana.23894 (2013).

112   Pasanen, P. *et al.* Novel alpha-synuclein mutation A53E associated with atypical multiple system atrophy and Parkinson's disease-type pathology. *Neurobiology of aging* **35**, 2180 e2181-2185, doi:10.1016/j.neurobiolaging.2014.03.024 (2014).

113   Greenbaum, E. A. *et al.* The E46K mutation in alpha-synuclein increases amyloid fibril formation. *The Journal of biological chemistry* **280**, 7800-7807, doi:10.1074/jbc.M411638200 (2005).

114   Chartier-Harlin, M. C. *et al.* Alpha-synuclein locus duplication as a cause of familial Parkinson's disease. *Lancet* **364**, 1167-1169, doi:10.1016/S0140-6736(04)17103-1 (2004).

115   Ibanez, P. *et al.* Causal relation between alpha-synuclein gene duplication and familial Parkinson's disease. *Lancet* **364**, 1169-1171, doi:10.1016/S0140-6736(04)17104-3 (2004).

116   Singleton, A. B. *et al.* alpha-Synuclein locus triplication causes Parkinson's disease. *Science* **302**, 841, doi:10.1126/science.1090278 (2003).

117   Maraganore, D. M. *et al.* Collaborative analysis of alpha-synuclein gene promoter variability and Parkinson disease. *Jama* **296**, 661-670, doi:10.1001/jama.296.6.661 (2006).

118   International Parkinson Disease Genomics, C. *et al.* Imputation of sequence variants for identification of genetic risks for Parkinson's disease: a meta-analysis of genome-wide association studies. *Lancet* **377**, 641-649, doi:10.1016/S0140-6736(10)62345-8 (2011).

119   Simon-Sanchez, J. *et al.* Genome-wide association study reveals genetic risk underlying Parkinson's disease. *Nature genetics* **41**, 1308-1312, doi:10.1038/ng.487 (2009).

120   Feany, M. B. & Bender, W. W. A Drosophila model of Parkinson's disease. *Nature* **404**, 394-398, doi:10.1038/35006074 (2000).

121   Masliah, E. *et al.* Dopaminergic loss and inclusion body formation in alpha-synuclein mice: implications for neurodegenerative disorders. *Science* **287**, 1265-1269 (2000).

122   Mazzulli, J. R. *et al.* Gaucher disease glucocerebrosidase and alpha-synuclein form a bidirectional pathogenic loop in synucleinopathies. *Cell* **146**, 37-52, doi:10.1016/j.cell.2011.06.001 (2011).

123   Gan-Or, Z., Giladi, N. & Orr-Utreger, A. Differential phenotype in Parkinson's disease patients with severe versus mild GBA mutations. *Brain : a journal of neurology* **132**, e125, doi:10.1093/brain/awp161 (2009).

124   Bandopadhyay, R. *et al.* The expression of DJ-1 (PARK7) in normal human CNS and idiopathic Parkinson's disease. *Brain : a journal of neurology* **127**, 420-430, doi:10.1093/brain/awh054 (2004).

125   Samaranch, L. *et al.* PINK1-linked parkinsonism is associated with Lewy body pathology. *Brain : a journal of neurology* **133**, 1128-1142, doi:10.1093/brain/awq051 (2010).

126   Neumann, J. *et al.* Glucocerebrosidase mutations in clinical and pathologically proven Parkinson's disease. *Brain : a journal of neurology* **132**, 1783-1794, doi:10.1093/brain/awp044 (2009).

127   Kalia, L. V. *et al.* Clinical correlations with Lewy body pathology in LRRK2-related Parkinson disease. *JAMA neurology* **72**, 100-105, doi:10.1001/jamaneurol.2014.2704 (2015).

128   Doherty, K. M. *et al.* Parkin disease: a clinicopathologic entity? *JAMA neurology* **70**, 571-579, doi:10.1001/jamaneurol.2013.172 (2013).

129   Ramirez, A. *et al.* Hereditary parkinsonism with dementia is caused by mutations in ATP13A2, encoding a lysosomal type 5 P-type ATPase. *Nature genetics* **38**, 1184-1191, doi:10.1038/ng1884 (2006).

130   Uversky, V. N., Li, J., Bower, K. & Fink, A. L. Synergistic effects of pesticides and metals on the fibrillation of alpha-synuclein: implications for Parkinson's disease. *Neurotoxicology* **23**, 527-536 (2002).

131   Uversky, V. N., Li, J. & Fink, A. L. Metal-triggered structural transformations, aggregation, and fibrillation of human alpha-synuclein. A possible molecular NK between Parkinson's disease and heavy metal exposure. *The Journal of biological chemistry* **276**, 44284-44296, doi:10.1074/jbc.M105343200 (2001).

132   Gaeta, A. & Hider, R. C. The crucial role of metal ions in neurodegeneration: the basis for a promising therapeutic strategy. *British journal of pharmacology* **146**, 1041-1059, doi:10.1038/sj.bjp.0706416 (2005).

133   Sian-Hulsmann, J., Mandel, S., Youdim, M. B. & Riederer, P. The relevance of iron in the pathogenesis of Parkinson's disease. *Journal of neurochemistry* **118**, 939-957, doi:10.1111/j.1471-4159.2010.07132.x (2011).

134   Zecca, L., Youdim, M. B., Riederer, P., Connor, J. R. & Crichton, R. R. Iron, brain ageing and neurodegenerative disorders. *Nature reviews. Neuroscience* **5**, 863-873, doi:10.1038/nrn1537 (2004).

135   Michaeli, S. *et al.* Assessment of brain iron and neuronal integrity in patients with Parkinson's disease using novel MRI contrasts. *Movement disorders : official journal of the Movement Disorder Society* **22**, 334-340, doi:10.1002/mds.21227 (2007).

136   Berg, D. Disturbance of iron metabolism as a contributing factor to SN hyperechogenicity in Parkinson's disease: implications for idiopathic and monogenetic forms. *Neurochemical research* **32**, 1646-1654, doi:10.1007/s11064-007-9346-5 (2007).

137   Sofic, E. *et al.* Increased iron (III) and total iron content in post mortem substantia nigra of parkinsonian brain. *J Neural Transm* **74**, 199-205 (1988).

138   Dexter, D. T. *et al.* Increased nigral iron content and alterations in other metal ions occurring in brain in Parkinson's disease. *Journal of neurochemistry* **52**, 1830-1836 (1989).

139   Ben-Shachar, D., Eshel, G., Riederer, P. & Youdim, M. B. Role of iron and iron chelation in dopaminergic-induced neurodegeneration: implication for Parkinson's disease. *Annals of neurology* **32 Suppl**, S105-110 (1992).

140   Zhang, X. *et al.* Neuroprotection by iron chelator against proteasome inhibitor-induced nigral degeneration. *Biochemical and biophysical research communications* **333**, 544-549, doi:10.1016/j.bbrc.2005.05.150 (2005).

141   Youdim, M. B., Stephenson, G. & Ben Shachar, D. Ironing iron out in Parkinson's disease and other neurodegenerative diseases with iron chelators: a lesson from 6-hydroxydopamine and iron chelators, desferal and VK-28. *Annals of the New York Academy of Sciences* **1012**, 306-325 (2004).

142   Kaur, D. *et al.* Genetic or pharmacological iron chelation prevents MPTP-induced neurotoxicity in vivo: a novel therapy for Parkinson's disease. *Neuron* **37**, 899-909 (2003).

143   Shachar, D. B., Kahana, N., Kampel, V., Warshawsky, A. & Youdim, M. B. Neuroprotection by a novel brain permeable iron chelator, VK-28, against 6-hydroxydopamine lession in rats. *Neuropharmacology* **46**, 254-263 (2004).

144   Levin, J. *et al.* Generation of ferric iron links oxidative stress to alpha-synuclein oligomer formation. *Journal of Parkinson's disease* **1**, 205-216, doi:10.3233/jpd-2011-11040 (2011).

145   Kostka, M. *et al.* Single particle characterization of iron-induced pore-forming alpha-synuclein oligomers. *The Journal of biological chemistry* **283**, 10992-11003, doi:10.1074/jbc.M709634200 (2008).

146   Turnbull, S. *et al.* alpha-Synuclein implicated in Parkinson's disease catalyses the formation of hydrogen peroxide in vitro. *Free radical biology & medicine* **30**, 1163-1170 (2001).

147   Alam, Z. I. *et al.* A generalised increase in protein carbonyls in the brain in Parkinson's but not incidental Lewy body disease. *Journal of neurochemistry* **69**, 1326-1329 (1997).

148   Manning-Bog, A. B. *et al.* The herbicide paraquat causes up-regulation and aggregation of alpha-synuclein in mice: paraquat and alpha-synuclein. *The Journal of biological chemistry* **277**, 1641-1644, doi:10.1074/jbc.C100560200 (2002).

149   Betarbet, R. *et al.* Chronic systemic pesticide exposure reproduces features of Parkinson's disease. *Nature neuroscience* **3**, 1301-1306, doi:10.1038/81834 (2000).

150   Pan-Montojo, F. & Reichmann, H. Considerations on the role of environmental toxins in idiopathic Parkinson's disease pathophysiology. *Translational neurodegeneration* **3**, 10, doi:10.1186/2047-9158-3-10 (2014).

151   Pan-Montojo, F. *et al.* Environmental toxins trigger PD-like progression via increased alpha-synuclein release from enteric neurons in mice. *Scientific reports* **2**, 898, doi:10.1038/srep00898 (2012).

152   Conway, K. A., Rochet, J. C., Bieganski, R. M. & Lansbury, P. T., Jr. Kinetic stabilization of the alpha-synuclein protofibril by a dopamine-alpha-synuclein adduct. *Science* **294**, 1346-1349, doi:10.1126/science.1063522 (2001).

153   Mazzulli, J. R., Armakola, M., Dumoulin, M., Parastatidis, I. & Ischiropoulos, H. Cellular oligomerization of alpha-synuclein is determined by the interaction of oxidized catechols with a C-terminal sequence. *The Journal of biological chemistry* **282**, 31621-31630, doi:10.1074/jbc.M704737200 (2007).

154   Conway, K. A., Harper, J. D. & Lansbury, P. T., Jr. Fibrils formed in vitro from alpha-synuclein and two mutant forms linked to Parkinson's disease are typical amyloid. *Biochemistry* **39**, 2552-2563 (2000).

155   Langston, J. W. *et al.* Novel alpha-synuclein-immunoreactive proteins in brain samples from the Contursi kindred, Parkinson's, and Alzheimer's disease. *Experimental neurology* **154**, 684-690, doi:10.1006/exnr.1998.6975 (1998).

156   Norris, E. H. *et al.* Reversible inhibition of alpha-synuclein fibrillization by dopaminochrome-mediated conformational alterations. *The Journal of biological chemistry* **280**, 21212-21219, doi:10.1074/jbc.M412621200 (2005).

157   Lansbury, P. T., Jr. Evolution of amyloid: what normal protein folding may tell us about fibrillogenesis and disease. *Proceedings of the National Academy of Sciences of the United States of America* **96**, 3342-3344 (1999).

158   Chen, S. W. *et al.* Structural characterization of toxic oligomers that are kinetically trapped during alpha-synuclein fibril formation. *Proceedings of the National Academy of Sciences of the United States of America* **112**, E1994-2003, doi:10.1073/pnas.1421204112 (2015).

159   Lorenzen, N. *et al.* The role of stable alpha-synuclein oligomers in the molecular events underlying amyloid formation. *Journal of the American Chemical Society* **136**, 3859-3868, doi:10.1021/ja411577t (2014).

160   Gosavi, N., Lee, H. J., Lee, J. S., Patel, S. & Lee, S. J. Golgi fragmentation occurs in the cells with prefibrillar alpha-synuclein aggregates and precedes the formation of fibrillar inclusion. *The Journal of biological chemistry* **277**, 48984-48992, doi:10.1074/jbc.M208194200 (2002).

161   Volles, M. J. & Lansbury, P. T., Jr. Zeroing in on the pathogenic form of alpha-synuclein and its mechanism of neurotoxicity in Parkinson's disease. *Biochemistry* **42**, 7871-7878, doi:10.1021/bi030086j (2003).

162   Cookson, M. R. & van der Brug, M. Cell systems and the toxic mechanism(s) of alpha-synuclein. *Experimental neurology* **209**, 5-11, doi:10.1016/j.expneurol.2007.05.022 (2008).

163   Kayed, R. *et al.* Common structure of soluble amyloid oligomers implies common mechanism of pathogenesis. *Science* **300**, 486-489, doi:10.1126/science.1079469 (2003).

164   Ostrerova-Golts, N. *et al.* The A53T alpha-synuclein mutation increases iron-dependent aggregation and toxicity. *The Journal of neuroscience : the official journal of the Society for Neuroscience* **20**, 6048-6054 (2000).

165   Hillmer, A. S. *et al.* Converse modulation of toxic alpha-synuclein oligomers in living cells by N'-benzylidene-benzohydrazide derivates and ferric iron. *Biochemical and biophysical research communications* **391**, 461-466, doi:10.1016/j.bbrc.2009.11.080 (2010).

166   Li, W. J., Jiang, H., Song, N. & Xie, J. X. Dose- and time-dependent alpha-synuclein aggregation induced by ferric iron in SK-N-SH cells. *Neuroscience bulletin* **26**, 205-210 (2010).

167   Huls, S. *et al.* AMPA-receptor-mediated excitatory synaptic transmission is enhanced by iron-induced alpha-synuclein oligomers. *Journal of neurochemistry* **117**, 868-878, doi:10.1111/j.1471-4159.2011.07254.x (2011).

168   Furukawa, K. *et al.* Plasma membrane ion permeability induced by mutant alpha-synuclein contributes to the degeneration of neural cells. *Journal of neurochemistry* **97**, 1071-1077, doi:10.1111/j.1471-4159.2006.03803.x (2006).

169   Winner, B. *et al.* In vivo demonstration that alpha-synuclein oligomers are toxic. *Proceedings of the National Academy of Sciences of the United States of America* **108**, 4194-4199, doi:10.1073/pnas.1100976108 (2011).

170   Ding, T. T., Lee, S. J., Rochet, J. C. & Lansbury, P. T., Jr. Annular alpha-synuclein protofibrils are produced when spherical protofibrils are incubated in solution or bound to brain-derived membranes. *Biochemistry* **41**, 10209-10217 (2002).

171   Schmidt, F. *et al.* Single-channel electrophysiology reveals a distinct and uniform pore complex formed by alpha-synuclein oligomers in lipid membranes. *PloS one* **7**, e42545, doi:10.1371/journal.pone.0042545 (2012).

172   Smith, D. P. *et al.* Formation of a high affinity lipid-binding intermediate during the early aggregation phase of alpha-synuclein. *Biochemistry* **47**, 1425-1434, doi:10.1021/bi701522m (2008).

173   Volles, M. J. *et al.* Vesicle permeabilization by protofibrillar alpha-synuclein: implications for the pathogenesis and treatment of Parkinson's disease. *Biochemistry* **40**, 7812-7819 (2001).

174   Fahn , S. Book Review. *New England Journal of Medicine* **335**, 2002-2003, doi:doi:10.1056/NEJM199612263352618 (1996).

175   Langston, J. W., Ballard, P., Tetrud, J. W. & Irwin, I. Chronic Parkinsonism in humans due to a product of meperidine-analog synthesis. *Science* **219**, 979-980 (1983).

176   Williams, A. MPTP parkinsonism. *British medical journal* **289**, 1401-1402 (1984).

177   Langston, J. W., Forno, L. S., Rebert, C. S. & Irwin, I. Selective nigral toxicity after systemic administration of 1-methyl-4-phenyl-1,2,5,6-tetrahydropyrine (MPTP) in the squirrel monkey. *Brain research* **292**, 390-394 (1984).

178   Klivenyi, P. *et al.* Mice lacking alpha-synuclein are resistant to mitochondrial toxins. *Neurobiology of disease* **21**, 541-548, doi:10.1016/j.nbd.2005.08.018 (2006).

179   Dauer, W. *et al.* Resistance of alpha -synuclein null mice to the parkinsonian neurotoxin MPTP. *Proceedings of the National Academy of Sciences of the United States of America* **99**, 14524-14529, doi:10.1073/pnas.172514599 (2002).

180   Li, W. W. *et al.* Localization of alpha-synuclein to mitochondria within midbrain of mice. *Neuroreport* **18**, 1543-1546, doi:10.1097/WNR.0b013e3282f03db4 (2007).

181   Ellis, C. E. *et al.* Mitochondrial lipid abnormality and electron transport chain impairment in mice lacking alpha-synuclein. *Molecular and cellular biology* **25**, 10190-10201, doi:10.1128/MCB.25.22.10190-10201.2005 (2005).

182   Martin, L. J. *et al.* Parkinson's disease alpha-synuclein transgenic mice develop neuronal mitochondrial degeneration and cell death. *The Journal of neuroscience : the official journal of the Society for Neuroscience* **26**, 41-50, doi:10.1523/JNEUROSCI.4308-05.2006 (2006).

183   Narendra, D., Walker, J. E. & Youle, R. Mitochondrial quality control mediated by PINK1 and Parkin: links to parkinsonism. *Cold Spring Harbor perspectives in biology* **4**, doi:10.1101/cshperspect.a011338 (2012).

184   Bartels, T., Choi, J. G. & Selkoe, D. J. alpha-Synuclein occurs physiologically as a helically folded tetramer that resists aggregation. *Nature* **477**, 107-110, doi:10.1038/nature10324 (2011).

185   Wang, W. *et al.* A soluble alpha-synuclein construct forms a dynamic tetramer. *Proceedings of the National Academy of Sciences of the United States of America* **108**, 17797-17802, doi:10.1073/pnas.1113260108 (2011).

186   Dettmer, U. *et al.* Parkinson-causing alpha-synuclein missense mutations shift native tetramers to monomers as a mechanism for disease initiation. *Nature communications* **6**, 7314, doi:10.1038/ncomms8314 (2015).

187   Zhu, M. & Fink, A. L. Lipid binding inhibits alpha-synuclein fibril formation. *The Journal of biological chemistry* **278**, 16873-16877, doi:10.1074/jbc.M210136200 (2003).

188   Jensen, M. B. *et al.* Membrane curvature sensing by amphipathic helices: a single liposome study using alpha-synuclein and annexin B12. *The Journal of biological chemistry* **286**, 42603-42614, doi:10.1074/jbc.M111.271130 (2011).

189   Middleton, E. R. & Rhoades, E. Effects of curvature and composition on alpha-synuclein binding to lipid vesicles. *Biophysical journal* **99**, 2279-2288, doi:10.1016/j.bpj.2010.07.056 (2010).

190   Dettmer, U., Newman, A. J., von Saucken, V. E., Bartels, T. & Selkoe, D. KTKEGV repeat motifs are key mediators of normal α-synuclein tetramerization: Their mutation causes excess monomers and neurotoxicity. *Proceedings of the National Academy of Sciences* **112**, 9596-9601, doi:10.1073/pnas.1505953112 (2015).

191   Fauvet, B. *et al.* alpha-Synuclein in central nervous system and from erythrocytes, mammalian cells, and Escherichia coli exists predominantly as disordered monomer. *The Journal of biological chemistry* **287**, 15345-15364, doi:10.1074/jbc.M111.318949 (2012).

192   Wagner, J. *et al.* Anle138b: a novel oligomer modulator for disease-modifying therapy of neurodegenerative diseases such as prion and Parkinson's disease. *Acta neuropathologica* **125**, 795-813, doi:10.1007/s00401-013-1114-9 (2013).

193   Sanchez, I., Mahlke, C. & Yuan, J. Pivotal role of oligomerization in expanded polyglutamine neurodegenerative disorders. *Nature* **421**, 373-379, doi:10.1038/nature01301 (2003).

194   Langley, G. The validity of animal experiments in medical research. *RSDA* **1:161–168** (2009).

195   Hartung, T. & Leist, M. Food for thought ... on the evolution of toxicology and the phasing out of animal testing. *Altex* **25**, 91-102 (2008).

196   Leist, M. *et al.* Consensus report on the future of animal-free systemic toxicity testing. *Altex* **31**, 341-356, doi:http://dx.doi.org/10.14573/altex.1406091 (2014).

197   Smirnova, L. *et al.* A LUHMES 3D dopaminergic neuronal model for neurotoxicity testing allowing long-term exposure and cellular resilience analysis. *Archives of Toxicology*, 1-19, doi:10.1007/s00204-015-1637-z (2015).

198   Krause, K. H., van Thriel, C., De Sousa, P. A., Leist, M. & Hengstler, J. G. Monocrotophos in Gandaman village: India school lunch deaths and need for improved toxicity testing. *Arch Toxicol* **87**, 1877-1881, doi:10.1007/s00204-013-1113-6 (2013).

199   Conway, K. A. *et al.* Accelerated oligomerization by Parkinson's disease linked alpha-synuclein mutants. *Annals of the New York Academy of Sciences* **920**, 42-45 (2000).

200   Danzer, K. M. *et al.* Different species of alpha-synuclein oligomers induce calcium influx and seeding. *The Journal of neuroscience : the official journal of the Society for Neuroscience* **27**, 9220-9232, doi:10.1523/JNEUROSCI.2617-07.2007 (2007).

201   Uversky, V. N., E, M. C., Bower, K. S., Li, J. & Fink, A. L. Accelerated alpha-synuclein fibrillation in crowded milieu. *FEBS letters* **515**, 99-103 (2002).

202   Bieschke, J. *et al.* Ultrasensitive detection of pathological prion protein aggregates by dual-color scanning for intensely fluorescent targets. *Proceedings of the National Academy of Sciences* **97**, 5468-5473, doi:10.1073/pnas.97.10.5468 (2000).

203   Giese, A., Bieschke, J., Eigen, M. & Kretzschmar, H. A. in *Prion Diseases: Diagnosis and Pathogenesis* (eds Martin H. Groschup & Hans A. Kretzschmar) 161-171 (Springer Vienna, 2000).

204   Schwille, P. Fluorescence correlation spectroscopy and its potential for intracellular applications. *Cell Biochemistry and Biophysics* **34**, 383-408, doi:10.1385/cbb:34:3:383 (2001).

205   Giese, A. *et al.* Single particle detection and characterization of synuclein co-aggregation. *Biochemical and biophysical research communications* **333**, 1202-1210, doi:10.1016/j.bbrc.2005.06.025 (2005).

206   Moussaud, S. *et al.* Targeting alpha-synuclein oligomers by protein-fragment complementation for drug discovery in synucleinopathies. *Expert opinion on therapeutic targets* **19**, 589-603, doi:10.1517/14728222.2015.1009448 (2015).

207   Hu, C. D., Chinenov, Y. & Kerppola, T. K. Visualization of interactions among bZIP and Rel family proteins in living cells using bimolecular fluorescence complementation. *Molecular cell* **9**, 789-798 (2002).

208   Morell, M., Ventura, S. & Aviles, F. X. Protein complementation assays: approaches for the in vivo analysis of protein interactions. *FEBS letters* **583**, 1684-1691, doi:10.1016/j.febslet.2009.03.002 (2009).

209   Remy, I. & Michnick, S. W. A highly sensitive protein-protein interaction assay based on Gaussia luciferase. *Nature methods* **3**, 977-979, doi:10.1038/nmeth979 (2006).

210   Danzer, K. M. *et al.* Exosomal cell-to-cell transmission of alpha synuclein oligomers. *Molecular neurodegeneration* **7**, 42, doi:10.1186/1750-1326-7-42 (2012).

211   Putcha, P. *et al.* Brain-permeable small-molecule inhibitors of Hsp90 prevent alpha-synuclein oligomer formation and rescue alpha-synuclein-induced toxicity. *The Journal of pharmacology and experimental therapeutics* **332**, 849-857, doi:10.1124/jpet.109.158436 (2010).

212   Danzer, K. M. *et al.* Heat-shock protein 70 modulates toxic extracellular alpha-synuclein oligomers and rescues trans-synaptic toxicity. *FASEB journal : official publication of the Federation of American Societies for Experimental Biology* **25**, 326-336, doi:10.1096/fj.10-164624 (2011).

213   Outeiro, T. F. *et al.* Formation of toxic oligomeric alpha-synuclein species in living cells. *PloS one* **3**, e1867, doi:10.1371/journal.pone.0001867 (2008).

214   Kerppola, T. K. Visualization of molecular interactions by fluorescence complementation. *Nature reviews. Molecular cell biology* **7**, 449-456, doi:10.1038/nrm1929 (2006).

215   Dimant, H. *et al.* Direct detection of alpha synuclein oligomers in vivo. *Acta neuropathologica communications* **1**, 6, doi:10.1186/2051-5960-1-6 (2013).

216   Tetzlaff, J. E. *et al.* CHIP targets toxic alpha-Synuclein oligomers for degradation. *The Journal of biological chemistry* **283**, 17962-17968, doi:10.1074/jbc.M802283200 (2008).

217   Takahashi, K. & Yamanaka, S. Induction of pluripotent stem cells from mouse embryonic and adult fibroblast cultures by defined factors. *Cell* **126**, 663-676, doi:10.1016/j.cell.2006.07.024 (2006).

218   Ryan, S. D. *et al.* Isogenic human iPSC Parkinson's model shows nitrosative stress-induced dysfunction in MEF2-PGC1alpha transcription. *Cell* **155**, 1351-1364, doi:10.1016/j.cell.2013.11.009 (2013).

219   Soldner, F. *et al.* Generation of isogenic pluripotent stem cells differing exclusively at two early onset Parkinson point mutations. *Cell* **146**, 318-331, doi:10.1016/j.cell.2011.06.019 (2011).

220   Lingor, P., Unsicker, K. & Krieglstein, K. Midbrain dopaminergic neurons are protected from radical induced damage by GDF-5 application. Short communication. *Journal of neural transmission* **106**, 139-144 (1999).

221   Tonges, L. *et al.* Inhibition of rho kinase enhances survival of dopaminergic neurons and attenuates axonal loss in a mouse model of Parkinson's disease. *Brain : a journal of neurology* **135**, 3355-3370, doi:10.1093/brain/aws254 (2012).

222   Fedorow, H. *et al.* Neuromelanin in human dopamine neurons: comparison with peripheral melanins and relevance to Parkinson's disease. *Progress in neurobiology* **75**, 109-124, doi:10.1016/j.pneurobio.2005.02.001 (2005).

223   Graham, F. L., Smiley, J., Russell, W. C. & Nairn, R. Characteristics of a human cell line transformed by DNA from human adenovirus type 5. *The Journal of general virology* **36**, 59-74, doi:10.1099/0022-1317-36-1-59 (1977).

224   Tabrizi, S. J. *et al.* Expression of mutant alpha-synuclein causes increased susceptibility to dopamine toxicity. *Human molecular genetics* **9**, 2683-2689 (2000).

225   Opazo, F., Krenz, A., Heermann, S., Schulz, J. B. & Falkenburger, B. H. Accumulation and clearance of alpha-synuclein aggregates demonstrated by time-lapse imaging. *Journal of neurochemistry* **106**, 529-540, doi:10.1111/j.1471-4159.2008.05407.x (2008).

226   Devine, M. J. *et al.* Pathogenic LRRK2 mutations do not alter gene expression in cell model systems or human brain tissue. *PloS one* **6**, e22489, doi:10.1371/journal.pone.0022489 (2011).

227   Deng, X. *et al.* Characterization of a selective inhibitor of the Parkinson's disease kinase LRRK2. *Nature chemical biology* **7**, 203-205, doi:10.1038/nchembio.538 (2011).

228   Hansen, C. *et al.* alpha-Synuclein propagates from mouse brain to grafted dopaminergic neurons and seeds aggregation in cultured human cells. *The Journal of clinical investigation* **121**, 715-725, doi:10.1172/JCI43366 (2011).

229   Tofaris, G. K., Layfield, R. & Spillantini, M. G. alpha-synuclein metabolism and aggregation is linked to ubiquitin-independent degradation by the proteasome. *FEBS letters* **509**, 22-26 (2001).

230   Danzer, K. M., Krebs, S. K., Wolff, M., Birk, G. & Hengerer, B. Seeding induced by alpha-synuclein oligomers provides evidence for spreading of alpha-synuclein pathology. *Journal of neurochemistry* **111**, 192-203, doi:10.1111/j.1471-4159.2009.06324.x (2009).

231   Pleasure, S. J., Page, C. & Lee, V. M. Pure, postmitotic, polarized human neurons derived from NTera 2 cells provide a system for expressing exogenous proteins in terminally differentiated neurons. *The Journal of neuroscience : the official journal of the Society for Neuroscience* **12**, 1802-1815 (1992).

232   Podrygajlo, G., Song, Y., Schlesinger, F., Krampfl, K. & Bicker, G. Synaptic currents and transmitter responses in human NT2 neurons differentiated in aggregate culture. *Neuroscience letters* **468**, 207-210, doi:10.1016/j.neulet.2009.10.092 (2010).

233   Klucken, J., Outeiro, T. F., Nguyen, P., McLean, P. J. & Hyman, B. T. Detection of novel intracellular alpha-synuclein oligomeric species by fluorescence lifetime imaging. *FASEB journal : official publication of the Federation of American Societies for Experimental Biology* **20**, 2050-2057, doi:10.1096/fj.05-5422com (2006).

234   Klucken, J. *et al.* Alpha-synuclein aggregation involves a bafilomycin A 1-sensitive autophagy pathway. *Autophagy* **8**, 754-766, doi:10.4161/auto.19371 (2012).

235   Hoshimaru, M., Ray, J., Sah, D. W. & Gage, F. H. Differentiation of the immortalized adult neuronal progenitor cell line HC2S2 into neurons by regulatable suppression of the v-myc oncogene. *Proceedings of the National Academy of Sciences of the United States of America* **93**, 1518-1523 (1996).

236   Lotharius, J. *et al.* Progressive degeneration of human mesencephalic neuron-derived cells triggered by dopamine-dependent oxidative stress is dependent on the mixed-lineage kinase pathway. *The Journal of neuroscience : the official journal of the Society for Neuroscience* **25**, 6329-6342, doi:10.1523/JNEUROSCI.1746-05.2005 (2005).

237   Scholz, D. *et al.* Rapid, complete and large-scale generation of post-mitotic neurons from the human LUHMES cell line. *Journal of neurochemistry* **119**, 957-971, doi:10.1111/j.1471-4159.2011.07255.x (2011).

238   Schildknecht, S. *et al.* Requirement of a dopaminergic neuronal phenotype for toxicity of low concentrations of 1-methyl-4-phenylpyridinium to human cells. *Toxicology and applied pharmacology* **241**, 23-35, doi:10.1016/j.taap.2009.07.027 (2009).

239   Depboylu, C. *et al.* Neuregulin-1 receptor tyrosine kinase ErbB4 is upregulated in midbrain dopaminergic neurons in Parkinson disease. *Neuroscience letters* **531**, 209-214, doi:10.1016/j.neulet.2012.10.050 (2012).

240   Xu, H. *et al.* Tau silencing by siRNA in the P301S mouse model of tauopathy. *Current gene therapy* **14**, 343-351 (2014).

241   Tatenhorst, L. *et al.* Fasudil attenuates aggregation of alpha-synuclein in models of Parkinson's disease. *Acta neuropathologica communications* **4**, 39, doi:10.1186/s40478-016-0310-y (2016).

242   Hollerhage, M. *et al.* Trifluoperazine rescues human dopaminergic cells from wild-type alpha-synuclein-induced toxicity. *Neurobiology of aging* **35**, 1700-1711, doi:10.1016/j.neurobiolaging.2014.01.027 (2014).

243   Schildknecht, S. *et al.* Generation of genetically-modified human differentiated cells for toxicological tests and the study of neurodegenerative diseases. *Altex* **30**, 427-444 (2013).

244   Shimomura, O., Johnson, F. H. & Saiga, Y. Extraction, purification and properties of aequorin, a bioluminescent protein from the luminous hydromedusan, Aequorea. *Journal of cellular and comparative physiology* **59**, 223-239 (1962).

245   Chalfie, M., Tu, Y., Euskirchen, G., Ward, W. W. & Prasher, D. C. Green fluorescent protein as a marker for gene expression. *Science* **263**, 802-805 (1994).

246   Heim, R., Prasher, D. C. & Tsien, R. Y. Wavelength mutations and posttranslational autoxidation of green fluorescent protein. *Proceedings of the National Academy of Sciences of the United States of America* **91**, 12501-12504 (1994).

247   Heim, R. & Tsien, R. Y. Engineering green fluorescent protein for improved brightness, longer wavelengths and fluorescence resonance energy transfer. *Current biology : CB* **6**, 178-182 (1996).

248   Shaner, N. C. *et al.* Improved monomeric red, orange and yellow fluorescent proteins derived from Discosoma sp. red fluorescent protein. *Nature biotechnology* **22**, 1567-1572, doi:10.1038/nbt1037 (2004).

249   Nagai, T. *et al.* A variant of yellow fluorescent protein with fast and efficient maturation for cell-biological applications. *Nature biotechnology* **20**, 87-90, doi:10.1038/nbt0102-87 (2002).

250   Rekas, A., Alattia, J. R., Nagai, T., Miyawaki, A. & Ikura, M. Crystal structure of venus, a yellow fluorescent protein with improved maturation and reduced environmental sensitivity. *The Journal of biological chemistry* **277**, 50573-50578, doi:10.1074/jbc.M209524200 (2002).

251   Kodama, Y. & Hu, C. D. Bimolecular fluorescence complementation (BiFC): a 5-year update and future perspectives. *BioTechniques* **53**, 285-298, doi:10.2144/000113943 (2012).

252   Gossen, M. *et al.* Transcriptional activation by tetracyclines in mammalian cells. *Science* **268**, 1766-1769 (1995).

253   Windl, O., Lorenz, H., Behrens, C., Romer, A. & Kretzschmar, H. A. Construction and characterization of murine neuroblastoma cell clones allowing inducible and high expression of the prion protein. *The Journal of general virology* **80 (Pt 1)**, 15-21, doi:10.1099/0022-1317-80-1-15 (1999).

254   Brand, A. H. & Perrimon, N. Targeted gene expression as a means of altering cell fates and generating dominant phenotypes. *Development (Cambridge, England)* **118**, 401-415 (1993).

255   Esengil, H., Chang, V., Mich, J. K. & Chen, J. K. Small-molecule regulation of zebrafish gene expression. *Nature chemical biology* **3**, 154-155, doi:10.1038/nchembio858 (2007).

256   No, D., Yao, T. P. & Evans, R. M. Ecdysone-inducible gene expression in mammalian cells and transgenic mice. *Proceedings of the National Academy of Sciences of the United States of America* **93**, 3346-3351 (1996).

257   Sawada, Y. *et al.* Synthesis and insecticidal activity of benzoheterocyclic analogues of N'-benzoyl-N-(tert-butyl)benzohydrazide: Part 1. Design of benzoheterocyclic analogues. *Pest management science* **59**, 25-35, doi:10.1002/ps.604 (2003).

258   Shimizu, B. *et al.* Molting hormonal and larvicidal activities of aliphatic acyl analogs of dibenzoylhydrazine insecticides. *Steroids* **62**, 638-642 (1997).

259   Hamilton, D. L. & Abremski, K. Site-specific recombination by the bacteriophage P1 lox-Cre system. Cre-mediated synapsis of two lox sites. *Journal of molecular biology* **178**, 481-486 (1984).

260   Feil, R., Wagner, J., Metzger, D. & Chambon, P. Regulation of Cre recombinase activity by mutated estrogen receptor ligand-binding domains. *Biochemical and biophysical research communications* **237**, 752-757, doi:10.1006/bbrc.1997.7124 (1997).

261   Nagy, A. Cre recombinase: the universal reagent for genome tailoring. *Genesis (New York, N.Y. : 2000)* **26**, 99-109 (2000).

262   Oberbek, A., Matasci, M., Hacker, D. L. & Wurm, F. M. Generation of stable, high-producing CHO cell lines by lentiviral vector-mediated gene transfer in serum-free suspension culture. *Biotechnology and bioengineering* **108**, 600-610, doi:10.1002/bit.22968 (2011).

263   Ibrahimi, A. *et al.* Highly efficient multicistronic lentiviral vectors with peptide 2A sequences. *Human gene therapy* **20**, 845-860, doi:10.1089/hum.2008.188 (2009).

264   de Felipe, P. *et al.* E unum pluribus: multiple proteins from a self-processing polyprotein. *Trends in biotechnology* **24**, 68-75, doi:10.1016/j.tibtech.2005.12.006 (2006).

265   Kim, J. H. *et al.* High cleavage efficiency of a 2A peptide derived from porcine teschovirus-1 in human cell lines, zebrafish and mice. *PloS one* **6**, e18556, doi:10.1371/journal.pone.0018556 (2011).

266   Ryan, M. D., King, A. M. & Thomas, G. P. Cleavage of foot-and-mouth disease virus polyprotein is mediated by residues located within a 19 amino acid sequence. *The Journal of general virology* **72 (Pt 11)**, 2727-2732, doi:10.1099/0022-1317-72-11-2727 (1991).

267   Doronina, V. A. *et al.* Site-specific release of nascent chains from ribosomes at a sense codon. *Molecular and cellular biology* **28**, 4227-4239, doi:10.1128/mcb.00421-08 (2008).

268   Hartley, J. L., Temple, G. F. & Brasch, M. A. DNA cloning using in vitro site-specific recombination. *Genome research* **10**, 1788-1795 (2000).

269   Landy, A. Dynamic, structural, and regulatory aspects of lambda site-specific recombination. *Annual review of biochemistry* **58**, 913-949, doi:10.1146/annurev.bi.58.070189.004405 (1989).

270   Madl, T. *et al.* Structural basis for nucleic acid and toxin recognition of the bacterial antitoxin CcdA. *Journal of molecular biology* **364**, 170-185, doi:10.1016/j.jmb.2006.08.082 (2006).

271 Bernard, P. & Couturier, M. Cell killing by the F plasmid CcdB protein involves poisoning of DNA-topoisomerase II complexes. *Journal of molecular biology* **226**, 735-745 (1992).

272 Lotharius, J. *et al.* Effect of mutant alpha-synuclein on dopamine homeostasis in a new human mesencephalic cell line. *The Journal of biological chemistry* **277**, 38884-38894, doi:10.1074/jbc.M205518200 (2002).

273 Smith, P. K. *et al.* Measurement of protein using bicinchoninic acid. *Analytical biochemistry* **150**, 76-85 (1985).

274 Kahle, P. J. *et al.* Subcellular localization of wild-type and Parkinson's disease-associated mutant alpha -synuclein in human and transgenic mouse brain. *The Journal of neuroscience : the official journal of the Society for Neuroscience* **20**, 6365-6373 (2000).

275 Nübling, G. & Giese, A. Scanning for Intensely Fluorescent Targets (SIFT) in the Study of Protein Aggregation at the Single-Particle Level-Chapter 15.

276 Schwille, P., Meyer-Almes, F. J. & Rigler, R. Dual-color fluorescence cross-correlation spectroscopy for multicomponent diffusional analysis in solution. *Biophysical journal* **72**, 1878-1886, doi:10.1016/s0006-3495(97)78833-7 (1997).

277 Schwille, P., Bieschke, J. & Oehlenschlager, F. Kinetic investigations by fluorescence correlation spectroscopy: the analytical and diagnostic potential of diffusion studies. *Biophysical chemistry* **66**, 211-228 (1997).

278 Bacia, K. & Schwille, P. A dynamic view of cellular processes by in vivo fluorescence auto- and cross-correlation spectroscopy. *Methods (San Diego, Calif.)* **29**, 74-85 (2003).

279 Kask, P., Palo, K., Ullmann, D. & Gall, K. Fluorescence-intensity distribution analysis and its application in biomolecular detection technology. *Proceedings of the National Academy of Sciences of the United States of America* **96**, 13756-13761 (1999).

280 Kask, P. *et al.* Two-dimensional fluorescence intensity distribution analysis: theory and applications. *Biophysical journal* **78**, 1703-1713, doi:10.1016/s0006-3495(00)76722-1 (2000).

281 Giese, A., Levin, J., Bertsch, U. & Kretzschmar, H. Effect of metal ions on de novo aggregation of full-length prion protein. *Biochemical and biophysical research communications* **320**, 1240-1246, doi:10.1016/j.bbrc.2004.06.075 (2004).

282 Levin, J. *et al.* Divergent molecular effects of desmin mutations on protein assembly in myofibrillar myopathy. *Journal of neuropathology and experimental neurology* **69**, 415-424, doi:10.1097/NEN.0b013e3181d71305 (2010).

283 Kodama, Y. & Hu, C. D. An improved bimolecular fluorescence complementation assay with a high signal-to-noise ratio. *BioTechniques* **49**, 793-805, doi:10.2144/000113519 (2010).

284 Pace, C. N., Shirley, B. A., McNutt, M. & Gajiwala, K. Forces contributing to the conformational stability of proteins. *FASEB journal : official publication of the Federation of American Societies for Experimental Biology* **10**, 75-83 (1996).

285 Nakagawa, C., Inahata, K., Nishimura, S. & Sugimoto, K. Improvement of a Venus-based bimolecular fluorescence complementation assay to visualize bFos-bJun interaction in living cells. *Bioscience, biotechnology, and biochemistry* **75**, 1399-1401 (2011).

286 Lin, J. *et al.* LEC-BiFC: a new method for rapid assay of protein interaction. *Biotechnic & histochemistry : official publication of the Biological Stain Commission* **86**, 272-279, doi:10.3109/10520295.2010.483068 (2011).

287 Meul, T. *Protein aggregation in Parkinson's disease - Improvement of a BiFC assay for visualisation of alpha-synuclein oligomerisation in cellular environment* B. Sc. thesis, Ludwig-Maximilian-Universität, (2013).

288 Giese, A. *et al.* (Google Patents, 2010).

289 Zhu, M. *et al.* The flavonoid baicalein inhibits fibrillation of alpha-synuclein and disaggregates existing fibrils. *The Journal of biological chemistry* **279**, 26846-26857, doi:10.1074/jbc.M403129200 (2004).

290 Deeg, A. A. *et al.* Anle138b and related compounds are aggregation specific fluorescence markers and reveal high affinity binding to alpha-synuclein aggregates. *Biochimica et biophysica acta* **1850**, 1884-1890, doi:10.1016/j.bbagen.2015.05.021 (2015).

291   Levin, J. *et al.* The oligomer modulator anle138b inhibits disease progression in a Parkinson mouse model even with treatment started after disease onset. *Acta neuropathologica* **127**, 779-780, doi:10.1007/s00401-014-1265-3 (2014).

292   Fellner, L. *et al.* Anle138b Partly Ameliorates Motor Deficits Despite Failure of Neuroprotection in a Model of Advanced Multiple System Atrophy. *Frontiers in neuroscience* **10**, 99, doi:10.3389/fnins.2016.00099 (2016).

293   Kerppola, T. K. Bimolecular fluorescence complementation (BiFC) analysis as a probe of protein interactions in living cells. *Annual review of biophysics* **37**, 465-487, doi:10.1146/annurev.biophys.37.032807.125842 (2008).

294   Goncalves, S. A., Matos, J. E. & Outeiro, T. F. Zooming into protein oligomerization in neurodegeneration using BiFC. *Trends in biochemical sciences* **35**, 643-651, doi:10.1016/j.tibs.2010.05.007 (2010).

295   Jones, W. D. The expanding reach of the GAL4/UAS system into the behavioral neurobiology of Drosophila. *BMB reports* **42**, 705-712 (2009).

296   Scott, E. K. The Gal4/UAS toolbox in zebrafish: new approaches for defining behavioral circuits. *Journal of neurochemistry* **110**, 441-456, doi:10.1111/j.1471-4159.2009.06161.x (2009).

297   Sauer, B. Functional expression of the cre-lox site-specific recombination system in the yeast Saccharomyces cerevisiae. *Molecular and cellular biology* **7**, 2087-2096 (1987).

298   Sauer, B. & Henderson, N. Site-specific DNA recombination in mammalian cells by the Cre recombinase of bacteriophage P1. *Proceedings of the National Academy of Sciences of the United States of America* **85**, 5166-5170 (1988).

299   Sauer, B. Inducible gene targeting in mice using the Cre/lox system. *Methods (San Diego, Calif.)* **14**, 381-392, doi:10.1006/meth.1998.0593 (1998).

300   Indra, A. K. *et al.* Temporally-controlled site-specific mutagenesis in the basal layer of the epidermis: comparison of the recombinase activity of the tamoxifen-inducible Cre-ER(T) and Cre-ER(T2) recombinases. *Nucleic acids research* **27**, 4324-4327 (1999).

301   Ahlfeld, J. *et al.* Sox2 requirement in sonic hedgehog-associated medulloblastoma. *Cancer research* **73**, 3796-3807, doi:10.1158/0008-5472.can-13-0238 (2013).

302   Borgna, J. L. & Rochefort, H. Hydroxylated metabolites of tamoxifen are formed in vivo and bound to estrogen receptor in target tissues. *The Journal of biological chemistry* **256**, 859-868 (1981).

303   Robertson, D. W., Katzenellenbogen, J. A., Long, D. J., Rorke, E. A. & Katzenellenbogen, B. S. Tamoxifen antiestrogens. A comparison of the activity, pharmacokinetics, and metabolic activation of the cis and trans isomers of tamoxifen. *Journal of steroid biochemistry* **16**, 1-13 (1982).

304   Jordan, V. C. Metabolites of tamoxifen in animals and man: identification, pharmacology, and significance. *Breast cancer research and treatment* **2**, 123-138 (1982).

305   Felker, A. *et al.* In Vivo Performance and Properties of Tamoxifen Metabolites for CreERT2 Control. *PloS one* **11**, e0152989, doi:10.1371/journal.pone.0152989 (2016).

306   Bruck, D., Wenning, G. K., Stefanova, N. & Fellner, L. Glia and alpha-synuclein in neurodegeneration: A complex interaction. *Neurobiology of disease* **85**, 262-274, doi:10.1016/j.nbd.2015.03.003 (2016).

307   Tak, H. *et al.* Bimolecular fluorescence complementation; lighting-up tau-tau interaction in living cells. *PloS one* **8**, e81682, doi:10.1371/journal.pone.0081682 (2013).

308   Hashimoto, T., Adams, K. W., Fan, Z., McLean, P. J. & Hyman, B. T. Characterization of oligomer formation of amyloid-beta peptide using a split-luciferase complementation assay. *The Journal of biological chemistry* **286**, 27081-27091, doi:10.1074/jbc.M111.257378 (2011).

309   Kwaks, T. H. & Otte, A. P. Employing epigenetics to augment the expression of therapeutic proteins in mammalian cells. *Trends in biotechnology* **24**, 137-142, doi:10.1016/j.tibtech.2006.01.007 (2006).

310   Magliery, T. J. & Regan, L. Reassembled GFP: detecting protein-protein interactions and protein expression patterns. *Methods of biochemical analysis* **47**, 391-405 (2006).

311   Cheng, P. *et al.* Dietary intake of iron, zinc, copper, and risk of Parkinson's disease: a meta-analysis. *Neurological sciences : official journal of the Italian Neurological Society and of the Italian Society of Clinical Neurophysiology* **36**, 2269-2275, doi:10.1007/s10072-015-2349-0 (2015).

312   Dexter, D. T. *et al.* Alterations in the levels of iron, ferritin and other trace metals in Parkinson's disease and other neurodegenerative diseases affecting the basal ganglia. *Brain : a journal of neurology* **114 (Pt 4)**, 1953-1975 (1991).

313   Riederer, P. *et al.* Transition metals, ferritin, glutathione, and ascorbic acid in parkinsonian brains. *Journal of neurochemistry* **52**, 515-520 (1989).

314   Hirsch, E. C., Brandel, J. P., Galle, P., Javoy-Agid, F. & Agid, Y. Iron and aluminum increase in the substantia nigra of patients with Parkinson's disease: an X-ray microanalysis. *Journal of neurochemistry* **56**, 446-451 (1991).

315   Rybicki, B. A., Johnson, C. C., Uman, J. & Gorell, J. M. Parkinson's disease mortality and the industrial use of heavy metals in Michigan. *Movement disorders : official journal of the Movement Disorder Society* **8**, 87-92, doi:10.1002/mds.870080116 (1993).

316   Zayed, J. *et al.* [Environmental factors in the etiology of Parkinson's disease]. *The Canadian journal of neurological sciences. Le journal canadien des sciences neurologiques* **17**, 286-291 (1990).

317   Gan, M., Moussaud, S., Jiang, P. & McLean, P. J. Extracellular ATP induces intracellular alpha-synuclein accumulation via P2X1 receptor-mediated lysosomal dysfunction. *Neurobiology of aging* **36**, 1209-1220, doi:10.1016/j.neurobiolaging.2014.10.037 (2015).

318   Ben-Shachar, D. & Youdim, M. B. Intranigral iron injection induces behavioral and biochemical "parkinsonism" in rats. *Journal of neurochemistry* **57**, 2133-2135 (1991).

319   Logroscino, G., Gao, X., Chen, H., Wing, A. & Ascherio, A. Dietary iron intake and risk of Parkinson's disease. *American journal of epidemiology* **168**, 1381-1388, doi:10.1093/aje/kwn273 (2008).

320   Tsien, R. Y. The green fluorescent protein. *Annual review of biochemistry* **67**, 509-544, doi:10.1146/annurev.biochem.67.1.509 (1998).

321   Vaikath, N. N. *et al.* Generation and characterization of novel conformation-specific monoclonal antibodies for alpha-synuclein pathology. *Neurobiology of disease* **79**, 81-99, doi:10.1016/j.nbd.2015.04.009 (2015).

322   Majbour, N. K. *et al.* Oligomeric and phosphorylated alpha-synuclein as potential CSF biomarkers for Parkinson's disease. *Molecular neurodegeneration* **11**, 7, doi:10.1186/s13024-016-0072-9 (2016).

323   Matsuda, W. *et al.* Single nigrostriatal dopaminergic neurons form widely spread and highly dense axonal arborizations in the neostriatum. *The Journal of neuroscience : the official journal of the Society for Neuroscience* **29**, 444-453, doi:10.1523/jneurosci.4029-08.2009 (2009).

324   Bolam, J. P. & Pissadaki, E. K. Living on the edge with too many mouths to feed: why dopamine neurons die. *Movement disorders : official journal of the Movement Disorder Society* **27**, 1478-1483, doi:10.1002/mds.25135 (2012).

325   Surmeier, D. J., Guzman, J. N., Sanchez-Padilla, J. & Goldberg, J. A. The origins of oxidant stress in Parkinson's disease and therapeutic strategies. *Antioxidants & redox signaling* **14**, 1289-1301, doi:10.1089/ars.2010.3521 (2011).

326   Guzman, J. N. *et al.* Oxidant stress evoked by pacemaking in dopaminergic neurons is attenuated by DJ-1. *Nature* **468**, 696-700, doi:10.1038/nature09536 (2010).

327   Chan, C. S. *et al.* 'Rejuvenation' protects neurons in mouse models of Parkinson's disease. *Nature* **447**, 1081-1086, doi:10.1038/nature05865 (2007).

328   Hengstler, J. G., Marchan, R. & Leist, M. Highlight report: towards the replacement of in vivo repeated dose systemic toxicity testing. *Arch Toxicol* **86**, 13-15, doi:10.1007/s00204-011-0798-7 (2012).

329   Stefanovic, A. N., Lindhoud, S., Semerdzhiev, S. A., Claessens, M. M. & Subramaniam, V. Oligomers of Parkinson's Disease-Related alpha-Synuclein Mutants Have Similar Structures but Distinctive Membrane Permeabilization Properties. *Biochemistry* **54**, 3142-3150, doi:10.1021/bi501369k (2015).

330   Rutherford, N. J. & Giasson, B. I. The A53E alpha-synuclein pathological mutation demonstrates reduced aggregation propensity in vitro and in cell culture. *Neuroscience letters* **597**, 43-48, doi:10.1016/j.neulet.2015.04.022 (2015).

331   Rutherford, N. J., Moore, B. D., Golde, T. E. & Giasson, B. I. Divergent effects of the H50Q and G51D SNCA mutations on the aggregation of alpha-synuclein. *Journal of neurochemistry* **131**, 859-867, doi:10.1111/jnc.12806 (2014).

332   Ghosh, D. *et al.* The newly discovered Parkinson's disease associated Finnish mutation (A53E) attenuates alpha-synuclein aggregation and membrane binding. *Biochemistry* **53**, 6419-6421, doi:10.1021/bi5010365 (2014).

333   Ghosh, D. *et al.* The Parkinson's disease-associated H50Q mutation accelerates alpha-Synuclein aggregation in vitro. *Biochemistry* **52**, 6925-6927, doi:10.1021/bi400999d (2013).

334   Ysselstein, D. *et al.* Effects of impaired membrane interactions on alpha-synuclein aggregation and neurotoxicity. *Neurobiology of disease* **79**, 150-163, doi:10.1016/j.nbd.2015.04.007 (2015).

335   Schulz, J. B. Update on the pathogenesis of Parkinson's disease. *Journal of neurology* **255 Suppl 5**, 3-7, doi:10.1007/s00415-008-5011-4 (2008).

8 Appendix

8.1 Plasmid Maps
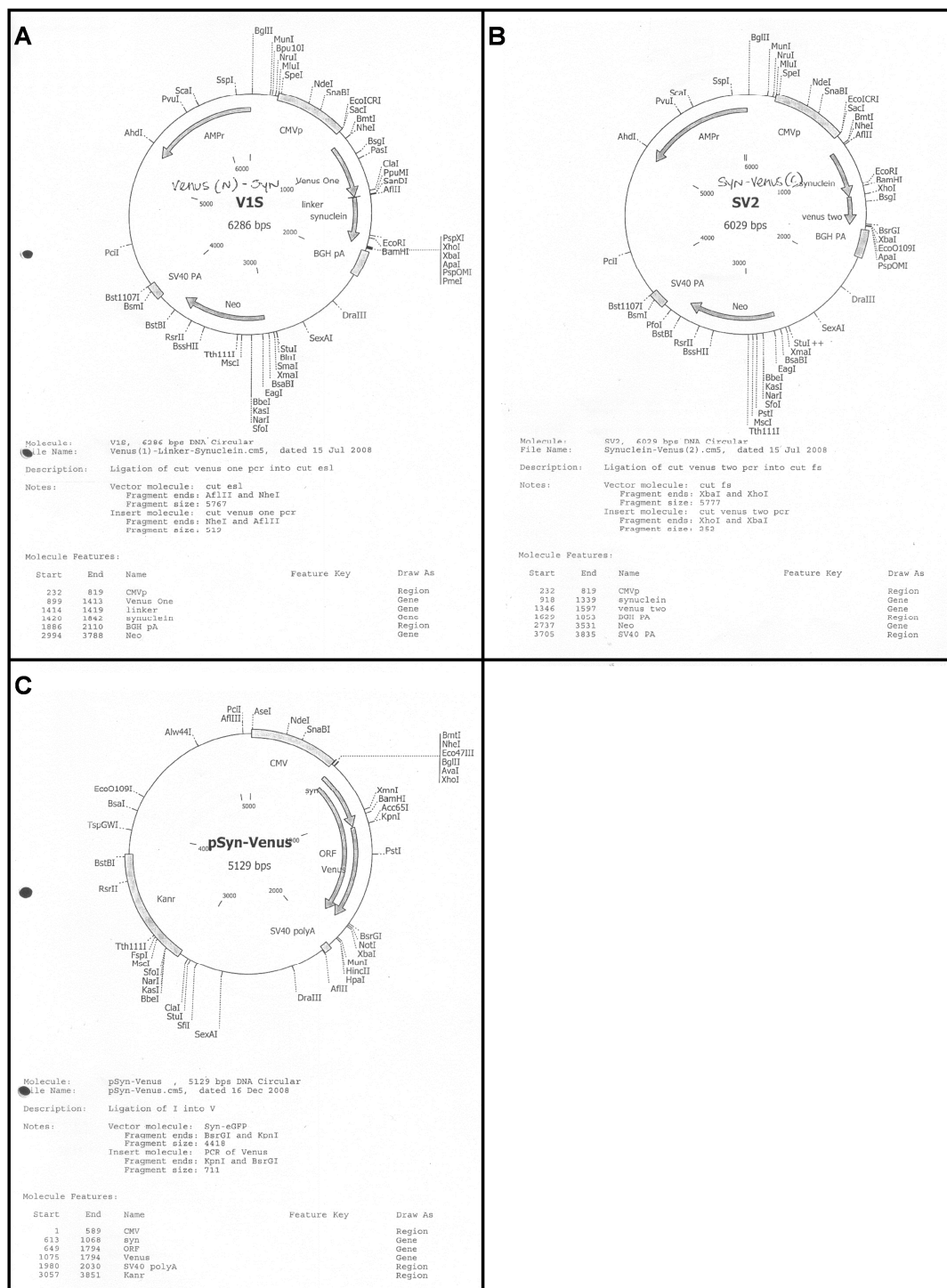
Figure 8-1: Plasmid maps I

A) Plasmid carrying the construct V1S (db #1)
B) Plasmid carrying the construct SV2 (db #2)
C) Plasmid carrying the construct αSyn-Venus (db #3)
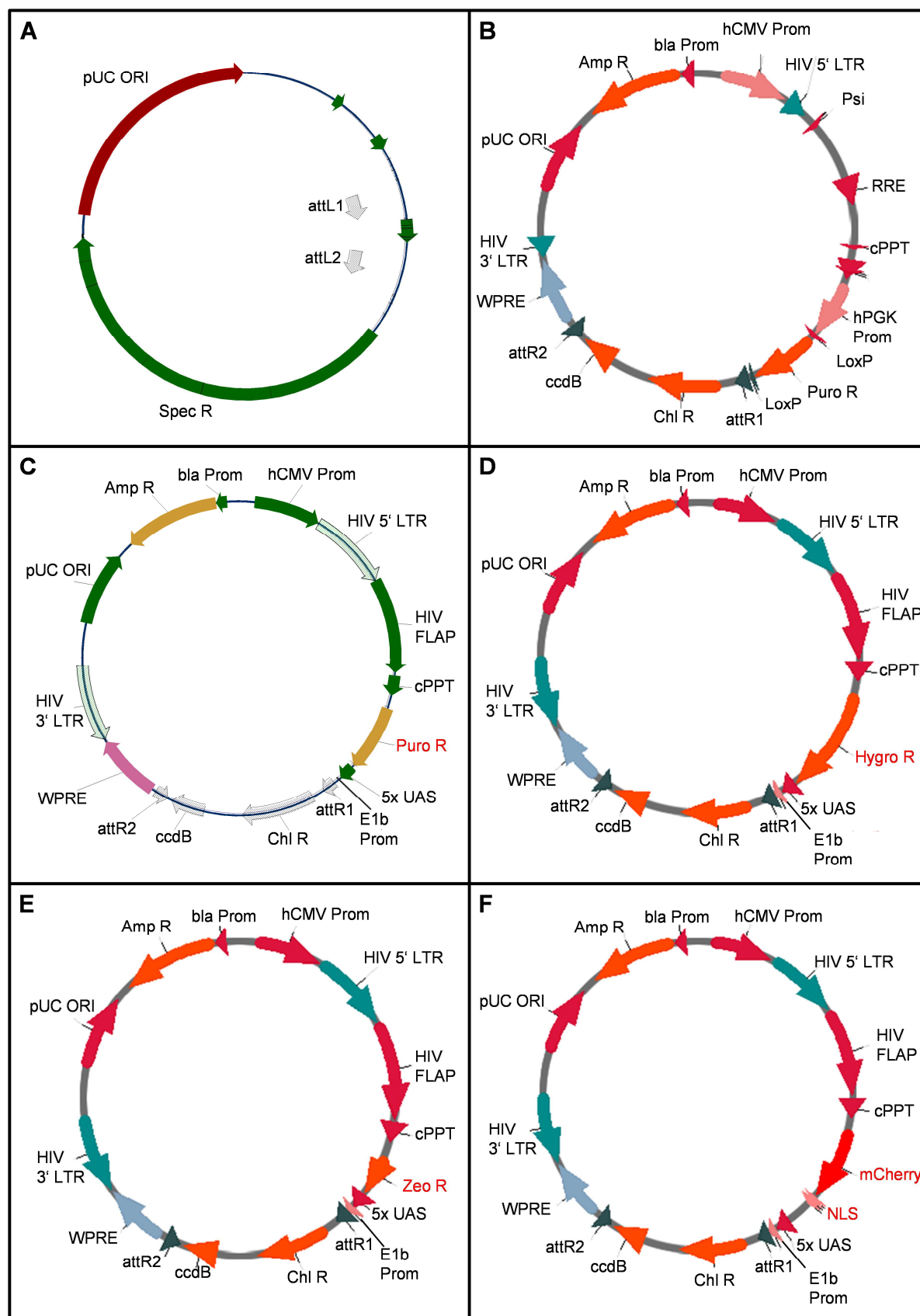
Figure 8-2: Plasmid maps II

Figure 8-2: Plasmid maps II

    A) pCR8/GW/TOPO+pCS2-MCS

    B) F2P-Delta Zeo-LoxP-Ko.Puro-LoxP-STNST-GW(DEST) (db 636)

    C) F2-Delta Zeo-Kozak-Puro-5XUAS-E1b-(GW)Dest (db 597)

    D) F2-Delta Zeo-Kozak-Hygro-5XUAS-E1b-(GW)Dest (db #44)

    E) F2-Delta Zeo-Kozak-Zeo-5XUAS-E1b-(GW)Dest (db #45)

    F) Delta Zeo-Kozak-mCherry-NLS-5X UAS-E1b-(GW)Dest (db #92)

Amp: ampicillin; att: attachment site for Gateway® cloning; bla: beta-lactamase; ccdB: control of cell death B; Chl: chloramphenicol; cPPT: central polypurine tract; hCMV: human cytomegalovirus; HIV: human immunodeficiency virus; hPGK: human phospho-glycero-kinase; Hygro: hygromycin; LTR: long terminal repeat; Prom: promoter; Psi: retroviral Psi packaging element; pUC Ori: pUC origin of replication; Puro: puromycin; R: resistance; RRE: rev response element; Spec: spectinomycin; UAS: upstream activation sequence; WPRE: woodchuck hepatitis virus posttranscriptional regulatory element; Zeo: zeocin^{TM}
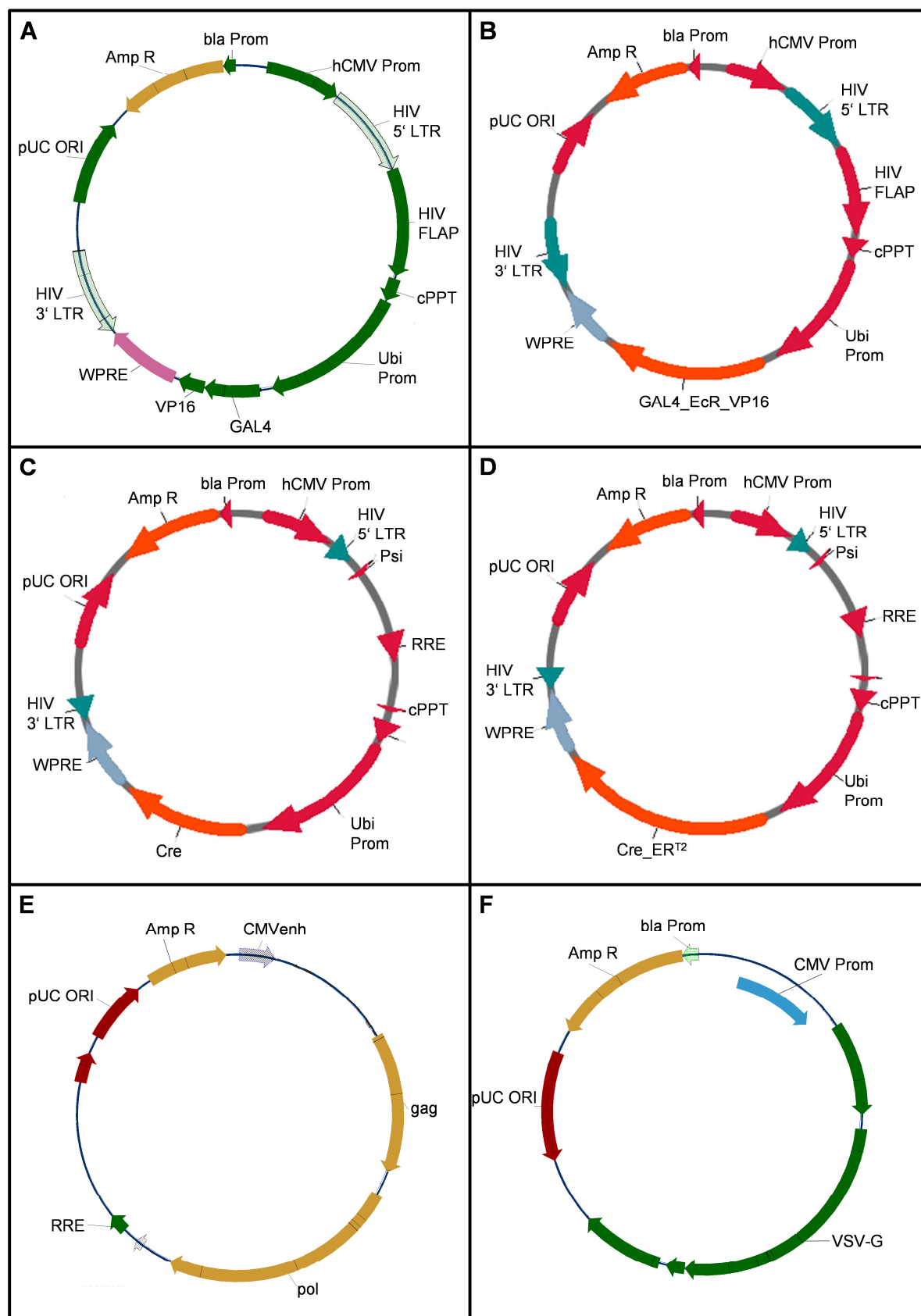
Figure 8-3: Plasmid maps III

Figure 8-3: Plasmid maps III

A) FUVALENTIN Delta Zeo-Gal4-VP16 (db #99)
B) FUVALENTIN Delta Zeo-Gal4-VP16-EcdR-F' (db #100)
C) F2U-Delta Zeo-iCre (db #101)
D) F2U-Delta Zeo-iCre-ERT2 (db #102)
E) psPAX2 (db #97)
F) pcDNAT3.1(-)VSVG (db #98)

Amp: ampicillin; bla: beta-lactamase; cPPT: central polypurine tract; Cre: Cre recombinase; EcR: ecdysone receptor; ER: estrogen receptor; hCMV: human cytomegalovirus; HIV: human immunodeficiency virus; LTR: long terminal repeat; Prom: promoter; Psi: retroviral Psi packaging element; pUC Ori: pUC origin of replication; R: resistance; RRE: rev response element; Ubi: ubiquitin; VSV-G: Vesicular stomatitis virus, glycoprotein G; WPRE: woodchuck hepatitis virus posttranscriptional regulatory element.

9 Acknowledgments

Unmentioned shall not remain Felix Schmidt's headhunter skills whose unconventional job interview (and Guinness and Tullamore Dew) turned the scale towards this PhD project.

Respectfully, I would like to thank my family and especially my parents for their love, patience, advice, and unconditional support over the last decades.

Especially, I would like to thank Agnes for love, company, and support without restrictions. Thank you for your patience when it comes to our "I-will-just-quickly-go-to-the-lab"-and-"Sorry-it-took-somewhat-longer"-weekends. I am looking forward to our common future and to Joining Our Next Adventure ☺.

10 Curriculum Vitae

Personal Data

Name   Martin Frank Bartels

Education

2012-Present   Graduate School for Systemic Neurosciences
                   PhD program

2009-2011   University of Munich
                   Degree: M.Sc. (Biochemistry)

2006-2009   University of Konstanz
                   Degree: B.Sc. (Biological Sciences)

11 List of Publications

Journal Articles

2014   **Wnt/β-catenin signaling inhibits the Shh pathway and impairs tumor growth in Shh-dependent medulloblastoma.**
Pöschl J, Bartels M, Ohli J, Bianchi E, Kuteykin-Teplyakov K, Grammel D, Ahlfeld J, Schüller U.
Acta Neuropathol. 2014 Apr;127(4):605-7. doi: 10.1007/s00401-014-1258-2. Epub 2014 Feb 15.

Talks

2015   **Etablierung eines neuen Zellkultur-Modells zur Untersuchung von Bildung, Modulation und Toxizität von alpha-Synuclein-Oligomeren**
Martin Bartels
Invited speaker at MODAG GmbH, MODAG Scientific Meeting, November 12th 2015, Munich

2012   **Etablierung eines neuen Zellkultur-Modells zur Untersuchung von Bildung, Modulation und Toxizität von alpha-Synuclein-Oligomeren**
Martin Bartels
Lüneburg-Seminar zur Pathophysiologie dopaminerger Zellen, December 10th 2012, Munich

Posters

2015   **Modelling alpha-synuclein pathology – transfer from *in vitro* studies to complex cellular models**

Martin Bartels, Peer-Hendrik Kuhn, Viktoria Ruf, Georg Nübling, Felix Schmidt, Daniel Weckbecker, Frits Kamp, Andrei Leonov, Sergey Ryazanov, Christian Griesinger, Kai Bötzel, Stefan F. Lichtenthaler, and Armin Giese

12th International Conference on Alzheimer's and Parkinson's Diseases and Related Neurological Disorders (AD/PD™ 2015), Nice (France)

Modelling alpha-synuclein pathology – transfer from *in vitro* studies to complex cellular models

Martin Bartels, Peer-Hendrik Kuhn, Viktoria Ruf, Georg Nübling, Felix Schmidt, Daniel Weckbecker, Frits Kamp, Andrei Leonov, Sergey Ryazanov, Christian Griesinger, Kai Bötzel, Stefan F. Lichtenthaler, and Armin Giese

GSN Orientation Week, October 5th to October 11th 2015, Munich (Germany)

Modelling alpha-synuclein pathology – transfer from *in vitro* studies to complex cellular models

Martin Bartels, Peer-Hendrik Kuhn, Viktoria Ruf, Georg Nübling, Felix Schmidt, Daniel Weckbecker, Frits Kamp, Andrei Leonov, Sergey Ryazanov, Christian Griesinger, Kai Bötzel, Stefan F. Lichtenthaler, and Armin Giese

GSN Retreat, July 3rd to July 5th 2015, Frauenchiemsee (Germany)

2014   **Novel cell-culture models to study formation, modulation, and toxicity of alpha-synuclein oligomers**

Martin Bartels, Peer-Hendrik Kuhn, Felix Schmidt, Kai Bötzel, Stefan Lichtenthaler, and Armin Giese

18th International Congress of Parkinson's Disease and Movement Disorders, June 8th to June 12th 2014, Stockholm (Sweden)

Novel cell-culture models to study formation, modulation, and toxicity of alpha-synuclein oligomers

Martin Bartels, Peer-Hendrik Kuhn, Felix Schmidt, Kai Bötzel, Stefan Lichtenthaler, and Armin Giese

GSN Retreat, July 4th to July 7th 2014, Spitzingsee (Germany)

A novel cell-culture model to study interaction of proteins with implication in neurodegenerative diseases

Martin Bartels, Peer-Hendrik Kuhn, Tabea Strauß, Kai Bötzel, Stefan Lichtenthaler, and Armin Giese

Neurowoche 2014, September 15th to September 19th 2014, Munich (Germany)

2013   **Establishment of a novel cell-culture model to study alpha-synuclein aggregation using single particle spectroscopy**

Martin Bartels

GSN NeuroSpin Winter School, April 27th to April 29th 2013, Obergurgl (Austria)

Establishment of a novel cell-culture model to study formation, modulation and toxicity of alpha-synuclein oligomers

Martin Bartels, Peer-Hendrik Kuhn, Kai Bötzel, Stefan Lichtenthaler, and Armin Giese

GSN Orientation Week, October 7th to October 12th 2013, Munich (Germany)

Eidesstattliche Versicherung/Affidavit

Hiermit versichere ich an Eides statt, dass ich die vorliegende Dissertation mit dem Titel „Establishment of Novel Cell Culture Models of Parkinson's Disease to Study Formation, Modulation, and Toxicity of α-Synuclein Oligomers" selbstständig angefertigt habe, mich außer der angegebenen keiner weiteren Hilfsmittel bedient und alle Erkenntnisse, die aus dem Schrifttum ganz oder annähernd übernommen sind, als solche kenntlich gemacht und nach ihrer Herkunft unter Bezeichnung der Fundstelle einzeln nachgewiesen habe.

I hereby confirm that the dissertation „Establishment of Novel Cell Culture Models of Parkinson's Disease to Study Formation, Modulation, and Toxicity of α-Synuclein Oligomers" is the result of my own work and that I have only used sources or materials listed and specified in the dissertation.

München, den   23.8.2017

Munich, date

_____

Martin Bartels

Declaration of Author Contributions

Plasmids for transient expression of V1S, SV2 and SV were kindly obtained from Prof. Dr. Pamela McLean.

Insertion of point mutations in V1 and V2 and evaluation of their effect on signal-to-noise ratio was part of a bachelor thesis of Thomas Meul which was supervised and coordinated by Martin Bartels.

Molecular cloning of most plasmids described in this work was perfomed by Martin Bartels during a lab rotation in Prof. Dr. Lichtenthaler's laboratory with help from Dr. Dr. Peer-Hendrik Kuhn. Gateway® plasmids and plasmids for the creation of lentiviruses, as well as protocols for creation and purification of lentiviruses were kindly obtained from Dr. Dr. Peer-Hendrik Kuhn.

Gateway® reaction to obtain plasmid #120 was performed by Tabea Strauß during an internship which was supervised and coordinated by Martin Bartels.

Experiments concerning the influence of metal ions on αSyn aggregation in H4_GE-V1S+SV2 cells and H4_GE-V cells were performed by Dr. Daniel Weckbecker and Martin Bartels. Sucrose gradient analysis was performed by Dr. Daniel Weckbecker.

Data evaluation script for cellular fluorescence analyzation from Opera® measurements was developed by Dr. Daniel Weckbecker, Dr. Achim Kirsch (Perkin Elmer) and Martin Bartels.

Mycoplasma tests were performed by Janina Mielke.

All additional parts of this work were performed by Martin Bartels.

_____ _____

Prof. Dr. med. Armin Giese Martin Bartels
1st supervisor